UNIVERSAL
LIBRARY

HARVARD MONOGRAPHS
IN APPLIED SCIENCE
NUMBER 2

EARTH WAVES

L. DON LEET
PROFESSOR OF GEOLOGY
HARVARD UNIVERSITY

1950
Cambridge, Massachusetts
HARVARD UNIVERSITY PRESS
New York: JOHN WILEY & SONS, INC.

PRINTED IN THE UNITED STATES OF AMERICA

FOREWORD

Fundamental research in applied science is characterized by diversity. Problems arise that overlap the tidy categories of academic science and demand the use of source material and methods of investigation drawn from many fields of knowledge. A wide range of applicability of the results further distinguishes this kind of research from the specialized objectivity of development work in engineering technology. With characteristic unpredictability, research in applied science is often of greatest potential value to those it might not reach through conventional specialized channels of publication.

The Harvard Monographs on Applied Science are designed to provide a medium for publishing the results of University research to a wider audience than would be reached by individual professional journals. The size and style of the monographs seem also to be well adapted for presentation of research results with due regard for a critical orientation of the work in its technical background.

The term "Applied Science" can be interpreted broadly enough to include all phases of science that influence the lives of men. Without accepting any narrower limitation of objective, this series of monographs will be devoted primarily to reports of significant research in the applied *physical* sciences, with especial emphasis on topics that involve intellectual borrowing among the academic disciplines.

THE EDITORIAL COMMITTEE

PREFACE

The purpose of this book is to present a compact summary of the present state of our knowledge about waves in the earth, with special reference to applications of that knowledge. The applications now being most widely made are in the fields of prospecting for minerals, studying hurricanes and other weather forms, measuring vibrations around dynamite blasts to determine their effects on buildings, and mapping broad earth structures of geologic interest.

The presentation is in a form which it is hoped will be of greatest value to readers with training in the fundamentals of some branch of engineering, physical, or geologic science, but it deals with first principles on the assumption that such readers have not necessarily been making daily use of all phases of the mathematics which that training included. Results of recent research, previously unpublished or available only in periodicals of limited circulation, are also presented on types of wave motion, interpretation of refraction profiles, and microseisms.

Much of the material was assembled in this form originally for presentation as a course of eight lectures on "Applications of Seismological Techniques to Engineering Problems," for The Lowell Institute of Boston in the autumn of 1946.

L. Don Leet

Harvard, Massachusetts
September 1949

CONTENTS

The point P_0, in completing one trip around its circular path, travels a distance $2\pi r$ in the time T. Since velocity is equal to distance divided by time,

$$v_0 = \frac{2\pi r}{T},$$

so that

$$a_0 = \frac{{v_0}^2}{r} = \frac{4\pi^2 r}{T^2}.$$

But

$$a = a_0 \frac{x}{r},$$

so the absolute value of the acceleration is

$$| a | = \frac{4\pi^2}{T^2} x = 4\pi^2 f^2 x.$$

If the direction in which it acts is considered, it must be given a negative sign to indicate that it is directed toward the position of zero displacement; that is,

$$a = -4\pi^2 f^2 x. \tag{1}$$

The quantity x of Eq. (1) appears in Fig. 2 as the distance by which P is displaced from the center of the reference circle O; it is called the *displacement* and varies according to the position of P. In fact, x is the only variable in the right-hand member of Eq. (1); hence *acceleration in simple harmonic motion is proportional to displacement.* The maximum displacement, when $x = OA$ or $x = OB$, is called the *amplitude* of the motion. Since force is equal to the product of mass and acceleration, or $F = ma$, force in simple harmonic motion is also proportional to displacement.

If, now, we wish to consider P as a particle in a physical system, O would be its position of rest, or the position it occupies when not in oscillation. We then know that if P is displaced from its rest position O, and if it is then acted upon by a restor-

ing force which is proportional to the displacement, then P, when released, will oscillate about O with simple harmonic motion. This condition—that the restoring force is proportional to the displacement—is met by all elastic bodies, including most earth materials and springs, and by a simple pendulum swinging through a small arc.

Complex Numbers

It happens that the circle can be used in the geometric representation of complex numbers, and complex notation is frequently employed in expressions for simple harmonic motion.[1]

The concept of complex numbers developed in algebra from investigations of the solutions of such equations as $x^2 - 2x + 5 = 0$. This equation has no real roots, but is formally satisfied by $1 \pm \sqrt{-4}$. Since $\sqrt{-4} = \sqrt{+4(-1)}$, it can be written as $2\sqrt{-1}$. Then, if we represent $\sqrt{-1}$ by the letter j the solution is written as $1 \pm 2j$. This is called a complex number and consists of a real part, 1 in this case, and an imaginary part, $2j$. In a similar manner, the solution of the quadratic equation $x^2 - 16x + 100 = 0$ is found to be $8 \pm 6j$, which is another complex number, with real part 8 and imaginary part $6j$.

A complex number can be expressed in the general form $a + bj$, where a and b are real numbers, not necessarily integers. Gauss, around the year 1800, proved that every algebraic equation with real coefficients has complex roots if we consider that real numbers are special types of complex numbers in which b, the coefficient of j, is zero. Complex numbers constitute a closed system for the elementary operations of addition, subtraction, multiplication, division by a nonvanishing divisor, and extraction of roots.

An important step in the study of complex numbers was made by Argand who, in 1806, published a discussion showing how to relate complex numbers to plane geometry by representing a

[1] D. R. Curtiss, *Analytic functions of a complex variable* (Open Court, Chicago, 1926), pp. 1–18.

complex number $x + jy$ by a point (x, y) in a system of plane Cartesian co-ordinates, as in Fig. 3. All real numbers are repre-

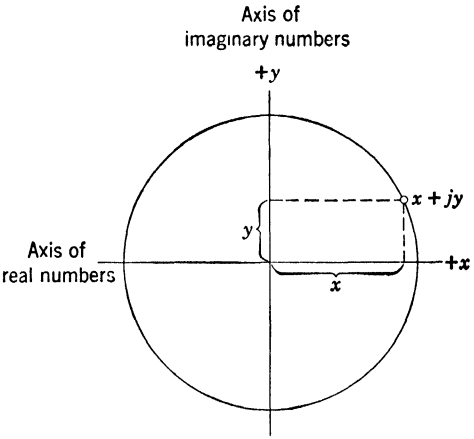

FIG. 3. Plotting $x + jy$.

sented by points on the axis of abscissas, all pure imaginaries by points on the axis of ordinates, and complex numbers by points elsewhere in the plane.

If a circle of radius $r = \sqrt{x^2 + y^2}$ is drawn around the origin of the X- and Y-axes as center, as in Fig. 4, it will be seen that the number represented by this point has for its real part $r \cos \varphi$ and for its imaginary part $rj \sin \varphi$. Accordingly, we may write $x + jy = r(\cos \varphi + j \sin \varphi)$. Furthermore, it has been shown by the standard series expansions that $\cos \varphi + j \sin \varphi = e^{j\varphi}$, φ being measured in radians, so we have as equivalent expressions for a complex number

$$x + jy = r(\cos \varphi + j \sin \varphi) = re^{j\varphi},$$

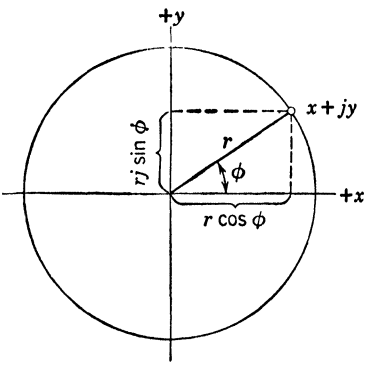

FIG. 4. Plotting $x + jy$.

where

$$x = r\cos\varphi, \qquad y = rj\sin\varphi,$$

$$r = \sqrt{x^2 + y^2}, \qquad \tan\varphi = y/x,$$

and r is a vector defined by its magnitude $\sqrt{x^2 + y^2}$ and its direction angle φ with reference to the axis of real numbers.

One interesting property of these expressions for a complex number is that as φ increases continuously, the vector r rotates uniformly and the value of $x + jy$ repeats itself periodically. This connects the graphical representation of complex numbers to our diagram and definition of Fig. 2. Moreover, $e^{\pi j} = -1$, $e^{\frac{1}{2}\pi j} = j$, $e^{\frac{3}{2}\pi j} = -j$, $e^{2\pi j} = e^{4\pi j} = \cdots = 1$; that is, the exponential is periodic with period $2\pi j$.

The complex numbers

$$x + jy = r(\cos\varphi + j\sin\varphi) = re^{+j\varphi}$$

and

$$x - jy = r(\cos\varphi - j\sin\varphi) = re^{-j\varphi},$$

which differ only in the sign of the imaginary part, are called conjugate complex numbers. The sum and product of a complex number and its conjugate are real.

In examining the theory of the seismograph, we are interested in expressions for the motion of a weight suspended by a spring. Obviously, such motion is real, so our final solution should be real. Differential equations are involved which lend themselves to complex exponential solutions. Under these circumstances, one procedure is to obtain a complex solution and take the real part. Geometrically, this amounts to defining a vector of fixed length revolving about the origin and using the projection of this vector on the axis of reals. This defines simple harmonic motion as illustrated in Fig. 2. Another form of solution consists of a complex vector and its conjugate. The sum of such vectors is real, and as φ increases at a constant rate this sum defines simple harmonic motion along the x-axis.

Consider Fig. 5, in which a mass m is supported on frictionless and massless rollers; m is attached to a spring k and k is attached to an infinite mass which is the frame of reference with respect to which the motion of m is described.

The mass m may be obtained by dividing the weight W by the acceleration g due to gravity; if W is expressed in pounds and g in inches per second per second, $m = W/386 = 0.00259W$ lb sec^2/in.

The spring constant k is the spring's restoring force per unit displacement, acting in a direction opposite to the displacement. It is the force required to extend the spring by unit distance, and we shall express it in pounds per inch.

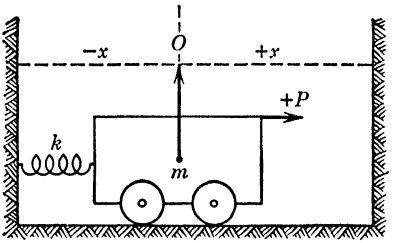

FIG. 5. Undamped linear vibratory system.

Now apply a force P, considered positive to the right, varying with time t. Let x be the displacement from the rest position, considered positive to the right.

Then

$$m\frac{d^2x}{dt^2} + kx = P(t) \tag{2}$$

or

$$\begin{pmatrix}\text{Force from acceleration}\\ \text{of the mass}\end{pmatrix} + \begin{pmatrix}\text{Restoring force}\\ \text{of spring}\end{pmatrix} = \begin{pmatrix}\text{Applied}\\ \text{force}\end{pmatrix}.$$

After an initial displacement of the system, if the force ceases to act, the equation becomes

$$m\frac{d^2x}{dt^2} + kx = 0$$

or

$$\frac{d^2x}{dt^2} + \frac{k}{m}x = 0, \tag{3}$$

and since the spring's restoring force is proportional to the displacement, the motion will be simple harmonic.

Using complex notation, we may assume $x = e^{jpt}$ and try to choose p so that x is a solution of Eq. (3). This is merely saying that we will let x be any complex number, with pt standing for the angle φ of Fig. 4. Substituting in Eq. (3),

$$\frac{dx}{dt} = \frac{d(e^{jpt})}{dt} = jpe^{jpt},$$

$$\frac{d^2x}{dt^2} = (jp)^2e^{jpt} = -p^2e^{jpt};$$

so

$$-p^2e^{jpt} + \frac{k}{m}e^{jpt} = 0,$$

$$-p^2 + \frac{k}{m} = 0,$$

$$p = \pm\sqrt{\frac{k}{m}}.$$

Now, for any homogeneous differential equation linear in x, that is, containing x only to the first power, such as Eq. (3), the sum of two solutions is a solution, so, since we have

$$x = e^{jpt}$$

and

$$x = e^{-jpt},$$

we can say that a solution of Eq. (3) is

$$x = Ce^{jpt} + De^{-jpt}. \tag{4}$$

The exponentials differ only in the sign of the term involving j, and accordingly are conjugates, the sum of which is real.

From series expansions, it has been shown that

$$e^{j\varphi} = \cos\varphi + j\sin\varphi,$$

$$e^{-j\varphi} = \cos(-\varphi) + j\sin(-\varphi)$$

$$= \cos\varphi - j\sin\varphi,$$

where φ is expressed in radians. Then

$$e^{j\varphi} + e^{-j\varphi} = 2\cos\varphi \quad \text{or} \quad \cos\varphi = \frac{e^{j\varphi} + e^{-j\varphi}}{2}$$

and

$$e^{j\varphi} - e^{-j\varphi} = 2j\sin\varphi \quad \text{or} \quad \sin\varphi = \frac{e^{j\varphi} - e^{-j\varphi}}{2j}.$$

Now, if we put

$$x = B\cos pt + A\sin pt,$$

where A and B are real numbers, we can write

$$x = B\left(\frac{e^{jpt} + e^{-jpt}}{2}\right) + A\left(\frac{e^{jpt} - e^{-jpt}}{2j}\right),$$

or, remembering that $1/j = -j$,

$$x = \left(\frac{B - jA}{2}\right)e^{jpt} + \left(\frac{B + jA}{2}\right)e^{-jpt},$$

which is the same as (Eq. (4) if $C = \frac{1}{2}(B - jA)$ and $D = \frac{1}{2}(B + jA)$. Thus, C and D are conjugate complex numbers, whose real parts are equal and whose imaginary parts have opposite signs. Hence, the solution of Eq. (3) may finally be written

$$x = A\sin pt + B\cos pt, \tag{4}$$

where A and B are real numbers, arbitrary constants depending on the initial conditions, and the quantity pt is expressed in radians.

Since pt is expressed in radians, p must be in radians per unit time, an angular velocity. It is actually the angular velocity with which the reference particle P_0 (Fig. 2) traverses its circular path so that its projection P will have the displacement defined by Eq. (4). We have already seen that $p = \sqrt{k/m}$ in terms of the quantities in Eq. (3).

Equation (4) describes oscillations of the mass in Fig. 5. Values of x are repeated each time the quantity pt is increased

by 2π radians. This occurs whenever the time t is increased by a certain interval T, the period. In other words,

$$pT = 2\pi \text{ radians},$$

$$T = \frac{2\pi}{p},$$

and

$$\frac{1}{T} = f = \frac{p}{2\pi},$$

or

$$2\pi f = p,$$

where f is the frequency. As a result of this relation, p, although it is a velocity term, is called the *angular frequency* of the mass oscillating with simple harmonic motion.

As an example of the determination of the constants A and B from the initial conditions, consider a situation in which the mass is at its zero position when we start counting time, but in motion with a velocity v'. Then the initial conditions are $x = 0$ and $v = v'$ when $t = 0$.

From Eq. (4), $\sin pt = 0$, $\cos pt = 1$ when $t = 0$, and the equation becomes

$$0 = 0 + B.$$

That is, $B = 0$ for these initial conditions, so that Eq. (4) becomes

$$x = A \sin pt.$$

Now when $t = 0$,

$$v = \frac{dx}{dt} = Ap \cos pt = v'$$

and $\cos pt = 1$, so that

$$A = \frac{v'}{p}.$$

Thus we have evaluated both constants for these initial conditions.

A graph of the solution for these initial conditions can be made in the manner of Fig. 2. It will show that the amplitude of motion (or radius of the reference circle) is v'/p and that φ [$= pt$] is the angle between the rotating radius and the Y-axis (instead of the X-axis as in Fig. 2).

As a second example, consider the mass at its maximum displacement and momentarily at rest, when we start counting time. Then $x = X$ and $v = 0$ when $t = 0$. Again, when $t = 0$, $\sin pt = 0$ and $\cos pt = 1$, so from Eq. (4)

$$X = 0 + B.$$

Now when $t = 0$,

$$v = \frac{dx}{dt} = Ap \cos pt - Bp \sin pt = 0$$

then

$$Ap \cos pt = 0;$$

but $\cos pt = 1$, so

$$Ap = 0$$

and since, by definition, p cannot be zero,

$$A = 0$$

and Eq. (4) becomes

$$x = X \cos pt.$$

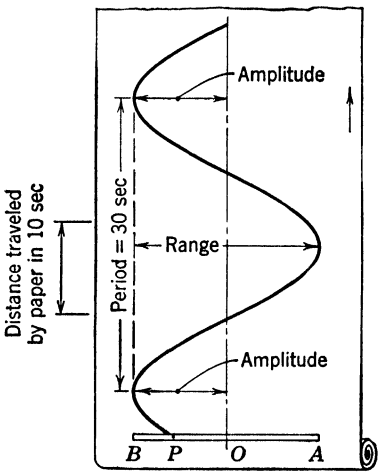

FIG. 6. Record of simple harmonic motion.

A graph for these initial conditions in the manner of Fig. 2 will have X for the amplitude of motion (or radius of the reference circle) and $pt = \varphi$, the angle between the rotating radius and the X-axis.

Simple harmonic motions are customarily recorded along a time axis. The relations of such a record to the elements of the motion are illustrated in Fig. 6.

Consider the particle P of Fig. 2 to be a pen, or a point of light, moving with simple harmonic motion along a slit AB

(Fig. 6), with a strip of paper moving under this slit with constant speed. Then P traces on the paper a curve that records displacement as a function of time. From this curve the amplitude and period of the motion can be measured, as indicated in the figure. It should be remembered that the amplitude is the maximum displacement from the central position, or position of rest, O. The total distance AB through which the particle moves is sometimes called the double amplitude, or range.

Forced Vibrations

There are many treatises dealing with various aspects of the subject of vibrations. Among these are such widely known textbooks as those of Rayleigh,[2] Timoshenko,[3] Den Hartog,[4] and Morse.[5] The very volume of the literature, however, has brought into use competing sets of nomenclature and symbols, which lead to confusion. Also, many of the relations are developed with emphasis on the theory and expressed in forms not well adapted to numerical computation. During the war, R. T. McGoldrick undertook, for the Structural Mechanics Division of the Navy's David Taylor Model Basin, to standardize notation and write formulas in such a way that numerical results could be obtained from them directly and simply.[6] The present discussion follows McGoldrick's notation and philosophy. All formulas will yield numerical answers in inch-pound-second (ips) units if the values substituted are in this system. The notation is summarized in Table 1.

If to the system of Fig. 5 we now add a means of resisting the motion of m by a force proportional to m's velocity, we have a damped vibratory system. A dashpot is used for the diagram-

[2] Lord Rayleigh, *The theory of sound* (Macmillan, London, 1929, 2 vols.; Dover, New York, 1945, 1 vol.).

[3] S. Timoshenko, *Vibration problems in engineering* (Van Nostrand, New York, 1928).

[4] J. P. Den Hartog, *Mechanical vibrations* (McGraw-Hill, New York, ed. 3, 1940).

[5] P. M. Morse, *Vibration and sound* (McGraw-Hill, New York, ed. 2, 1948).

[6] R. T. McGoldrick, *A vibration manual for engineers* (David Taylor Model Basin, Washington, D. C., 1944).

TABLE 1. Summary of notation.

Symbol	Quantity	Units	Dimensions—Force, Length, Time (FLT)
a	Instantaneous acceleration	(in./sec)/sec	LT^{-2}
c	Linear damping force per unit velocity	lb/(in./sec)	$FL^{-1}T$
c_c	Critical damping force per unit velocity	lb/(in./sec)	$FL^{-1}T$
e	Base of natural logarithms: 2.718	numeric	—
f	Frequency	cycles/sec	T^{-1}
f_n	Natural frequency of damped system	cycles/sec	T^{-1}
F	Magnification factor: ratio of single amplitude produced by exciting force $P_0 \sin \omega t$ to static deflection that would be produced by force P_0	numeric	—
g	Acceleration due to gravity	(in./sec)/sec	LT^{-2}
k	Linear spring constant	lb/in.	FL^{-1}
l	Length	in.	L
m	Mass: determined by dividing weight (lb) by acceleration due to gravity [(in./sec)/sec] [$= W/386 = 0.00259\ W$]	lb/(in./sec^2)	$FL^{-1}T^2$
p	Natural angular frequency without damping, or resonant angular frequency, of weight and spring system	rad/sec	T^{-1}
P	Instantaneous value of exciting force	lb	F
P_0	Maximum value of sinusoidal exciting force	lb	F
t	Time	sec	T
T	Period: time required for one complete oscillation; reciprocal of frequency	sec	T
W	Weight	lb	F
x	Instantaneous value of displacement	in.	L
X	Maximum value of sinusoidal displacement; amplitude	in.	L
Z	Resonance factor: ratio of steady state amplitude of mass subjected to forced vibration to actual amplitude of its support; X_1/X	numeric	—
δ	Logarithmic decrement	numeric	—
φ	Phase angle; in forced vibration, angle by which applied force leads displacement	rad	—
ω	Angular frequency [$= 2\pi f$]	rad/sec	T^{-1}
ω_n	Natural angular frequency of damped system	rad/sec	T^{-1}

matic representation but in seismographs the damping is usually achieved by some variation of the principle of a copper vane moving in a magnetic field to set up eddy currents which dissipate energy in the form of heat and thus retard the motion.

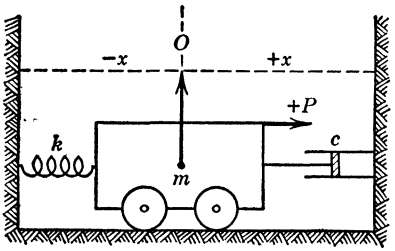

FIG. 7. Damped linear vibratory system.

A quantity c is used to represent the damping force per unit velocity, always acting in a direction opposite to that of the velocity. It is expressed in pounds per inch per second, that is, pound-seconds per inch (lb sec/in.).

If the mass in Fig. 7 is now displaced by a force P and the force is then removed, the equation for the motion of m becomes

$$m\frac{d^2x}{dt^2} + c\frac{dx}{dt} + kx = 0$$

or

$$\frac{d^2x}{dt^2} + \frac{c}{m}\frac{dx}{dt} + \frac{k}{m}x = 0. \tag{5}$$

If we assume $x = e^{at}$, then

$$\frac{dx}{dt} = ae^{at},$$

$$\frac{d^2x}{dt^2} = a^2e^{at},$$

and, substituting,

$$\left(a^2 + \frac{c}{m}a + \frac{k}{m}\right)e^{at} = 0.$$

Since $e^{at} \neq 0$, we have a quadratic equation in a, namely,

$$a^2 + \frac{c}{m}a + \frac{k}{m} = 0.$$

So long as the constant coefficients do not depend upon the time, and a satisfies the quadratic equation, the exponential will satisfy the differential equation. The solution of the quadratic equation is

$$a = -\frac{c}{2m} \pm \sqrt{\frac{c^2}{4m^2} - \frac{k}{m}}.$$

Substituting in our originally assumed expression, $x = e^{at}$, we have

$$x = Ce^{\left(-\frac{c}{2m}+\sqrt{\frac{c^2}{4m^2}-\frac{k}{m}}\right)t} + De^{\left(-\frac{c}{2m}-\sqrt{\frac{c^2}{4m^2}-\frac{k}{m}}\right)t}, \tag{6}$$

where C and D are arbitrary constants depending on initial conditions. This is a solution of Eq. (5), but since we shall be particularly interested in the case where $k/m > c^2/4m^2$ it is desirable to reduce it to a more convenient form, in which the quantity under the radical is positive. Since

$$\sqrt{\frac{c^2}{4m^2} - \frac{k}{m}} = j\sqrt{\frac{k}{m} - \frac{c^2}{4m^2}},$$

we have

$$x = e^{-\frac{c}{2m}t}\left(Ce^{j\sqrt{\frac{k}{m}-\frac{c^2}{4m^2}}\,t} + De^{-j\sqrt{\frac{k}{m}-\frac{c^2}{4m^2}}\,t}\right). \tag{6}$$

If we put

$$\omega_n = \sqrt{\frac{k}{m} - \frac{c^2}{4m^2}} = 2\pi f_n,$$

Eq. (6) becomes

$$x = e^{-\frac{c}{2m}t}\left(Ce^{j\omega_n t} + De^{-j\omega_n t}\right). \tag{6}$$

The term in parentheses will be recognized as the right-hand member of Eq. (4), with ω_n in place of p, so as a final step we write

$$x = e^{-\frac{c}{2m}t}\left(A \sin \omega_n t + B \cos \omega_n t\right). \tag{6}$$

This equation shows that x is a periodic function of the time, with decreasing amplitude—determined by the exponential

term. Hence the mass undergoes *damped oscillations;* ω_n is the *natural angular frequency with damping*, expressed in radians per second, and A and B are real numbers and arbitrary constants depending on the initial conditions.

As has been pointed out, Eq. (6) is actually a solution of Eq. (5) for the case where $k/m > c^2/4m^2$, which is described as the one for which damping is less than critical. If $k/m < c^2/4m^2$, the

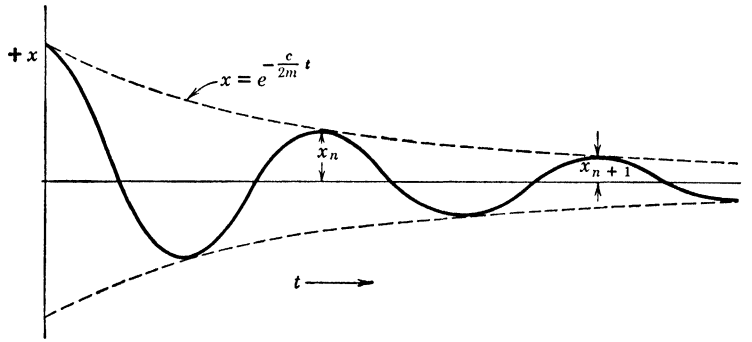

FIG. 8. Free vibration with less than critical damping.

mass will not oscillate but will gradually return to its rest position. If $k/m = c^2/4m^2$, the system is critically damped, or deadbeat, and the constant c is assigned a special value c_c. Then

$$\frac{k}{m} = \frac{c_c^2}{4m^2}$$

and

$$c_c = \sqrt{\frac{4m^2k}{m}} = 2\sqrt{mk}.$$

The solution represented by Eq. (6) has been plotted as a function of time in Fig. 8.

The term $e^{-(c/2m)t}$ approaches zero as the time increases. The term in parentheses represents an oscillation like that given by Eq. (4). The effect of the exponential term introduced by the damping is to reduce each succeeding amplitude by a constant

raction. The period does not change with a decrease in amplitude.

The rate at which the amplitude dies down is of interest. It :an be calculated by considering two successive maxima, such as X_n and X_{n+1} in Fig. 8. The time that elapses between these naxima is the period, $2\pi/\omega_n$. During that time, the amplitude ıas decreased from $e^{-(c/2m)t}$ to $e^{-(c/2m)(t+2\pi/\omega_n)}$. The second of .hese quantities can be obtained by multiplying the first by $:^{-\pi c/m\omega_n}$, which is less than unity. This quantity is the same for ıny two successive maxima and is independent of both ampli- .ude and time. The ratio of successive maxima is constant and .he amplitudes decrease in a geometric series.

The quantity $\delta[= \pi c/m\omega_n]$ is known as the *logarithmic decrement*. Since

$$X_{n+1} = X_n e^{-\frac{\pi c}{m\omega_n}},$$

$$\ln \frac{X_{n+1}}{X_n} = -\frac{\pi c}{m\omega_n} = -\delta. \tag{7}$$

For small damping,

$$\delta = 2\pi \frac{c}{c_c}.$$

If we now subject the mass of Fig. 7 to a sinusoidal driving 'orce $P = P_0 \sin \omega t$, the equation for the motion of m becomes

$$m\frac{\mathrm{d}^2x}{\mathrm{d}t^2} + c\frac{\mathrm{d}x}{\mathrm{d}t} + kx = P_0 \sin \omega t. \tag{8}$$

The general solution of this equation is

$$x = e^{-\frac{c}{2m}t}(A \sin \omega_n t + B \cos \omega_n t) + \frac{P_0 \sin (\omega t - \varphi)}{\sqrt{(c\omega)^2 + (k - m\omega^2)^2}}, \tag{9}$$

where A and B as before are arbitrary constants depending on :he initial conditions,

$$\omega_n = \sqrt{\frac{k}{m} - \frac{c^2}{4m^2}},$$

and

$$\tan \varphi = \frac{c\omega}{k - m\omega^2} = \frac{2\frac{\omega}{p}\frac{c}{c_c}}{1 - \left(\frac{\omega}{p}\right)^2};$$

the first term in the right-hand member is the so-called transient term and the second is the steady-state term.

The motion of the mass m, with reference to the rigid frame of Fig. 7, is thus compounded of the transient, which represents the natural vibration of the mass when it is displaced and the force removed, as in Eq. (6), and the steady state imposed by the external force P. This is shown graphically in Fig. 9.

The amplitude of the steady-state oscillation is given by

$$X = \frac{P_0/k}{\sqrt{\left[1 - \left(\frac{\omega}{p}\right)^2\right]^2 + \left[2\frac{c}{c_c}\frac{\omega}{p}\right]^2}}, \tag{10}$$

where, as before, $p[= \sqrt{k/m}]$ is the undamped angular frequency and ω is the angular frequency of the applied force.

The numerator of the right-hand member of Eq. (10) is the displacement that would be produced by the force P_0 applied statically. It appears from this expression for X that *a given force acting on the mass of Fig. 7 can produce widely varying amplitudes of m, depending on the damping and on the ratio of the forcing frequency to the natural frequency of the system.* This is the key to the subject of forced vibrations.

The ratio of the steady-state amplitude in forced vibrations to that which would result from static application of the same force may be called the *amplitude factor*, F. That is,

$$F = \frac{X}{P_0/k} = \frac{1}{\sqrt{\left[1 - \left(\frac{\omega}{p}\right)^2\right]^2 + \left[2\frac{c}{c_c}\frac{\omega}{p}\right]^2}}.$$

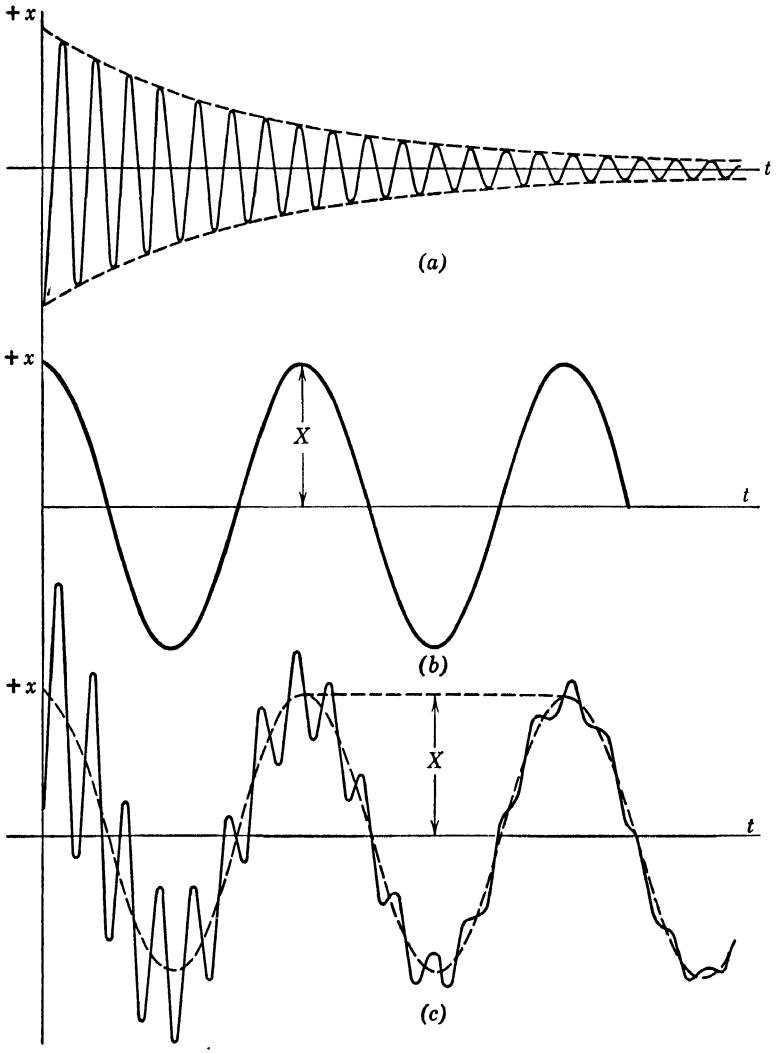

FIG. 9. Forced vibration. (*a*) Free vibration, with frequency p, of the mass of Fig. 7, with damping adjusted to cause an amplitude decrease of 10 percent per cycle. (*b*) Steady-state vibration due to an applied force P with frequency ω [$= p/8$]. (*c*) The actual motion—the sum of curves (*a*) and (*b*)—represented by Eq. (9). (After Den Hartog.)

The factor F is plotted as a function of ω/p for several values of c/c_c in Fig. 10. The phase angle φ, by which the force leads the displacement, is plotted in Fig. 11.

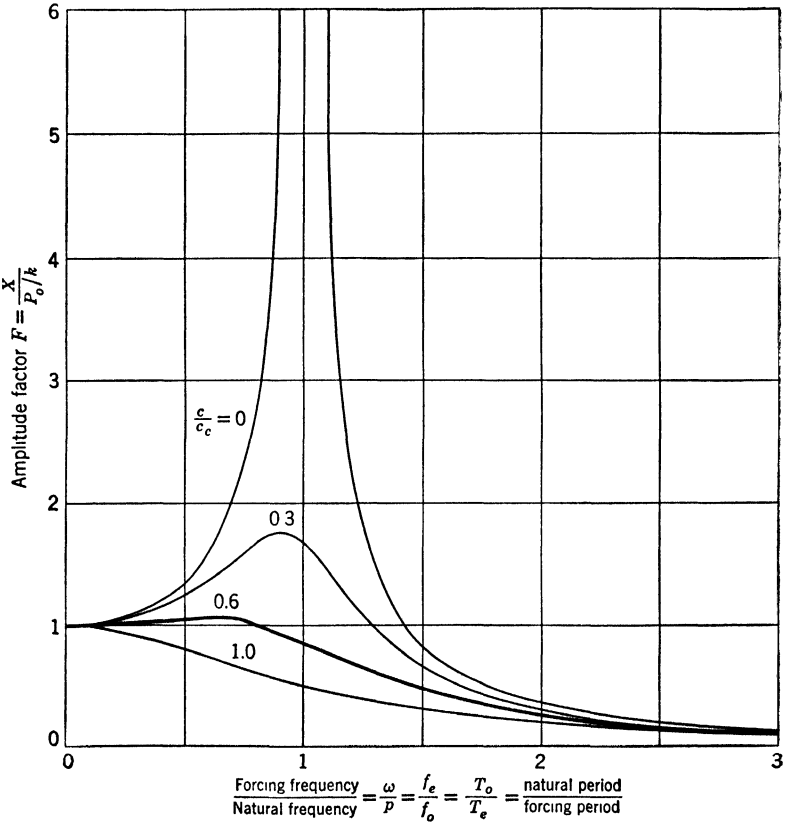

FIG. 10. Magnification factor for a damped system subjected to a force $P_o \sin \omega t$.

Equation (8) and its solution have a direct analogy in an electric circuit containing capacitance, inductance, resistance, and impressed electromotive force, the equation for which is

$$L\frac{d^2Q}{dt^2} + R\frac{dQ}{dt} + \frac{1}{C}Q = E_0 \sin \omega t, \qquad (8a)$$

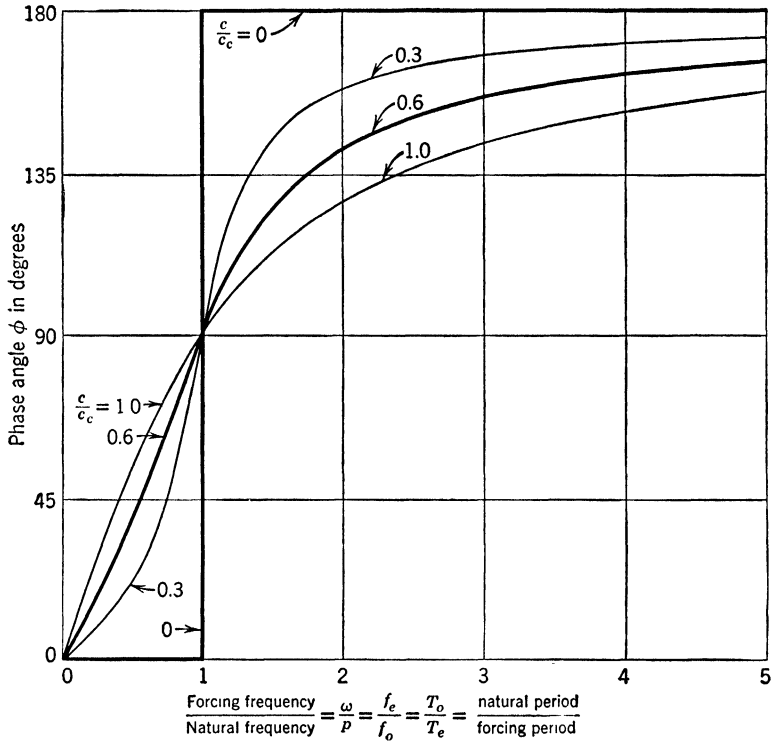

FIG. 11. Phase angle for a damped system subjected to a force $P_o \sin \omega t$.

where L is self-inductance; C, capacitance; R, resistance; E_0, emf; Q, charge; dQ/dt $[= i]$, current.

The Seismograph

A seismograph is basically an inertia member, subjected to a restoring force and damping when displaced, mounted in a frame or case which rests on or is attached to the structure whose vibrations are to be measured. This is shown diagrammatically in Fig. 12. In practice, displacement of the inertia member m relative to the case is multiplied by mechanical or electrical means and recorded as a function of time. For purposes of discussing the theory of its operation, however, the multiplication and registration features need not be considered here.

In Fig. 12, x represents the absolute displacement of the structure measured on axes fixed in space, and x_1 represents displacement of the inertia member m relative to the case, which leads

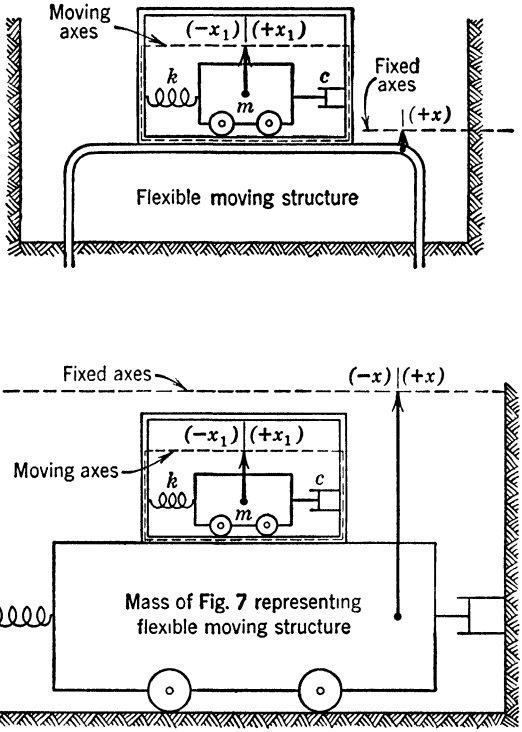

FIG. 12. Seismograph on a flexible moving structure.

to the recorded motion. The displacement x_1 is measured on axes which move (without rotation) with the case.

The differential equation for the motion of m relative to the moving axes in Fig. 12 is

$$m\frac{d^2x_1}{dt^2} + c\frac{dx_1}{dt} + kx_1 = -m\frac{d^2x}{dt^2}. \tag{11}$$

This is identical with Eq. (5) if x_1 is substituted for x and $-m(d^2x/dt^2)$ for the force which was applied and removed.

Let us assume that the structure has a simple harmonic motion $X \sin \omega t$; then the acceleration is

$$\frac{d^2X}{dt^2} = -X\omega^2 \sin \omega t,$$

and Eq. (11) becomes

$$m\frac{d^2x_1}{dt^2} + c\frac{dx_1}{dt} + kx_1 = mX\omega^2 \sin \omega t \tag{12}$$

The steady-state amplitude of the system subjected to such a motion is

$$X_1 = \frac{mX\omega^2/k}{\sqrt{\left[1 - \left(\frac{\omega}{p}\right)^2\right]^2 + \left[2\frac{c}{c_c}\frac{\omega}{p}\right]^2}}.$$

As before, we define the undamped angular frequency of m as p, and $p^2 = k/m$.

Dividing both numerator and denominator of the steady-state part of the solution of Eq. (12) by ω^2/p^2 gives

$$X_1 = \frac{X}{\sqrt{\left[\left(\frac{p}{\omega}\right)^2 - 1\right]^2 + \left[2\frac{c}{c_c}\frac{p}{\omega}\right]^2}},$$

which may be written

$$X_1 = XZ.$$

This shows that the steady-state amplitude of the mass m is equal to the actual amplitude of the base modified by a factor Z whose value depends upon the damping ratio and the ratio of natural to impressed frequency. This factor Z has been called the *resonance factor*. Figure 13 is a graph of Z as a function of the ratio of impressed to natural frequency for different values of c/c_c.

When the resonance factor is unity, the mass m is recording most faithfully the motion of the structure on which it rests.

That actually means that m is standing still in space while the axes on which x_1 is measured move with the supporting structure. From Fig. 13, it can be seen that this condition obtains prac-

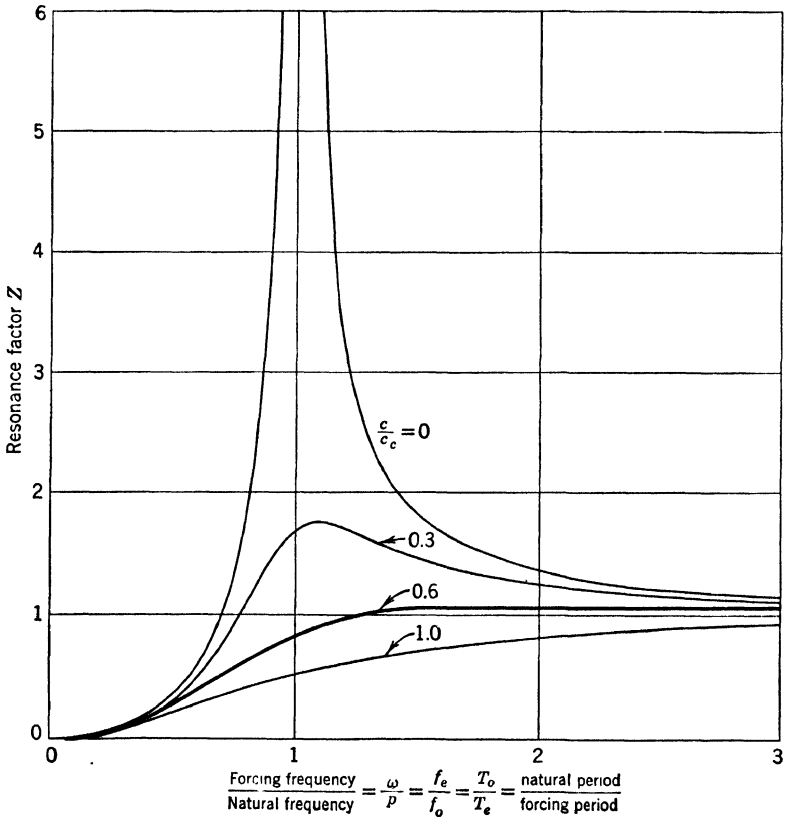

FIG. 13. Resonance factor for a damped system subjected to a force $P_o \sin \omega t$.

tically for impressed frequencies that are three or more times the natural undamped frequency of m for wide variations in damping. When c/c_c is about 0.6, the instrument records amplitudes accurately at impressed frequencies down practically to the natural frequency itself. Stated in terms of periods, when the forcing

period is one-third or less that of the natural period, for nearly all damping, or when the forcing period is equal to or less than the natural period for $c/c_c = 0.6$, the seismograph records displacements well.

Figure 13 and the steady-state solution of Eq. (12) also show that if the supporting structure vibrates at frequencies lower than the natural frequency of the instrument, or at periods greater than the natural period of the instrument,

$$\frac{X_1}{X} \approx \frac{1}{\sqrt{p^4/\omega^4}} \approx \left(\frac{\omega}{p}\right)^2.$$

For values of ω/p less than 0.5, X_1/X is parabolic for wide variations in damping. If the damping is 0.6 critical, this condition is approximated for values of ω/p nearly down to unity. Within this zone, the instrument writes a record that is proportional to the acceleration of the forcing motion, since, as was shown in Eq. (12), this acceleration is proportional to ω^2.

In general, then, such an instrument responds as a **displacement recorder** *for frequencies greater than its own (periods less than its own) and as an* **acceleration recorder** *for frequencies less than its own (periods greater than its own).*

If the motion applied in Fig. 12 is not a steady-state vibration, a transient term appears in the solution of Eq. (11). Fundamentally, the instrument responds to acceleration at all times, but the transient displacement of the structure may be obtained from the recorded displacement x_1. If we multiply Eq. (11) by p^2/k it becomes

$$\frac{d^2x_1}{dt^2} + 2\frac{c}{c_c}p\frac{dx_1}{dt} + p^2x_1 = -\frac{d^2x}{dt^2}. \tag{13}$$

A double integration gives

$$x_1 + 2\frac{c}{c_c}p\int_0^t x_1\,dt + p^2\int_0^t\int_0^t x_1\,dt\,dt = -x, \tag{14}$$

where the constants of integration drop out if $x = 0$ when $t = 0$. Thus the displacement up to time t can be obtained by adding the recorded displacement and the indicated integrals. The shorter the time interval, the smaller the correction to the first term, so for short intervals the displacement is recorded directly.

In connection with Fig. 12, everything that has been said about the behavior of m as a seismograph applies regardless of the physical nature of the "flexible moving structure," so long as the so-called structure moves according to the laws assumed in the discussion. In other words, the "flexible moving structure" might be solid earth set into motion by the passage of elastic waves. In this case, the "fixed axes" are, in imagination, hung in space.

Some Types of Seismographs

All seismographs are divided into three parts: (1) inertia system, (2) coupling system, (3) recording system.

The inertia system is illustrated diagrammatically in Fig. 12 and is the core of the instrument. Discussion of the theory was directed toward studying the response of this inertia system to external vibrations. Several methods have been used to suspend the mass m. In some, its freedom is limited to a single horizontal direction; in others, to the vertical. Lever systems and combinations of springs have been employed to control the value of p and obtain desired values for ω/p. These modify the equations of motion only by the introduction of constants which depend upon the shape of the instrument and the position of m relative to the axis about which it moves.

The coupling system is introduced for the purpose of transforming relative motion of the mass m and its case into a form that can be recorded. This may or may not include magnifying the motion. The coupling is sometimes accomplished by an *electromechanical transducer*, a device actuated by power from a mechanical system and supplying power to an electrical system,

or the reverse. Sometimes the coupling is accomplished by a simple mechanical or mechanical-optical lever.

The recording system presents a graph of some function of the motion of m on a time scale.

Since the inertia systems that are best adapted to use in a seismograph possess only one degree of freedom, it is necessary to have three components to obtain a full record of any general displacement. Two of these respond to horizontal motion in directions perpendicular to each other, and the third to vertical motion.

Vibrations from Artificial Sources

Seismographs for the registration of vibrations other than those resulting from earthquakes fall into two general classes: (1) high-sensitivity units for seismic prospecting, and (2) low-sensitivity or strong-motion units for registration of vibrations from large blasts, traffic, and heavy industry.

The seismic method for mapping geologic structures involves detonation of small charges of dynamite, registration of the resulting vibrations at distances from a few tens to a few thousands of feet, and interpretation of the pattern of travel times to those distances. For this purpose, it has been customary to use only seismographs that record vertical motion. Earth frequencies of the order of 10 to 50 c/sec are most commonly involved, and instrumental frequencies are usually in that same range. High amplifications are achieved by electronic circuits, since one objective is to keep down operating costs by employing small quantities of dynamite. Values from 10,000 to several million have been made available, though the highest can be used only on extremely favorable occasions owing to the background level of ground unrest from the movement of trees, animals, traffic, distant trains, and other sources. Time marks every 0.01 sec are standard.

Vibrations from large blasts have frequencies ranging from about 50 c/sec down to 3 c/sec, with an extreme of 1 c/sec from

the atomic-bomb test in New Mexico, July 16, 1945. For these vibrations, a three-component seismograph with magnification of about 50 and natural period of 1 sec for each element is well adapted. Time marks every 0.01 sec again are standard.

Vibrations from Earthquakes

Waves in the earth from an earthquake cover such a wide range of periods and amplitudes that no single seismograph can record all of them with equal effectiveness. Two sets of instruments have been used in many places, one a short-period high-magnification combination, the other a long-period low-magnification. An exception to this occurs for instruments placed for the purpose of getting complete records at very short distances from large earthquakes. These so-called strong-motion seismographs necessarily have small magnifications, regardless of their periods. In Japan, for example, many have been in service with magnifications of less than unity, that is, one-half, one-tenth, or other fractional values.

Earth-wave periods range from about 0.3 sec at short distances to periods of 60 and even 120 sec for waves that travel around the globe. Very useful records of distant earthquakes have been obtained for years on seismographs that have a period of 12 sec and static magnification of 250 to 1000. The static magnification is the ratio of recorded displacement to static displacement of the mass m, that is, the magnification effective when the amplitude factor F (Fig. 10) is unity. Seismographs of longer period would be desirable for studies of certain of the surface waves, but instruments with such periods are difficult to maintain with sufficient stability for continuous operation. The short-period service is performed well by a seismograph with natural period of 1 to 3 sec and magnification of 10,000 to 100,000.

Some modern seismographs have transducers that respond in proportion to the velocity with which m moves, rather than to its displacement. These seismographs usually drive a galvanom-

eter to make the record and the over-all response of the system includes the characteristics of the galvanometer as an oscillating element. In general, the record produced by such a system must be integrated three times and differentiated once to obtain the original ground displacement.[7] Motion of the galvanometer may be recorded photographically or, as in some of the most recent developments, by a pen writing on a continuous strip of inexpensive paper. The time scale is provided by marks placed on the record at intervals of 1 min by a circuit including contacts on a well-rated clock.

Portable Strong-Motion Seismograph

The Leet seismograph is an example of a portable three-component seismograph designed primarily for the registration of vibrations from blasts, traffic, machinery, and general industrial sources. Each component has a natural frequency of 1 c/sec. Magnetic damping is 0.6 critical. For frequencies above 1 c/sec, displacements are multiplied 50 times on the record.

A cutaway perspective view of the interior of this seismograph is shown in Fig. 14. The inertia members are suspended by flat springs; the spring for the vertical element is supplemented by a stabilizing coil spring. The horizontal components are at right angles to each other. The inertia element for one of the horizontal components is shown in detail in Fig. 14. It consists of a cylindrical brass mass. Above and below it are plugs that close in on the cylinder and lock it for transportation when they are actuated by a knob on the top panel. Attached to the mass is a copper vane that swings between the extended poles of an Alnico magnet, for damping. Also attached to the mass is an arm which extends forward to support the concave mirror for that component so that it is in the same plane as the mirrors for the other elements.

[7] F. B. Galitzin, *Vorlesungen über Seismometrie* (German translation from Russian, Teubner, Berlin, 1914), pp. 452–469; English translation in L. D. Leet, *Practical seismology and seismic prospecting* (Appleton-Century-Crofts, New York, 1938), pp. 221–226.

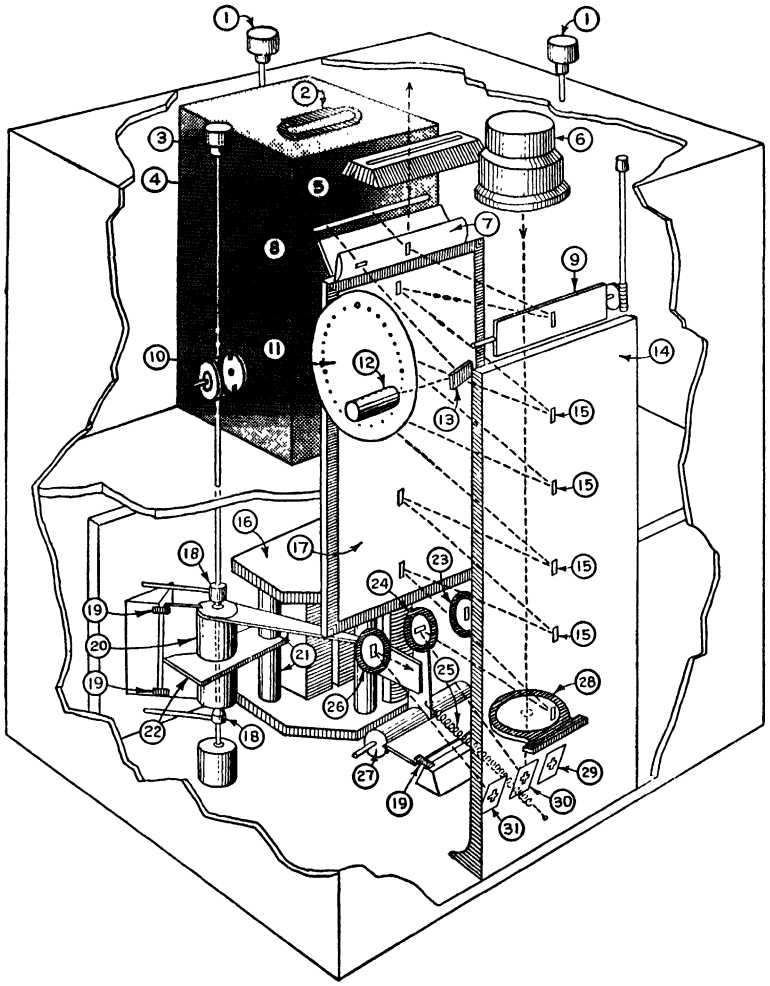

FIG. 14. Leet three-component portable seismograph. (1) Knobs controlling leveling feet; (2) camera handle; (3) knob for locking inertia member; (4) camera; (5) viewing slit; (6) light-source housing; (7) cylindrical lens; (8) half-silvered mirror; (9) adjustable mirror; (10) camera-drive clutch; (11) timing-line shutter; (12) timing-line light housing; (13) timing-line mirror; (14) and (17) plane mirrors; (15) point of reflection; (16) permanent magnet; (18) locking nut; (19) spring; (20) and (27) inertia members; (21) magnet poles; (22) damping vane; (23), (24) and (26) inertia member mirrors; (25) stabilizing spring; (28) condensing lens; (29), (30), and (31) fixed mirrors.

Light is supplied by a straight-filament galvanometer lamp in a housing on the top panel. It travels directly to a condensing lens just above three fixed mirrors. The concave mirror attached to the inertia element for each of the horizontal components receives from its fixed mirror a rectangular patch of converging light, with the long axis vertical. It returns the light to the face of the outer of two long parallel plane mirrors. From this the light goes to the inner long mirror, and so on by eleven reflections to a cylindrical lens which brings it to a focus on the surface of the photographic paper for registration. The eleventh reflection is from a small mirror that can be adjusted about a horizontal axis.

The history of the light beam for the vertical component is slightly different, owing to the fact that the moving mirror for that component moves at right angles to those for the horizontal components, and without some correction its light would move up and down on the large plane mirrors instead of from side to side, as it must to record properly at the camera. To provide the correction, two prisms are interposed in the light path for the vertical component. Neither prism is shown in Fig. 14.

In principle, this seismograph is a simple mechanical-optical lever with a beam of light substituted for a portion of the long arm of the lever in Fig. 1. If we denote by a the distance from the center of mass, for the element illustrated, to the hinge axis, and note that motion is now rotation through an angle θ instead of translation through a distance x_1, the equation for undamped motion of the mass becomes

$$ma^2 \frac{d^2\theta}{dt^2} + ka^2\theta = -ma \frac{d^2x}{dt^2}.$$

The angular frequency is given by the equation $p^2 = k/m$, as before.

With the cover in place for carrying, the seismograph occupies a space 12 x 14 x 20 in. and weighs 65 lb.

Velocity Transducers

Transducers that respond to the velocity of the inertia member have been widely used in seismographs for earthquake registration, as well as for portable service in prospecting. They are very efficient, can be made rugged, and do not respond to slow drifts of the inertia member from temperature changes, elastic fatigue, or tilt of horizontal members. For some aspects of earthquake research, they have the disadvantage of giving records that strongly favor certain frequencies and cannot be interpreted readily in terms of true ground motion.

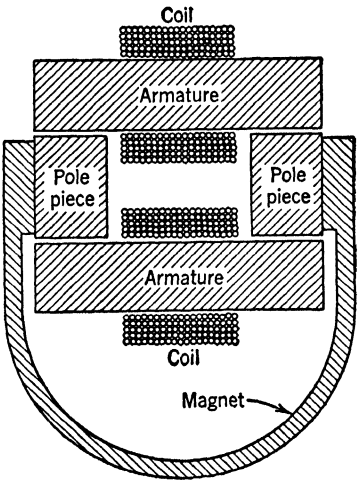

FIG. 15. Benioff transducer.

One standard form of this type of transducer is a coil moving in a magnetic field. Another is a variable reluctance system. An example of the latter is one of the Benioff transducers, shown diagrammatically in Fig. 15.[8]

In the type illustrated, used for earthquake registration, one of the coils is matched to a long-period galvanometer (14 to 60 sec) and the other to a short-period galvanometer (0.2 sec). The armatures are rigidly fastened together and to the inertia member or mass. The pole pieces are fastened to the base. Although the magnet is shown schematically as a U-magnet, it is actually constructed of two rectangular magnets, of dimensions $\frac{3}{8}$ x 2 x 7 in. No electronic amplification is employed.

Two versions of the variable-reluctance transducer used in seismic prospecting are shown in Fig. 16. In prospecting, the output from these transducers is connected through high-gain amplifiers to the recording galvanometers.

[8] L. D. Leet, *Practical seismology and seismic prospecting* (Appleton-Century-Crofts, New York, 1938), pp. 213–216.

A Displacement Transducer

For service in the registration of earthquakes as well as the registration of earth waves from artificial sources for certain

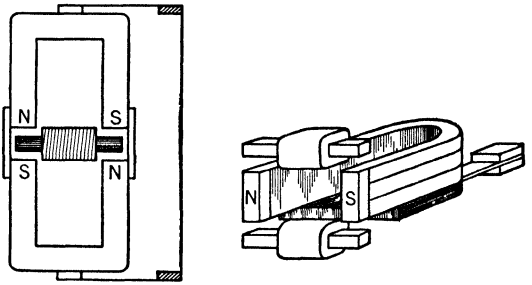

FIG. 16. Types of variable-reluctance transducer used in seismic prospecting.

research purposes, a new seismograph incorporating a displacement transducer has been developed at Harvard by Roland K. Blumberg.[9]

This seismograph has an adjustable natural frequency, and uniform response over a wide range of frequencies. The record is written in ink, at a point remote from the seismometer, or inertia member, with the three components side by side on a continuous strip of inexpensive paper. The inertia member for each component has a primary spring that keeps it in neutral position, and a lever system which is the equivalent of a secondary spring that partially opposes the primary spring and permits adjustment of the period. The period can be made infinite, theoretically. Attached to the mass are two plates. These, with two other plates that are fixed to the base by electric insulators, form two variable condensers which are the transducer of the seismograph. These two variable condensers are the capacitances in two electric tank circuits. The tanks determine the frequencies of two electronic oscillators. The two frequencies are mixed and the difference frequency is detected. Changes of this beat frequency

[9] R. K. Blumberg, *A new displacement seismograph* (Doctoral thesis, Harvard University, 1948).

are converted to changes in its amplitude by a frequency-discriminator circuit. This signal is rectified and becomes the signal for the pen amplifier. The frequency-response curve of the transducer is flat from zero to several thousand cycles per second, a frequency higher than any that would be of interest to a seismologist. The curves for the pen amplifier and the pen are flat from zero to about 20 c/sec.

An automatic compensator maintains the mass at true zero and eliminates trouble from drift in the vertical or slow tilts in the horizontal.

With the mass adjusted to a natural period of 1 sec, and with a gain of the order of 100,000, this instrument records earth waves from blasts and local earthquakes, as well as the preliminary waves from earthquakes, with very good written amplitudes. Under these same conditions, when the surface waves from earthquakes come in—with periods most commonly from 20 to 40 sec—displacements of the mass fall off greatly, in accordance with the laws of forced vibrations. The true earth amplitudes of these surface waves increase, however, in nearly inverse proportion to the loss of sensitivity in the seismograph, so good records are written of those waves as well. As a result, this seismograph with a displacement transducer covers the spectrum of waves from an earthquake in a manner which can be equaled only by two sets of the velocity transducers currently in use.

Seismic Prospecting Equipment

The procedure in commercial seismic prospecting involves generation of earth waves by detonation of a small charge of dynamite at an instant recorded by the equipment, and registration of the waves on a number of detectors distributed along the ground at different distances. The record carries a time scale that permits measurement of the time required for the waves to travel to the detectors.

In principle, the components of a complete prospecting outfit do not differ from those already described. The detectors, or

seismometers, are subject to the laws of forced vibration. Their output is amplified electronically until ground movements from earth waves of the order of 10^{-8} in. can be detected under favorable conditions. Seismometers may be of any of the types employed in other services. In certain types of prospecting, notably

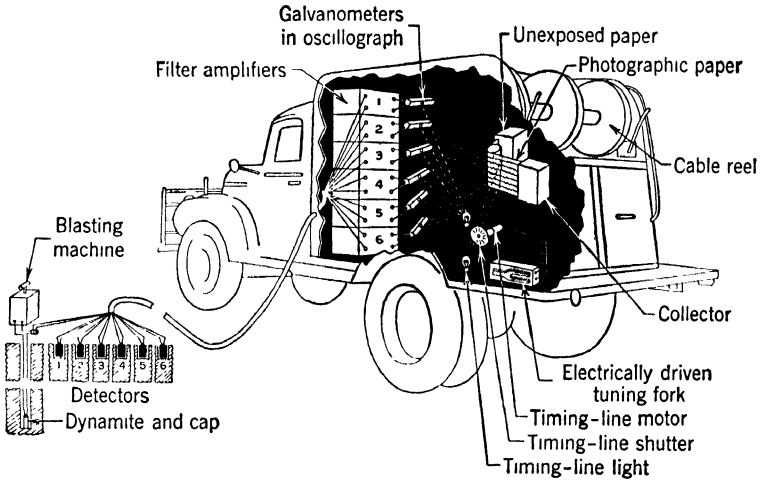

FIG. 17. Schematic diagram showing components of seismic prospecting equipment.

by the reflection method, special volume-control devices are employed to limit the amplitudes arising from large surface waves near a shot so that the galvanometers can bring through a record of small higher-frequency waves from depth. These are procedural details of which there are about as many variations as there are companies using the method.

A schematic layout is given in Fig. 17 to illustrate the relationships of components in prospecting equipment. The number of channels may run up to 24 or more. Sometimes two or more detectors may be connected in series to one recording channel in such a way that surface waves cancel each other while waves from below reinforce and give a larger signal.

CHAPTER II

Observed Types of Earth Waves

Waves in the earth supply the basic data of seismology. They are to it what electromagnetic waves are to radio, or sound waves to acoustics. Nevertheless, the literature of the subject is surprisingly lacking in quantitative observational evidence on just what types of waves earth materials in place will transmit. This lack is due in part to the youth of the science and in part to the difficulty of controlling conditions at the source in an experiment designed to generate and record earth waves. Earthquakes, of course, are out of the controlled class of source. Dynamite blasts are pretty good, although attempts have been made by some theoretical experts to discredit them on the assumption that they apply radially symmetric simple expansive forces around a point and are, therefore, too special in nature to generate all possible types of waves. This assumption is reasonable theory, but it does not accord with observation. The first atomic bomb supplied the best experimental source yet observed.

Elastic Constants [1]

The speed with which any wave travels through earth materials is controlled by the elastic properties of the material. These are defined in various ways. In general, the most widely used method

[1] A. E. H. Love, *A treatise on the mathematical theory of elasticity* (Cambridge University Press, Cambridge, ed. 4, 1927; Dover, New York, 1944); J. B. Macelwane, *Introduction to theoretical seismology, Part I, Geodynamics* (Wiley, New York, 1936), pp. 10–145; L. D. Leet, *Practical seismology and seismic prospecting* (Appleton-Century-Crofts, New York, 1938), pp. 81–107.

is to determine certain numbers called elastic moduli, each of which describes a material's response to a certain type of stress. The modulus itself is the ratio of stress to strain, or of the force applied in a certain way to the deformation that results.

One of the earliest of the elastic moduli to be studied was the modulus of stretch, known as *Young's modulus*, after Thomas Young, who is known also for his discovery of the interference of light. If a wire or rod of a material is stretched by a force acting parallel to its long axis, the length is changed. The modulus E (originally standing for elasticity) is then

$$E = \frac{\text{Stress}}{\text{Strain}} = \frac{\text{Force per unit area}}{\text{Change in length per unit length}}.$$

It is expressed in units of stress intensity, such as pounds per square inch.

Under this type of stress, a change in diameter accompanies the change in length, and the ratio of these changes per unit length has been given a special name, *Poisson's ratio;* it is designated by μ (mu) and defined by the equation

$$\mu = \frac{\text{Change in diameter per unit diameter}}{\text{Change in length per unit length}}.$$

It is a dimensionless number. For ordinary elastic materials, it lies between 0 and 0.5.

Two important properties of a material are its resistance to change of shape without change of volume and its resistance to change of volume without change of shape. The first of these is measured by the modulus of rigidity G, also known as the shear modulus;

$$G = \frac{\text{Stress}}{\text{Strain}} = \frac{\text{Force per unit area}}{\text{Shear}}.$$

It is to be noticed that the force is here *parallel* to the area on which it acts. Shear is defined as the relative displacement of parallel planes unit distance apart, or as the angle through which

a plane normal to the force is rotated. The second is measured by the *bulk modulus*, or *modulus of incompressibility*, B;

$$B = \frac{\text{Stress}}{\text{Strain}} = \frac{\text{Increase in hydrostatic pressure}}{\text{Change in volume per unit volume}}.$$

Each of these moduli is expressed in units of stress intensity, such as pounds per square inch.

The reciprocal of B is the *compressibility factor* k.[2]

The *density* of a material is not an elastic constant, but it is a property that affects the transmission of elastic waves in the material. It is the mass of a unit volume of a substance. In the inch-pound-second (ips) system of units, as previously mentioned, the mass is obtained by dividing the weight in pounds by 386 in./sec^2, the acceleration due to gravity. For example, 1 ft^3 of water weighs 62.5 lb and 1 in.^{3} weighs 0.036 lb, approximately. The mass of 1 in.^{3} of water in ips units is therefore $0.036/386 = 9.3 \times 10^{-5}$ lb sec^2/in. and the density of water is 9.3×10^{-5} lb sec^2 in.$^{-1}$/in.^{3} The symbol ρ (rho) is used for density.

The specific gravity of a material, or the ratio of its density to the density of water, is relatively easy to measure and is usually listed in tables of constants for various substances. When it is available, the density is obtained by multiplying the specific gravity by the density of water.

Wave Motion

Rocks and many accumulations of unconsolidated sand, gravel, and clay are elastic, and resist an applied stress by a force that is approximately proportional to displacement. Accordingly, they oscillate with simple harmonic motion. When one portion of

[2] In this monograph we use in general the American Standard letter symbols for physics, listed in the American Standards Publication ASA Z 10.6—1948 (American Society of Mechanical Engineers, New York, 1948); see also *Am. J. Physics* **16**, 164 (1948). Some of these standard symbols differ from those that have formerly been used in the literature of seismology. In particular, the elastic moduli that we here designate μ, G, B, and k will be found in the literature with the symbols σ, μ, K, and β, respectively.

such a medium is displaced, adjacent particles are displaced and as time passes more and more particles are included in the displaced portion. The result is the advance of an elastic wave through the medium.

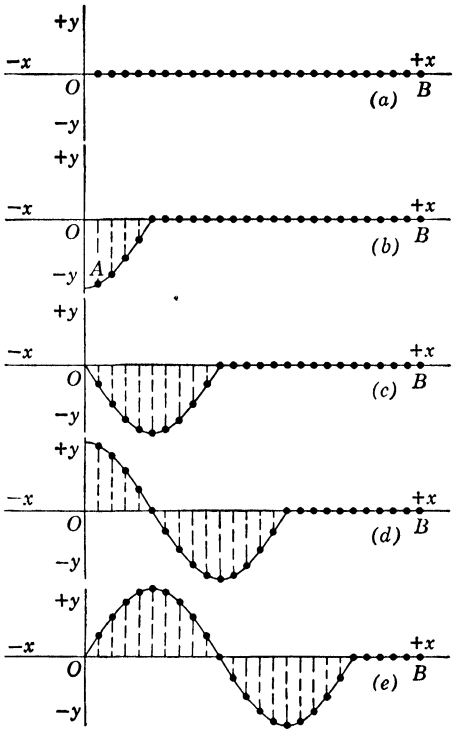

FIG. 18. Wave motion.

To examine this wave motion, in the simplest case of two dimensions, consider an indefinite number of particles elastically bound together along the line *OB* in Fig. 18(*a*). If the particle at *O* is displaced, particles adjacent to it will be disturbed progressively, until by the time the displacement of the particle on the Y-axis is *A* they will be arranged as in Fig. 18(*b*). If the particle on the Y-axis is allowed to move with simple harmonic motion

back through O to an equal displacement A on the opposite side, and then to return to O, successive arrangements of the adjacent particles will be as shown in Fig. 18(c, d, e).

As the process continues, each particle oscillates up and down across the X-axis with simple harmonic motion. Its position at a given time is determined by its distance from O. The motion of the particle at O is defined by the equation

$$y = A \sin pt,$$

A being the amplitude, but other particles along the X-axis are delayed in reaching corresponding positions by an amount depending on their distance from O. We can express this by saying that a particle is out of phase with the one on the Y-axis by, say, κ radians per unit distance along the X-axis. The total phase difference due to position along the X-axis will then be κx rad, and the motion of any particle can be expressed by the equation

$$y = A \sin (pt - \kappa x). \tag{15}$$

By holding x constant and solving Eq. (15) for different values of t, we obtain the motion of the particle at that special value of x. It is simple harmonic motion with amplitude A and angular frequency p rad/sec. Its period is then

$$\frac{2\pi \text{ (rad)}}{p \text{ (rad/sec)}} = T \text{ (sec)}.$$

By holding t constant and solving Eq. (15) for different values of x, we obtain the wave shape as shown, say, in Fig. 18(e). Here particles which are separated by distances that are multiples of $2\pi/\kappa$ have a common displacement at all times. Hence each section of the wave of length $2\pi/\kappa$ is identical in form. Accordingly, this distance is called the *wavelength*. It is usually designated by λ (lambda), so

$$\frac{2\pi \text{ (rad)}}{\kappa \text{ (rad/in.)}} = \lambda \text{ (in.)}.$$

If in Eq. (15) we hold the value of $(pt - \kappa x)$ constant, thereby defining a fixed amplitude on the wave, and then allow t to increase, it is evident that x will have to increase also. This means that as t increases our arbitrarily selected reference amplitude moves along the X-axis in the positive direction.

The dimensions of the constants in Eq. (15) have been indicated; p is expressed in radians per second and κ in radians per unit length. That being the case, p/κ is a velocity, since (rad/sec)/(rad/in.) = in./sec.

Accordingly, Eq. (15) describes a wave form with period $T = 2\pi/p$ and wavelength $\lambda = 2\pi/\kappa$, advancing in the positive x-direction with a velocity p/κ. It is, of course, obvious that as the wave form advances each particle in its path oscillates about its starting position but does not itself advance with the wave.

In Fig. 18 and Eq. (15), the particles oscillated along paths at right angles to the direction in which the wave form advanced. Such a wave is called *transverse*. Another type of motion would result if each particle moved back and forth along the X-axis. If we denote the displacement of a particle in that direction by c, then a progressive wave of this type is given by the equation

$$c = A \sin (pt - \kappa x). \tag{16}$$

By holding t constant and plotting c against x we obtain from Eq. (16) a series of condensations and rarefactions. Continuous increase of t gives an advance of this wave form. The relationships of p and κ to wavelength, period, and velocity are the same as for Eq. (15). A wave of this type is called *longitudinal*.

Recalling that $p = 2\pi/T$ and $\kappa = 2\pi/\lambda$ we can also write Eqs. (15) and (16) in the forms

$$\begin{aligned} y &= A \sin 2\pi \left(\frac{t}{T} - \frac{x}{\lambda}\right), \\ c &= A \sin 2\pi \left(\frac{t}{T} - \frac{x}{\lambda}\right) \end{aligned} \tag{17}$$

for waves moving in the positive x-direction, or

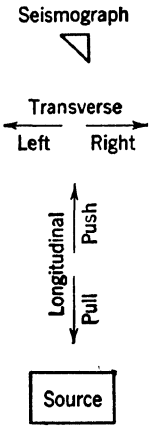

FIG. 19. Directional terminology.

$$y = A \sin 2\pi\left(\frac{t}{T} + \frac{x}{\lambda}\right), \qquad c = A \sin 2\pi\left(\frac{t}{T} + \frac{x}{\lambda}\right) \tag{18}$$

for waves moving in the opposite direction.

If two transverse waves, with amplitudes A and B, moving in opposite directions are superposed, the displacements are given by

$$y = A \sin 2\pi\left(\frac{t}{T} - \frac{x}{\lambda}\right) + B \sin 2\pi\left(\frac{t}{T} + \frac{x}{\lambda}\right), \tag{19}$$

and similarly for c. Such superposition results, for example, when a wave is reflected at a boundary.

Figure 19 illustrates the directional terminology with which earth motion during the passage of waves will be discussed.

Body Waves

Two of the basic waves of the science of seismology are well known from both theory [3] and observation. They are body waves, that is, they travel through the interior of an elastic medium, as distinct from types bound to a free surface.

1. Longitudinal (Compressional), P-Waves

One of the body waves advances by alternating compressions and rarefactions, as in Eq. (16). It is the type that carries sound, and has been variously known as *compressional*, *irrotational*, or *longitudinal*. The last name is applied because of the sense of motion of a particle along the direction of the wave's advance. In seismology, the symbol P is used for this wave type because

[3] S. D. Poisson, "Note sur les vibrations des corps sonores," *Ann. Chim.* **36**, 86–93 (1827); G. G. Stokes, "Propagation of an arbitrary disturbance in an elastic medium," *Mathematical and physical papers* (Cambridge University Press, Cambridge, 1880), vol. 2, pp. 257–280.

it arrives first from an earthquake, and in the early days these first waves were christened *Undae Primae*, or first waves, before their nature was understood. The velocity v_P of P-waves may be expressed by the equation

$$v_P \text{ (ft/sec)} = \frac{1}{12}\sqrt{\frac{R\left(\frac{\text{lb}}{\text{in.}^2}\right) + \frac{4}{3}G\left(\frac{\text{lb}}{\text{in.}^2}\right)}{\rho\left(\frac{\text{lb sec}^2\ \text{in.}^{-1}}{\text{in.}^3}\right)}}$$

$$= \frac{1}{12}\sqrt{\frac{E\left(\frac{\text{lb}}{\text{in.}^2}\right)}{\rho\left(\frac{\text{lb sec}^2\ \text{in.}^{-1}}{\text{in.}^3}\right)}\frac{1-\mu}{(1+\mu)(1-2\mu)}}. \qquad (20)$$

2. Transverse (Shear), S-Waves

The second type of body wave advances by shearing displacements, of which Eq. (15) gives one example, and has been known as the *shear*, *equivoluminal*, or *transverse wave*. Such waves, as the second prominent group from an earthquake, were christened *Undae Secundae*, or second waves, and given the symbol S by seismologists. An expression for the velocity of S-waves is given by

$$v_S \text{ (ft/sec)} = \frac{1}{12}\sqrt{\frac{G\left(\frac{\text{lb}}{\text{in.}^2}\right)}{\rho\left(\frac{\text{lb sec}^2\ \text{in.}^{-1}}{\text{in.}^3}\right)}}$$

$$= \frac{1}{12}\sqrt{\frac{E\left(\frac{\text{lb}}{\text{in.}^2}\right)}{\rho\left(\frac{\text{lb sec}^2\ \text{in.}^{-1}}{\text{in.}^3}\right)}\frac{1}{2(1+\mu)}}. \qquad (21)$$

If the density of a material is known or can be estimated within useful limits, as is frequently the case, determination of

the velocities of P- and S-waves leads to values of all the elastic constants through the following connecting equations,

$$G = \frac{E}{2(1+\mu)}, \qquad B = \frac{E}{3(1-2\mu)},$$

$$\mu = \frac{\frac{1}{2}\left(\frac{v_P}{v_S}\right)^2 - 1}{\left(\frac{v_P}{v_S}\right)^2 - 1}, \qquad \left(\frac{v_P}{v_S}\right)^2 = \frac{\mu - 1}{\mu - \frac{1}{2}}. \qquad 0 < \mu < \tfrac{1}{2} \qquad (22)$$

A particle in the path of a transverse wave may oscillate in any direction in the plane normal to the direction of advance of the wave. For a transverse wave traveling parallel to the earth's surface, if particles in its path oscillate up and down, the wave is given the special symbol SV; if the particles oscillate in a horizontal plane, it is called SH. The motion is defined by Eq. (15).

From Eq. (21) it will be seen that transverse waves cannot exist in a medium that has zero rigidity. For practical purposes, this includes most fluids.

Surface Waves

As opposed to the body waves, which travel through the interior of an elastic medium, there are certain types that can exist only on the surface of such a medium.

3. Rayleigh, R-Waves

Included among early volumes on the theory of elasticity and elastic waves was a treatise published in 1885 by Lord Rayleigh [4] discussing the type of wave motion that would be propagated along the plane surface of a homogeneous elastic solid. This has since been called the Rayleigh wave, and given the symbol R.

Detailed quantitative observational data confirming the exist-

[4] John William Strutt, Baron Rayleigh, "On waves propagated along the plane surface of an elastic solid," *Proc. London Math. Soc.* **17**, 4–11 (1885); *Scientific papers* (Cambridge University Press, Cambridge, 1900), vol. 2, p. 447.

ence on earthquake records of the waves predicted by Rayleigh were first published in 1931 [5] and have been augmented since that time by controlled experiments.[6,7]

Lord Rayleigh described the motion of a surface particle in the path of these waves on material for which $\mu = 0.25$ by the simultaneous equations

$$\begin{aligned} c &= 0.4227 \sin (pt + \kappa x), \\ z &= -0.6204 \cos (pt + \kappa x), \end{aligned} \tag{23}$$

where c is particle displacement along the X-axis as in Eq. (16), and z is displacement in the vertical direction.

As discussed in connection with Eq. (15), the motion of an earth particle as defined by these equations is determined by allowing t to increase while x remains constant. Taking the positive direction of the X-axis toward the right and of the Z-axis downward (as Rayleigh did), and assigning successive values to t, we find that as the quantity $(pt + \kappa x)$ increases by steps of $\pi/2$ rad the displacements in the x- and z-directions reach maxima in the directions and sequence shown in Table 2.

TABLE 2. Sequence of c and z for Rayleigh waves.

$pt + \kappa x$			
(rad)	(deg)		
0	0	0	− (up)
$\frac{1}{2}\pi$	90	+ (pull)	0
π	180	0	+ (down)
$\frac{3}{2}\pi$	270	− (push)	0
2π	360	0	− (up)

[5] L. D. Leet, "Empirical investigation of surface waves generated by distant earthquakes," *Publications of the Dominion Observatory* (Ottawa, 1931), vol. 7, *Seismology*, No. 6.

[6] L. D. Leet, "Ground vibrations near dynamite blasts," *Bull. Seis. Soc. Am.* **29**, 487–496 (1939).

[7] L. D. Leet, "Earth motion from the atomic bomb test," *Am. Scientist* **34**, 198–211 (1946).

As before, the direction of propagation of the disturbance is given by holding the argument $(pt + \kappa x)$ constant while t and x vary; hence x decreases as t increases, and the direction of propagation is from right to left. The particle traces out an elliptic path in a clockwise sense while the wave moves from right to left. The motion of the particle at its maximum "up"

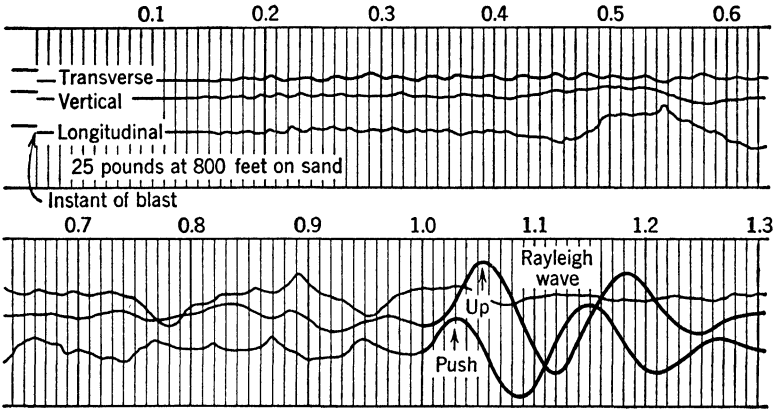

FIG. 20. Record of a Rayleigh wave.

position is thus opposite to the direction of propagation of the wave form, and for that reason its sense of rotation has been designated as retrograde.

The direction and sequence of the maxima and minima, using the terminology of Fig. 19, are *push—up—pull—down*. For a medium in which $\mu = 0.25$, the velocity of Rayleigh waves is approximately $0.9\ v_S$.

In Fig. 20, distance and velocity relations have permitted a true Rayleigh wave to stand out clearly, beginning at about 1 sec on an experimental record for which the horizontal components were aligned in the longitudinal and transverse directions (Fig. 19). It happens here that horizontal transverse motion is practically absent or so irregular that it is obviously unrelated to the longitudinal or vertical.

4. Love, Q-Waves

Another type of surface wave is that in which the particles of the medium vibrate transverse to the direction of the wave's travel, with *no vertical component.* They are called *Q*-waves, the symbol being derived from the German *Querwellen.* The English mathematician Love [8] has shown that such waves can be propagated in a medium that is bounded above by an ideal reflecting surface, such as a rock-air discontinuity, and below by a medium in which the velocity of body shear waves is greater than in the first medium. Their mode of propagation is analogous to the optical case of a wave of light moving nearly parallel to the faces of a plate, with matter of a different refractive index in optical contact with the lower face and an ideal reflecting surface over the upper face. If the velocity of light in the plate is less than that in the underlying medium, light incident on the boundary at an angle exceeding the critical angle will be totally reflected, and will continue to be propagated in the plate. If, however, the velocity of light is greater in the plate, light can pass freely from it to the underlying matter, whatever its angle of incidence may be. Thus, the light will gradually be lost into the underlying medium as it advances and the propagation of a train of waves of constant form would be impossible. The waves described theoretically by Love are equivalent to *SH*-waves reflected up and down within the upper layer of the earth's crust, with associated movement in the lower layer of the type that always arises in total reflection.

A German investigator, E. Meissner,[9] has shown that such transverse surface waves can also exist in a medium without marked discontinuities, but in which the velocity of body transverse waves increases with depth.

[8] A. E. H. Love, *Some problems of geodynamics* (Cambridge University Press, 1911), pp. 144–178.

[9] E. Meissner, "Elastische Oberflächenquerwellen," *Verhandlungen international Kongress für technische Mechanik, Zurich, No. 2* (1927), pp. 3–11; reported in *Z. Geophysik* **3,** XL (1928) and in *Gerlands Beitr. Geophysik* **18,** 360 (1927).

A characteristic of Q-waves observed in controlled experiments is that a group consists of three or four complete waves, the first having the greatest amplitude and the rest progressively decreasing in amplitude.

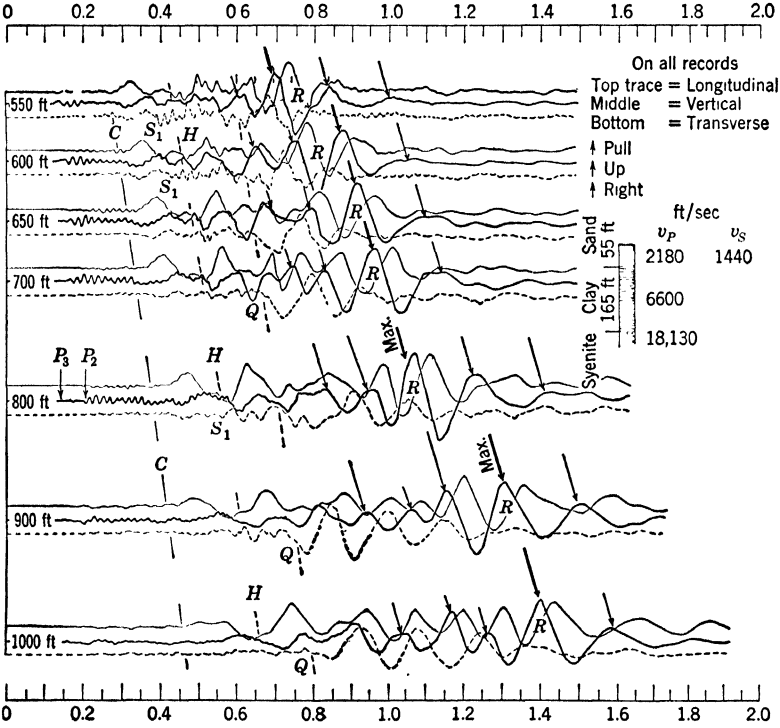

FIG. 21. Experimental profile illustrating wave types; discovery records for coupled waves.

Equation (15) describes the motion of a particle in the path of a Q-wave, with appropriate orientation of the axes in the plane of the earth's surface, and x along the line of the wave's advance.

Figure 21 shows records of Q-waves, best represented at 900 ft and 1000 ft.

5. Hydrodynamic, H-Waves

A new type of wave was first recognized on a record of earth motion at the test of the first atomic bomb in New Mexico on Monday, July 16, 1945.[7] To date, it has been identified only on records obtained from controlled experiments on unconsolidated surface materials.

Motion of a particle in the path of these waves can be described by the simultaneous equations

$$\begin{aligned} c &= A \sin (pt + \kappa x), \\ z &= B \cos (pt + \kappa x), \end{aligned} \tag{24}$$

which will be recognized as the same as Eqs. (23) except for a change in the sign of the right-hand member of the second equation. As before, x is positive to the right and z is positive downward. If we hold x constant while increasing t, as the quantity $(pt + \kappa x)$ increases by steps of $\pi/2$ rad the displacements in the x- and z-directions reach maxima in the directions and sequence shown in Table 3.

TABLE 3. Sequence of c and z for hydrodynamic waves.

$pt + \kappa x$ (rad)	$pt + \kappa x$ (deg)	c	z
0	0	0	+ (down)
$\frac{1}{2}\pi$	90	+ (pull)	0
π	180	0	− (up)
$\frac{3}{2}\pi$	270	− (push)	0
2π	360	0	+ (down)

The direction of propagation is from right to left, as for the Rayleigh waves in Eqs. (23), but the particle in Eqs. (24) traces out a path in a counterclockwise sense and is moving forward at its maximum "up" position, just the opposite of the Rayleigh wave.

In the terminology of Fig. 19, the direction and sequence of the maxima and minima are *push—down—pull—up*.

In the three cases where these waves have been identified to date, the horizontal motion is nearly twice the vertical, that is, $A \approx 2B$.

The discovery record for these waves is shown in Fig. 22, with a key in Fig. 23, showing the other wave types identified on this record.

These so-called hydrodynamic or H-waves are present but poorly developed and confused with other types at the distances represented on Fig. 21.

6. Coupled, C-Waves

Coupled waves were first described in 1939 [6] from the records of Fig. 21, and were later observed on the atomic-bomb record of Fig. 22. As with H-waves, to date they have been positively identified only on records obtained from controlled experiments on unconsolidated surface materials, though motion of approximately this type has been found on records of quarry blasts and on earthquake records such as Fig. 24, where superposed motion from other waves confuses the picture.

Motion of a particle in the path of these waves can be described by the simultaneous equations

$$\begin{aligned} c &= A \sin (pt + \kappa x), \\ y &= \pm B \sin (pt + \kappa x), \\ z &= C \sin (pt + \kappa x), \end{aligned} \tag{25}$$

where x is on the surface in a direction along the line of the waves' advance, y is on the surface at right angles to x, and z is positive downward, while c is particle displacement along the x-direction.

As in Eqs. (23) and (24), the waves advance along the negative direction of x. Now, if we hold x constant and increase t, as the quantity $(pt + \kappa x)$ increases by steps of $\pi/2$ rad, the dis-

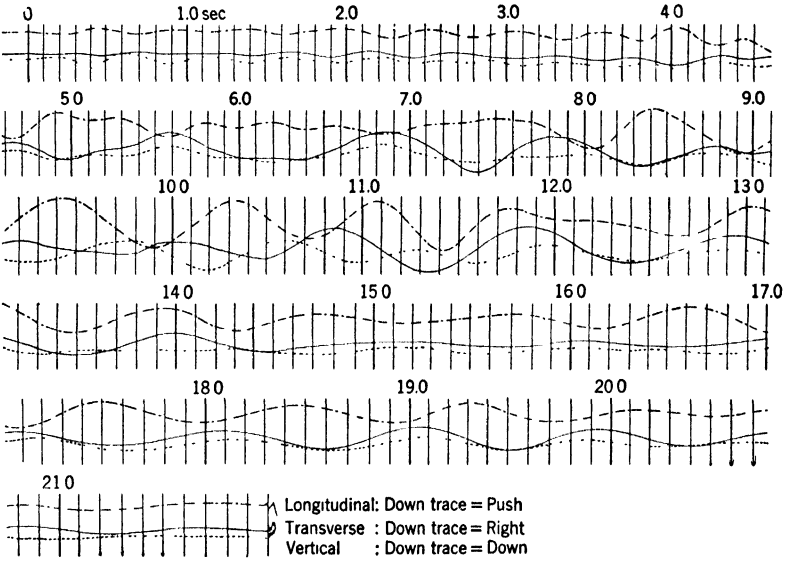

FIG. 22. Record of earth motion from atomic-bomb test; discovery record for hydrodynamic waves. Recorded on Leet seismograph, 5:30 A.M. MWT, Monday, July 16, 1945.

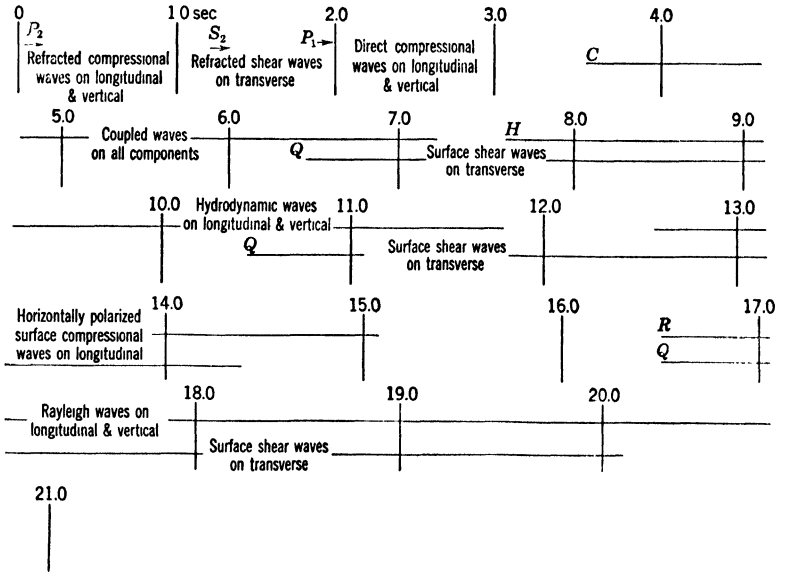

FIG. 23. Key to wave types on Fig. 22.

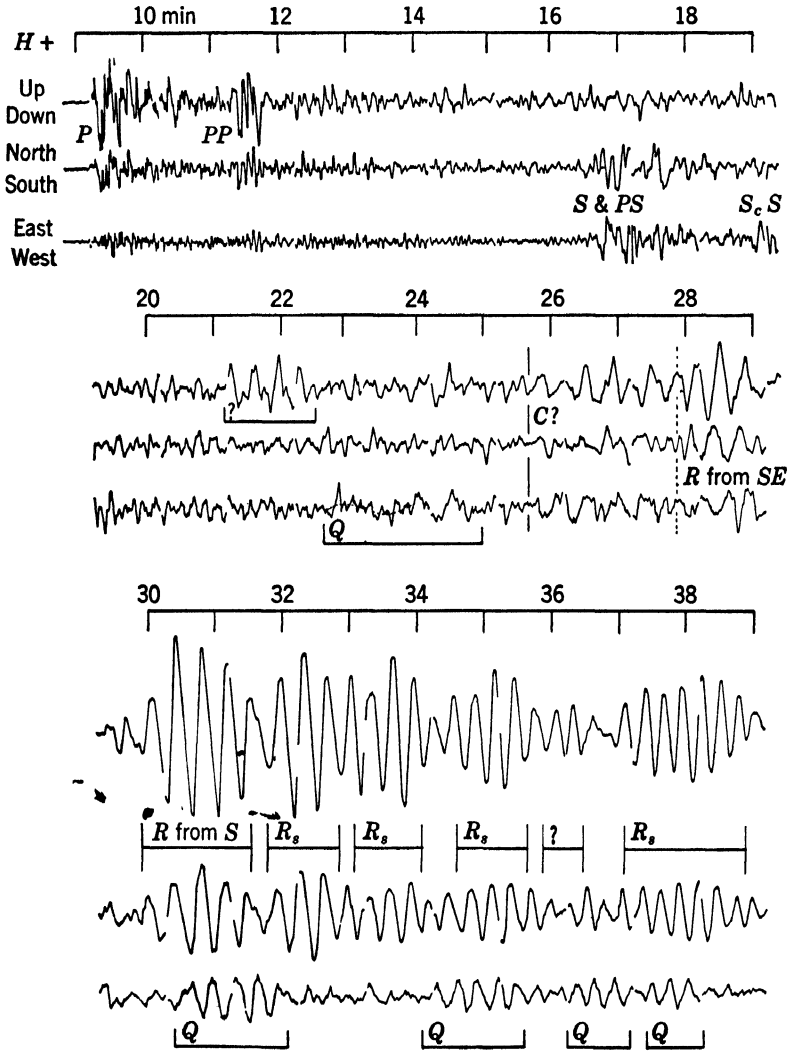

FIG. 24. Wave types on an earthquake record. Recorded on Harvard Benioffs, November 1, 1947; distance, 53.1° (5900 km, 3665 mi); azimuth, 185°.

placements in the x-, y-, and z-directions reach maxima simultaneously in the directions and sequence shown in Table 4.

TABLE 4. Sequence of c, y, and z for coupled waves.

$pt + \kappa x$ (rad)	$pt + \kappa x$ (deg)	c	y	z
0	0	0	0	0
$\frac{1}{2}\pi$	90	+ (pull)	+ (left)	+ (down)
			− (right)	
π	180	0	0	0
$\frac{3}{2}\pi$	270	− (push)	− (right)	− (up)
			+ (left)	
2π	360	0	0	0

In the terminology of Fig. 19, the directions and sequence of the maxima and minima are *push, left, up—pull, right, down* or *push, right, up—pull, left, down.*

Only two examples of these waves have been described to date. They are shown in Figs. 21 and 22. In both, the longitudinal amplitude A was greatest and the vertical amplitude C was smallest. The transverse amplitude B was nearly equal to A in Fig. 22, and about half of A in Fig. 21.

According to the best data available, over a uniform terrain the velocity of C-waves is greatest of the four surface types, with the others following in the order H, Q, R.

Mathematical discussions of H- and C-waves have not yet been developed as they have been for R- and Q-waves.

The appearance of P-, S-, Q-, and R-waves on an earthquake record is illustrated in Fig. 24. These waves were from the earthquake of Nov. 1, 1947, located at 11° South Latitude, 75° West Longitude, in Peru, and recorded at the Harvard Seismograph Station, nearly due north at a distance of 5900 km (3665 mi). Elapsed time from the instant of the quake, approximately $14^h\ 59^m$ GCT, is shown. The first P-waves, beginning at $9^m\ 10^s$,

show a period of about 15 sec, which is abnormally long for these waves, with waves of about 1-sec period superposed. The *S*-waves beginning at $16^m\ 40^s$ have the travel time of shear waves but do not show motion conforming to Eq. (15). This may be due in part to the fact that at this distance two sets of shear waves arrived at nearly the same time. One followed a direct course from the earthquake source to the recording station. The other, called *PS*, was generated by *P*-waves upon reflection at a point on the surface between source and station.

A poorly developed *Q*-wave begins at about $22^m\ 50^s$, and is confused by a shorter-period motion of unknown type.

Motion on all three components from $25^m\ 40^s$ to about $27^m\ 40^s$ may be *C*-waves underlying irregular motion of indeterminate type.

Pure *R*-waves begin on the N–S and vertical components at $29^m\ 53^s$. They show a sequence of maxima in the order *north-up-south-down*. Five separate groups appear in the figure. There are others in the continuation of the record, which is not shown.

During the interval in which *R*-waves were being recorded, motion on the E–W component followed an independent pattern and represents *Q*-waves.

The multiplicity of groups of these surface waves has not been fully explained. Beginning at about $27^m\ 50^s$, there appear to be *R*-waves reaching the station from SSE instead of South. These may have followed a curved course including part of the Atlantic basin, where the velocity is greater than over a continental path. The series of groups arriving from the south at different times, however, cannot be explained readily in an analogous manner.

A type of motion which has been observed from other quakes, but was not included in the list of wave types, begins at 21^m on the vertical component only. It has no counterpart on either horizontal component. Such a wave has also been observed occasionally on experimental records.

In sharp contrast to the pattern of Fig. 24 are the surface waves in Fig. 25 from the earthquake of Oct. 7, 1947 in central

Alaska, 64.5° North Latitude, 146° West Longitude, at $01^h\ 53.4^m$ G.C.T. This was 5100 km (3165 mi) from the Harvard station in an azimuth of 327°, or N 57° W of the station. In this record, *Q*-waves begin $24^m\ 20^s$ after the time of the quake, with

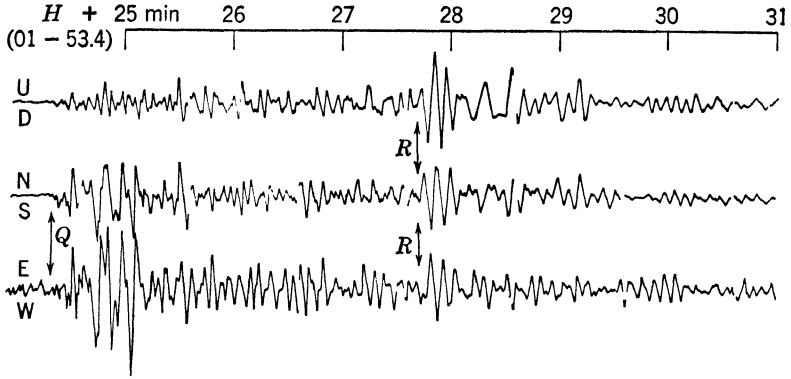

FIG. 25. Wave types on an earthquake record. Recorded on Harvard Benioffs, October 7, 1947; distance, 46° (5100 km, 3165 mi); azimuth, 327°.

maximum amplitude of the E–W nearly double that of the N–S component.

A single simple group of *R*-waves begins at $27^m\ 40^s$, with the horizontal amplitudes nearly equal. These show a velocity of 3.07 km/sec and a period of 7 sec. In contrast to this, the first direct *R*-waves in Fig. 24 show a velocity of 3.29 km/sec and a period of 23 sec.

Figures 24 and 25 are shown not so much to illustrate what is known about types of waves generated by earthquakes as to suggest the range of unsolved problems which they present.

CHAPTER III

Transmission of Earth Waves

The propagation paths of waves in materials of the earth are determined by laws of geometric optics. One method is to employ *Huygens' principle*, developed by Christian Huygens in connection with studies of light, and described in his *Traité de la lumière* in 1690. The front of a wave at time $t = 0$ is pictured as the locus of centers of an indefinitely large number of spherical wavelets, each starting from one of the centers as a new source. At time t, then, each wavelet will have a radius vt, where v is the velocity of advance, and the envelope of these wavelets will form a new surface which is the position of the original wave front at the later time.

The concept of a wave front has as a corollary that of the *ray*, which is at all times perpendicular to the wave front and is the trace of positions occupied by a given point on the wave front throughout its course. The geometry of ray paths is governed by *Fermat's principle*, named for Pierre Fermat, whose collected works were published in 1679. As with the work of Huygens, the original developments were made in connection with the propagation of light. Fermat's principle demonstrates by the calculus of variations [1] that the ray representing the path of a wave in going from one point to another will follow a course that permits the wave to make the trip in minimum time. Such a ray is called the *brachistochronic*, or shortest-time, path.

[1] G. A. Bliss, *Calculus of variations* (Open Court, Chicago, 1927).

If a material in which P- and S-waves travel with certain velocities, say v_1 and v_1', adjoins another material in which they travel with velocities v_2 and v_2', a wave of either type, say P, encountering the boundary between the materials will in general produce displacements at that boundary which result in

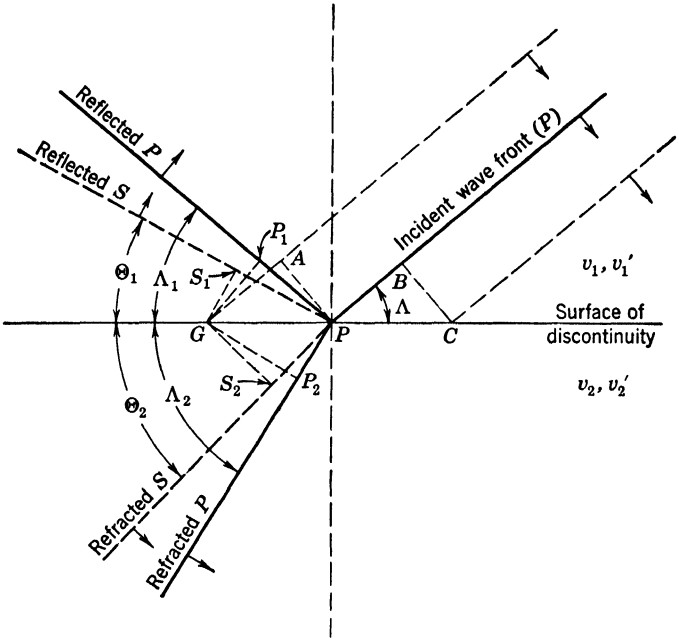

FIG. 26. Huygens construction at a velocity discontinuity.

the setting up of (i) a reflected P-wave, (ii) a refracted P-wave advancing into the new material, (iii) a reflected S-wave, and (iv) a refracted S-wave advancing into the new material. The distribution of the initial energy among the derived waves is determined by the angle at which the wave approaches the dividing surface or *discontinuity*, and the contrast in elastic properties of the two materials.

The angles at which the energy leaves such a surface in the form of P- and S-waves can be determined by Huygens' principle with the aid of Fig. 26. The advancing wave front PB was

in position GA 1 sec before the instant under consideration and will be at position C 1 sec later. During the advance of the incident wave from A to P, there traveled out from generating point G, on the interface, four waves: (i) PP_1, the reflected longitudinal or P-wave; (ii) PS_1, the reflected transverse or S-wave; (iii) PP_2, the refracted P-wave; and (iv) PS_2, the refracted S-wave. Since each traveled the distances indicated in unit time, we have *numerically* $GP_1 = v_1$, $GS_1 = v_1'$, $GP_2 = v_2$, and $GS_2 = v_2'$. Subscript 1 designates waves in medium 1, and 2 those in medium 2. Angles are represented by Λ (lambda, for Longitudinal) and Θ (theta, for Transverse). Now, by construction, $GP = PC$ and $AP = BC = GP_1$. Then

$$GP_1 = v_1 = GP \sin \Lambda_1 = BC = PC \sin \Lambda;$$

hence

$$\Lambda = \Lambda_1.$$

Similarly,

$$GS_1 = v_1' = GP \sin \Theta_1,$$

$$GP_2 = v_2 = GP \sin \Lambda_2,$$

$$GS_2 = v' = GP \sin \Theta_2.$$

Hence

$$\frac{v_1}{\sin \Lambda} = \frac{v_1}{\sin \Lambda_1} = \frac{v_1'}{\sin \Theta_1} = \frac{v_2}{\sin \Lambda_2} = \frac{v_2'}{\sin \Theta_2}. \tag{26}$$

Here Λ is the angle of P-wave incidence, Λ_1 the angle of P-wave reflection, Λ_2 the angle of P-wave refraction, Θ_1 the angle of S-wave reflection, and Θ_2 the angle of S-wave refraction. If an incident S-wave were considered, the ratio $v_1'/\sin \Theta$ would be included in Eqs. (26).

It is more common practice to use rays in designating the relationships in reflection and refraction, as in Fig. 27.

Equations (26) state relations for special cases of Fermat's principle and are sometimes referred to as expressions of the *law of reflection* and the *law of refraction*. The law of reflection is that the angle of reflection for a given wave is equal to the

angle of incidence. The law of refraction is that the sine of the angle of incidence is to the sine of the angle of refraction as the velocity in the first medium is to the velocity in the second, that is,

$$\frac{v_1}{v_2} = \frac{\sin \Lambda}{\sin \Lambda_2} = \frac{\sin i}{\sin r},$$

where i and r stand for the angles of incidence and refraction, respectively.

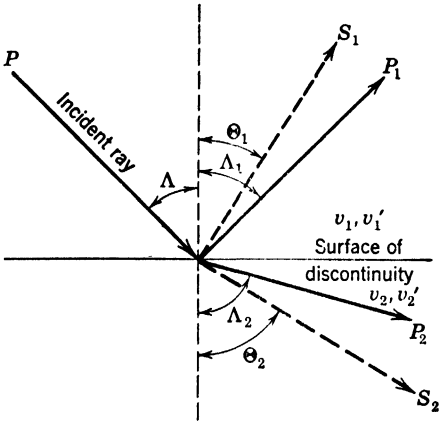

FIG. 27. Ray paths at a velocity discontinuity.

Equations for the computation of energy distribution among the derived waves at a surface of velocity discontinuity were developed by C. G. Knott.[2] As a preface to their presentation, the symbols involved are summarized in Table 5.

For a longitudinal wave, in a medium having bulk modulus B_1, rigidity G_1, and density ρ_1, and with longitudinal velocity v_1 and transverse velocity v_1', incident upon a second medium for which these constants are designated by the subscript 2,

$$\begin{aligned}(\rho_1 v_1^2)(\epsilon^2 + 1) &= \rho_1\omega^2 = G_1(\gamma_1^2 + 1),\\ (\rho_2 v_2^2)(\epsilon_2^2 + 1) &= \rho_2\omega^2 = G_2(\gamma_2^2 + 1).\end{aligned} \tag{27}$$

[2] C. G. Knott, "Reflexion and refraction of elastic waves with seismological applications," *Phil. Mag.* [5] **48**, 64–97 (1899); *Physics of earthquake phenomena* (Clarendon Press, Oxford, 1908).

TABLE 5. Summary of symbols used in formulas for computing energy partition in reflection and refraction of earth waves.

Wave	Type	Velocity	Amplitude Factor	Angle of Ray with Normal	
				Angle	Cotangent
Incident	Longitudinal	v	P	Λ	ϵ
	Transverse	v'	S	Θ	γ
Reflected	Longitudinal	v_1	P_1	Λ_1	ϵ_1
	Transverse	v_1'	S_1	Θ_1	γ_1
Refracted	Longitudinal	v_2	P_2	Λ_2	ϵ_2
	Transverse	v_2'	S_2	Θ_2	γ_2

Solution of these equations under the boundary conditions gives

$$\begin{aligned} S_1 + \epsilon(P - P_1) &= S_2 + \epsilon_2 P_2, \\ \gamma_1 S_1 + (P + P_1) &= -\gamma_2 S_2 + P_2, \\ -2\gamma_1 S_1 + (\gamma_1^2 - 1)(P + P_1) &= 2\left(\frac{G_2}{G_1}\right)\gamma_2 S_2 + \left(\frac{G_2}{G_1}\right)(\gamma_2^2 - 1)P_2, \\ (\gamma_1^2 - 1)S_1 - 2\epsilon(P - P_1) &= \left(\frac{G_2}{G_1}\right)(\gamma_2^2 - 1)S_2 - 2\left(\frac{G_2}{G_1}\right)\epsilon_2 P_2. \end{aligned} \tag{28}$$

By taking the difference of the products of the first and third, and of the second and fourth, of these equations, and by suitable substitution according to Eqs. (27), the energy equation is obtained in the form

$$\epsilon\rho_1 P^2 - \epsilon\rho_1 P_1^2 = \epsilon_2\rho_2 P_2^2 + \gamma_1\rho_1 S_1^2 + \gamma_2\rho_2 S_2^2. \tag{29}$$

The transverse waves are of SV type.

Equation (29) shows how the original energy $\epsilon\rho_1 P^2$ of the incident wave is distributed among the four waves into which it breaks up at the interface. In detailed numerical calculations

of the ratios of P and S quantities in any particular case, the energy equation supplies a check on the accuracy of the work.

Equations (27) give the relations among the quantities ϵ, ϵ_2, γ_1, and γ_2 for any assumed values of the densities and elastic constants. Hence, for any chosen value of ϵ—that is, for any chosen angle of incidence—the corresponding values of ϵ_2, γ_1, and γ_2 may be calculated. Or, if the respective velocities are known, Eqs. (26) relate any assumed angle of incidence to the other quantities, while from Eq. (21) the modulus of rigidity may be computed. The numerical values of the coefficients in Eqs. (28) can then be filled in. That leaves four numerical equations from which any four of the five quantities can be determined in terms of the fifth. Knott suggested that it makes for greater speed and accuracy to fill in the numerical values in the equations as they stand and then solve them for each individual case, rather than to work out the several algebraic expressions for each ratio and then substitute. Except when $G_1 = G_2$, or when either vanishes, the expressions are unwieldy. With the aid of tables of squares, square roots, and trigonometric functions, the four equations with numerical coefficients can be worked out with a little care and patience. Values of S_1 and S_2 follow at once. Finally, by calculating the terms in the energy equation (29) and dividing through by $\epsilon\rho_1 P^2$, numbers may be obtained that show the partition of energy among the reflected and refracted waves. When any one of the quantities ϵ_2, γ_1, or γ_2 becomes zero or imaginary, there is no wave of that type. In such cases, the P and S quantities may work out in the form $p + js$ and it is then necessary to take the expression $\sqrt{p^2 + s^2}$ as the number on which the energy depends.

Analogous equations were developed for incident SV- and SH-waves.

If the velocity of earth waves increases continuously with depth, the brachistochronic path becomes a continuous curve. This can be demonstrated by constructing paths for a sequence

of parallel constant-velocity layers, if the layers are made successively thinner and more numerous. For n layers,

$$\frac{v_1}{\sin i_{1_n}} = \frac{v_2}{\sin i_{2_n}} = \frac{v_3}{\sin i_{3_n}} = \cdots = v_n,$$

and in the limit of indefinitely large n, that is, continuous increase of velocity with depth and continuous curvature of path, if the subscript o is used for the surface, and m for the midpoint

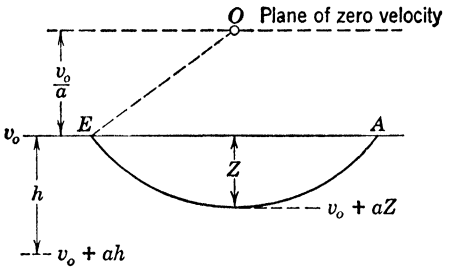

FIG. 28. Ray in a medium in which the velocity increases linearly with depth.

or point of maximum penetration of the curved ray, the first and last members of these equations become

$$\frac{v_o}{\sin i_o} = v_m.$$

In the special case in which the velocity increases linearly,[3] so that a velocity v_o at the surface becomes a velocity $v_o + ah$ at a depth h, the path is the arc of a circle with its center at a height v_o/a above the surface, as in Fig. 28. This is the height at which the velocity would be zero if it decreased upward at the same rate that it increases downward from the surface.

If at a depth h the velocity suddenly changes from $v_o + ah$ to a different value v_1, and if below the discontinuity the velocity

[3] O. Meisser, "Beiträge zu einer experimentellen Seismik," *Veröffentlichungen der Reichsanstalt für Erdbebenforschung in Jena* (G. Fischer, Jena, 1929), No. 9, p. 24.

again increases linearly, at a different rate A ft/sec per foot of depth, so that at depth H below the discontinuity it is $v_1 + AH$, reflection and refraction occur and the paths are constructed as in Fig. 29.

Figures 28 and 29 show curved rays below a plane representing the earth's surface, as for cases involved in seismic prospecting or studies of earthquake waves at short distances from their

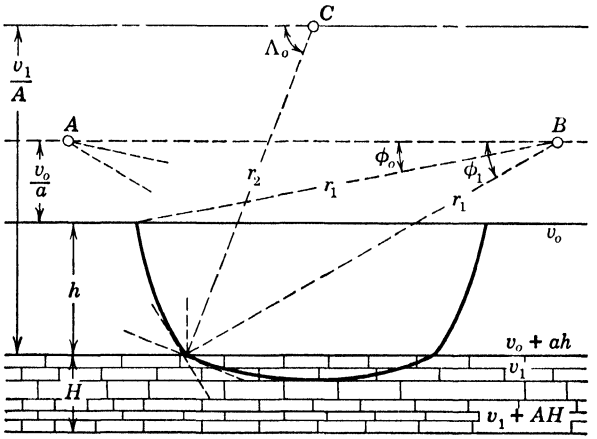

FIG. 29. Rays in two mediums in which the velocity increases linearly with depth; ϕ_o, angle of incidence at surface; ϕ_1, angle of incidence in medium 1; Λ_o, angle of refraction in medium 1.

sources. The laws governing all rays at distances great enough to require allowance for the earth's curvature are the same, but the terminology introduces a symbol for depth in terms of distance from the earth's center rather than depth below the surface plane (see p. 78).

Travel Time

The travel history of earth waves is reconstructed from observations of the time required to reach different distances along the surface. These are plotted on a graph of time versus distance. Under the controlled conditions of seismic prospecting, the exact

instant of firing the dynamite at the source is known and this graph is in all cases a *travel-time graph.* In early studies of earthquake waves, the time of arrival at recording stations from a known source was sometimes known, but the time of starting was not, so the graph became simply a *time–distance graph.* As data accumulated, it became possible to extrapolate back to the origin and set a time for the starting of the earthquake waves. We are now equipped with reasonably complete travel-time data for such waves.

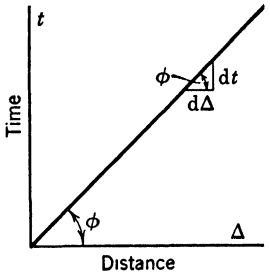

FIG. 30. Travel-time graph.

The travel-time graph for waves from a surface source in a medium in which their velocity is constant is a straight line, as shown in Fig. 30. The slope of this line, tan φ, is an increment of time divided by the corresponding increment of distance, $dt/d\Delta$, which is equal to the reciprocal of the velocity of the waves, $1/v$.

Although, strictly speaking, the mathematical slope of this line is the reciprocal of the velocity, it is general practice in seismology to speak of the slope of the line as measuring the velocity.

Now consider three layers in each of which the velocity is constant, with $v_1 < v_2 < v_3$. By the method of Huygens, it is a simple and instructive exercise to construct wave fronts for the advance of a disturbance from a source on the surface. The result is shown in Fig. 31 for layers in which the velocities of the advancing wave are 5000 ft/sec, 7500 ft/sec, and 10,000 ft/sec, respectively.[4] The positions of the wave front for successive tenths of seconds are shown. An important feature of the process is illustrated along the interface between mediums 1 and 2. Once the disturbance has entered medium 2, it quickly outruns the portion still in medium 1, and the wave in 2 is the first to reach

[4] H. R. Thornburgh, "Wave-front diagrams in seismic interpretation," *Bull. Am. Assoc. Petroleum Geol.* **14,** 185–200 (1930).

points along the discontinuity. As it traverses the lower side of the interface it sets up a progressive series of disturbances moving toward the upper surface of medium 1. If the discontinuity is plane, the front of this derived disturbance is plane, and the angle that it makes with the interface depends on the ratio of the velocities. The curve AB represents points in medium 1

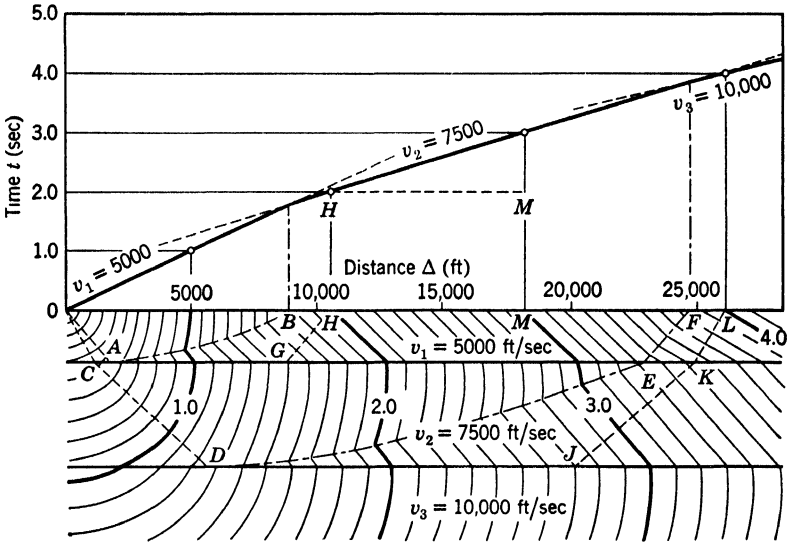

FIG. 31. Wave-front diagram and travel-time graph for three layers bounded by parallel discontinuities. (After Thornburgh.)

that are reached simultaneously by direct waves from O and waves derived from passage of the disturbance in medium 2 along the interface. Since only the front of the disturbance is being considered, the waves in medium 1 are not drawn beyond that line, though, of course, they actually continue outward, and the waves generated by passage of the waves in medium 2 along the discontinuity do not stop at AB.

The curve DE is a similar equal-time locus in medium 2, and EF is its continuation to the surface. The picture has been carried through 4 sec, to a surface distance of 28,000 ft, where first

arrivals are those which have followed rays like *OCDJKL*, including travel in medium 3 in the path.

In the upper half of Fig. 31, arrival time of this first wave at different surface distances has been plotted. From *O* to *B* the graph has a slope of 5000 ft/sec, the velocity v_1. Beyond *B*, where the equal-time locus *AB* reaches the surface, the travel-time line takes a slope of 7500 ft/sec, or v_2. At *F*, it takes the slope of 10,000 ft/sec, or v_3. These relations obtain for the case where the velocity discontinuities are parallel to the surface.

A ray that is refracted in such a way that it travels along the interface between mediums 1 and 2, such as *OAGH*, must reach that interface at an angle of incidence which will make the angle of refraction 90°. From Eq. (26), we would have

$$\frac{v_1}{v_2} = \frac{\sin \Lambda}{\sin \Lambda_2};$$

but, as has just been pointed out, $\Lambda_2 = 90°$; therefore $\sin \Lambda_2 = 1$ and this particular angle of incidence, called the *critical angle*, is the one whose sine is equal to v_1/v_2. This angle is given the symbol i_{12} when it stands for the angle of incidence of a ray in medium 1 refracted at 90° along the surface of medium 2. For such an angle in medium 2, refracted along the top of medium 3, the symbol would be i_{23}, and similarly for other combinations. Thus,

$$\sin i_{12} = \frac{v_1}{v_2}, \tag{30}$$

$$\sin i_{23} = \frac{v_2}{v_3}. \tag{31}$$

If we denote by i_{13} the angle that the ray *OCD* must make at *C* in order to reach medium 3 at the critical angle i_{23}, we have

$$\frac{v_1}{v_2} = \frac{\sin i_{13}}{\sin i_{23}} = \frac{\sin i_{13}}{v_2/v_3} = \frac{v_3 \sin i_{13}}{v_2}$$

and

$$\sin i_{13} = \frac{v_1}{v_3}. \tag{32}$$

This use of subscripts in connection with angles of incidence for critical rays allows the first number to represent the medium in which the incident angle is made, and the second to represent the medium in which the ray is finally critical, that is, refracted at 90°.

Figure 32 illustrates the terms that enter into formulas for computation of the depth of a discontinuity parallel to the surface and separating layers in which the velocities are v_1 and v_2, with v_1 less than v_2. The first energy that returns to the surface after refraction along the top of medium 2 arrives at the distance Δ_c. Figure 33 shows a refracted wave appearing first at $\Delta_c = 32{,}000$ ft. From that distance outward, waves arrive on the schedule represented by the v_2-line. Beyond the distance Δ_{12}, these are the first arrivals. Although no refracted waves exist between the origin and Δ_c, extrapolation of the v_2-line back to the axis of zero distance gives a time T_2 which is useful in certain formulas. The distance m, which is called the *mirage distance*, is the distance from the origin to a point on the surface vertically above the point of incidence of the critical ray on medium 2. From Fig. 32,

$$m = h_1 \tan i_{12}$$

and

$$\Delta_c = 2m = 2h_1 \tan i_{12}.$$

The depth h_1 is given by the equation

$$h_1 = \frac{\Delta_{12}}{2}\sqrt{\frac{v_2 - v_1}{v_2 + v_1}} = \frac{v_1 T_2}{2 \cos i_{12}}. \tag{33}$$

For any number of parallel layers, the intercept times on the axis of zero distance can be expressed as

$$T_n = 2 \sum_{k=1}^{k=n-1} \frac{h_k \cos i_{kn}}{v_k}, \tag{34}$$

from which the thickness of each layer can be computed if a travel-time graph is available.

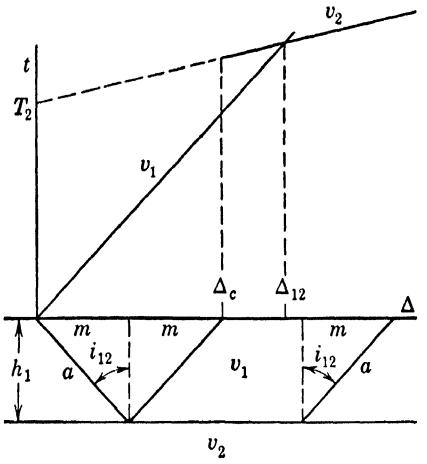

FIG. 32. Quantities involved in formulas for computation of the depth to a discontinuity.

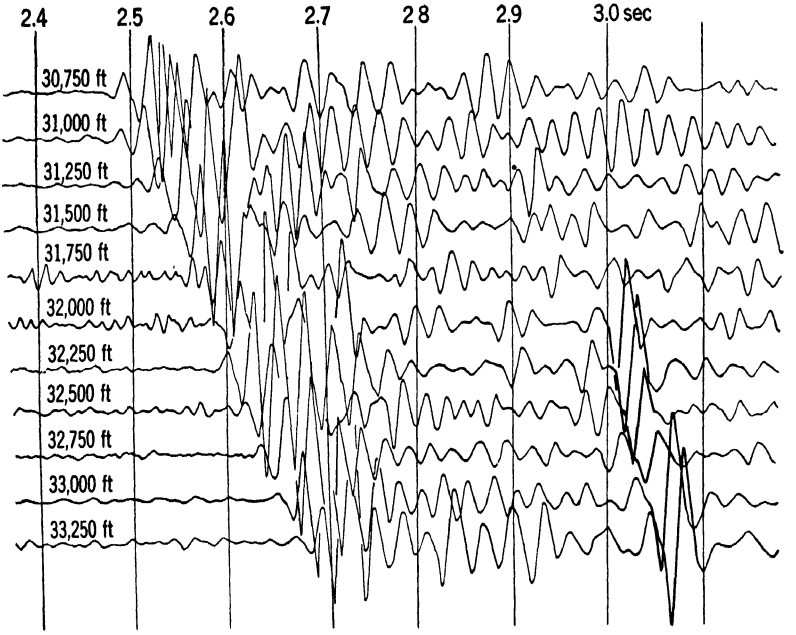

FIG. 33. First appearance of a wave refracted through a deep layer.

In connection with Fig. 31, it was pointed out that beyond B the travel-time line has a slope of 7500 ft/sec, and beyond F, of 10,000 ft/sec. The observations leading to these results, however, were made by instruments located on the top of medium 1, in which the true velocity was 5000 ft/sec. Thus the observed velocity under certain circumstances is an *apparent velocity*. This apparent velocity is governed by the angle at which the emerging waves reach the surface.

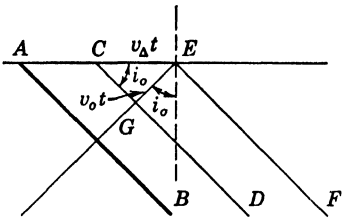

FIG. 34. Relation of apparent velocity to true velocity and angle of incidence.

In Fig. 34, consider an emerging wave front AB sweeping through successive positions CD and EF and incident upon the surface at the angle i_o. As the wave advances from G to E with its true velocity v_o, it sweeps the surface from C to E with an apparent velocity v_Δ. If it requires a time t to travel from G to E, then $GE = v_o t$ and $CE = v_\Delta t$. But

$$\frac{v_o t}{v_\Delta t} = \sin i_o,$$

so

$$v_\Delta = \frac{v_o}{\sin i_o}.$$

This concept of apparent velocity is extremely important in all developments of formulas for the interpretation of travel times of earth waves. As i_o varies from 90° to 0°, the value of v_Δ ranges from v_o to infinity.

Referring again to Fig. 31, it can be seen that if the upper boundary of medium 2 is not parallel to the surface, the slope of the v_2 travel-time line will not be a measure of the true v_2.

The wave fronts make angles with the discontinuities that are independent of the orientations of those discontinuities relative to the surface, since the angles are determined solely by

velocity ratios. As a result, if a discontinuity slopes away from the energy source, the apparent velocity with which waves reach the surface is less than if the discontinuity is parallel, that is, less than the true v_2. The reverse is true if the discontinuity slopes so that it approaches the surface as distance from the source increases. When slope in this direction is at an angle equal to the critical angle, the wave fronts emerge parallel to the surface, which they reach with an apparently infinite velocity, since all points are reached simultaneously. If the angle of slope is greater than this, distant points are reached before nearer ones, and the apparent velocity is negative.

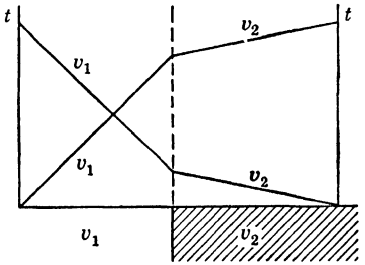

FIG. 35. Reversed profiles over a vertical discontinuity.

When instruments for recording earth waves are arranged in an approximately straight line away from an energy source, their records are said to constitute a *profile*. If the profile runs in the downward direction of the slope of a discontinuity with reference to the surface, it is said to run *downslope*. The travel-time graph for a downslope profile shows an apparent velocity for medium 2 that is less than the true velocity.

If a series of records is obtained from one shot point, at stations aligned in profile, and if, without moving the instruments, the observers locate a new shot point at the most distant station and take another series of records, the profiles are the reverse of each other, and are called *reversed profiles*.

When a discontinuity slopes with reference to the surface, it is necessary to observe travel times along reversed profiles to obtain data for computing the true v_2, the dip, and the depth. Reversed profiles are also necessary, strictly speaking, to determine whether a break in slope of the travel-time graph is caused by a horizontal or a vertical discontinuity. An example of the effect of the latter on reversed profiles is shown in Fig. 35.

The terminology employed in formulas for depth computation in the case of sloping discontinuities is illustrated in Fig. 36. Here ω_{12} is the angle by which the top of medium 2 slopes with reference to the top of medium 1—the surface; ω_{23} is the angle

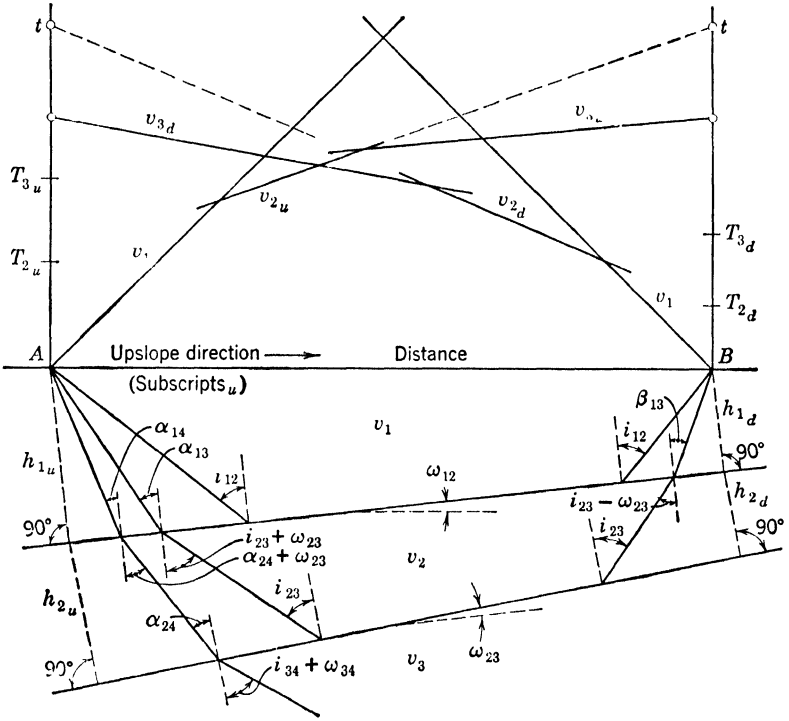

FIG. 36. Terminology used in formulas for depth computation—sloping layers.

by which the top of medium 3 slopes with reference to the top of medium 2, and similarly for other layers; v_{2_u} is the apparent value of v_2 in the upslope direction, and v_{2_d} that in the downslope direction. The slope of the first discontinuity fixes the upslope and downslope directions of the profiles for purposes of computation. If the next discontinuity slopes in the opposite direction, its angle of slope is called negative, but the so-called

upslope profile direction remains unchanged, as fixed by the attitude of the first discontinuity relative to the surface. The time required for waves to travel from A to B by any combination of paths is the same as the time required to travel from B to A over the same combination of paths in the reverse direction. Such times are called *reverse times*. They are marked by circles on the time axes in Fig. 36.

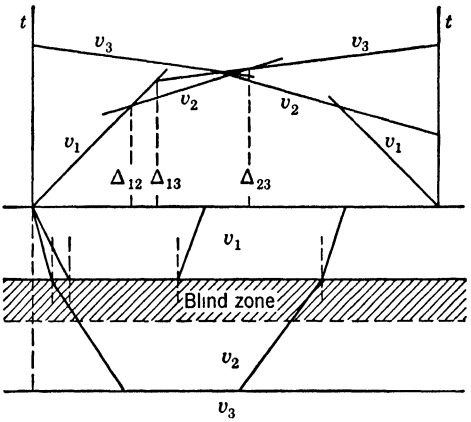

FIG. 37. Blind zone, with parallel discontinuities.

Formulas for depth computation with layers in which wave velocities are constant are summarized in Table 6.

It has been the practice in some types of work, particularly commercial prospecting, to base interpretations primarily, if not entirely, upon the times at which the first waves are recorded, the so-called *first breaks*. When this is done, the possibility of a *blind zone* which is not represented in the graph of first breaks needs to be taken into account.[5] This is illustrated by Fig. 37, in which the layers are left parallel for simplicity.

If layer 2 is made progressively thinner, the v_3-line moves down the graph parallel to itself until a point is reached where

[5] G. Brinckmeier, "Sonderfälle aus der Praxis des seismischen Verfahrens," *Beitr. angew. Geophysik* **4**, 152–164 (1934); R. Maillet and J. Bazerque, "La prospection séismique du sous-sol," *Ann. mines* [12] **20**, 314 (1931).

TABLE 6. Depth Formulas for Constant-Velocity Layers

$$\sin i_{12} = \frac{v_1}{v_2} \qquad (30)$$

$$\sin (i_{12} + \omega_{12}) = \frac{v_1}{v_{2_d}} \qquad (35)$$

$$\sin (i_{12} - \omega_{12}) = \frac{v_1}{v_{2_u}} \qquad (36)$$

$$\sin (\beta_{13} - \omega_{12}) = \frac{v_1}{v_{3_u}} \qquad (37)$$

$$\sin (\alpha_{13} + \omega_{12}) = \frac{v_1}{v_{3_d}} \qquad (38)$$

$$\sin i_{23} = \frac{v_2}{v_3} \qquad (31)$$

$$\frac{v_1}{v_2} = \frac{\sin \beta_{13}}{\sin (i_{23} - \omega_{23})} = \frac{\sin \alpha_{13}}{\sin (i_{23} + \omega_{23})} \qquad (39)$$

Similar formulas for additional layers

Two Layers—Discontinuity Parallel to Surface

$$h_1 = \frac{\Delta_{12}}{2} \sqrt{\frac{v_2 - v_1}{v_2 + v_1}} = \frac{v_1 T_2}{2 \cos i_{12}} \qquad (33)$$

Multiple Layers—All Parallel to Surface

$$T_n = 2 \sum_{k=1}^{k=n-1} \frac{h_k \cos i_{k_n}}{v_k} \qquad (34)$$

Formulas for Sloping Discontinuities

$$T_{2_u} = \frac{2h_{1_u} \cos i_{12}}{v_1}$$

$$T_{3_u} = \frac{2h_{2_u} \cos i_{23}}{v_2} + \frac{h_{1_u}(\cos \alpha_{13} + \cos \beta_{13})}{v_1}$$

$$T_{n_u} = \frac{2h_{(n-1)u} \cos i_{(n-1)n}}{v_{n-1}} + \sum_{k=1}^{k=(n-2)} \frac{h_{k_u}(\cos \alpha_{k_n} + \cos \beta_{k_n})}{v_k} \qquad (40)$$

Δ_{13} coincides with Δ_{12}. For the thickness of layer 2 that produces this condition, no v_2-line appears on a graph of first arrivals. Under a fairly wide variety of velocity conditions, however, this may occur while layer 2 actually has an appreciable thickness.

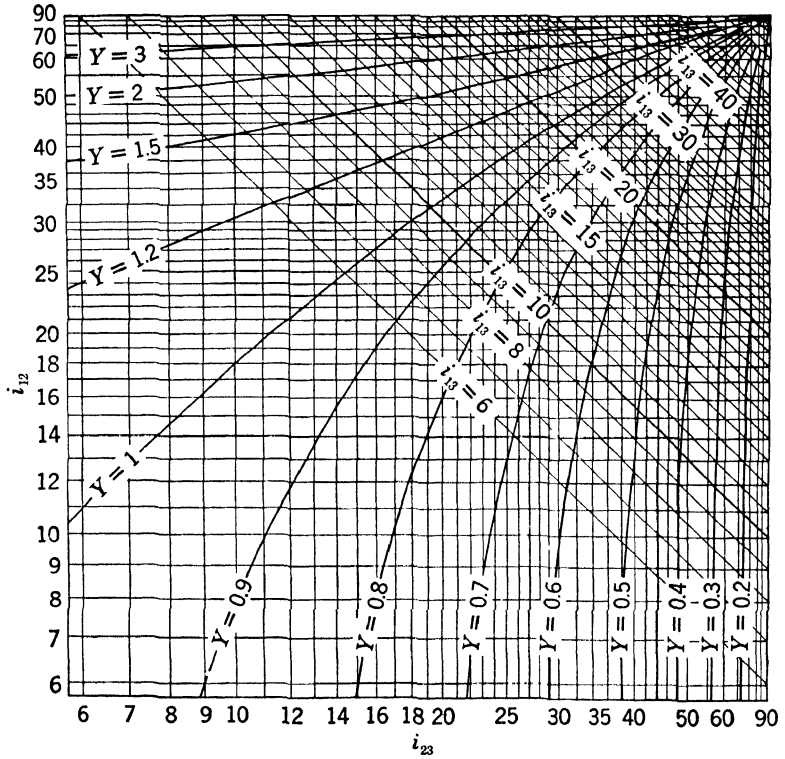

FIG. 38. Graph for computing thickness of a blind zone, with parallel discontinuities.

For example, in Fig. 37, with $v_1 = 3280$ ft/sec, $v_2 = 6560$ ft/sec, $v_3 = 16{,}400$ ft/sec, and $h_1 = 95$ ft, the second layer will not appear on a graph of first arrivals if it is less than 86 ft thick. The magnitude of the effect is clearly influenced by the extent to which v_3 exceeds v_2. A Huygens wave-front diagram illustrates the situation by showing that the waves that penetrate to the top of layer 3 reach the surface at the same time and

place as the waves that penetrated only to the top of layer 2, for the critical depth.

Figure 38 can be used to determine the minimum value of h_2/h_1 for which the v_2-line is defined by first arrivals. A quantity Y is defined by the equation

$$Y = \frac{\cos i_{12} - \cos i_{23} + \sin (i_{12} - i_{13})}{\sin i_{12} \cos i_{23} (1 - \sin i_{12})},$$

with

$$\sin i_{13} = \sin i_{12} \sin i_{23};$$

then the line for v_2 passes above the point (Δ_{13}, t_{13}) unless h_2/h_1 is greater than Y.

Travel-Time Graphs for Curved Paths

In connection with Fig. 28, wave paths were shown to become continuous curves as the number of constant-velocity layers increased to the limit where velocity increased continuously with

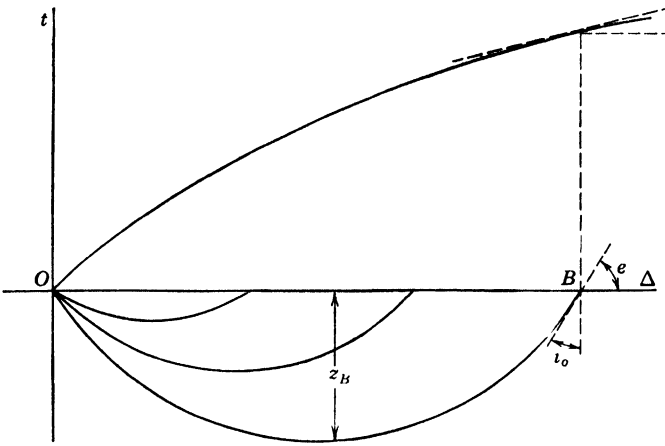

FIG. 39. Travel-time graph for curved paths.

depth. The travel-time graph likewise becomes a continuous curve under this condition.

Wave paths, or rays, and travel times are shown in Fig. 39 for a medium of this kind. The slope of the travel-time line is

measured by the slope of the tangent to it at any point. In the illustration, for example, it is $\tan \varphi = \mathrm{d}t/\mathrm{d}\Delta$ at $\Delta = B$.

This slope actually measures the apparent velocity with which the emerging wave front sweeps along the surface, and varies continuously because the angle of emergence varies continuously with distance. The apparent velocity thus represented may be designated for any distance Δ by the symbol v_Δ, as was done in connection with Fig. 34. As developed for that figure, it can be shown in the same manner for Fig. 39 that

$$v_\Delta = \frac{v_o}{\sin i_o}.$$

But in going to the limit of a large number of separate layers merging into a medium in which velocity increases continuously with depth, it was shown that

$$v_m = \frac{v_o}{\sin i_o},$$

so we find that $v_m = v_\Delta$; thus the slope of the travel-time graph at any distance yields the maximum velocity of the ray emerging at that distance, which is the true velocity at the midpoint of its path.

For earthquake waves, the curvature of the earth must be taken into account at the larger distances; the formula for computing depth of penetration is [6]

$$R \ln \left[\frac{R}{(R - z)}\right] = \frac{1}{\pi} \int_{\Delta=0}^{\Delta=B} \ln \left(p + \sqrt{p^2 - 1}\right) \mathrm{d}x,$$

where R is the radius of the earth, z is the depth of penetration,

[6] G. Herglotz, "Über das Benndorfsche Problem der Fortpflanzungsgeschwindigkeit der Erdbebenstrahlen," *Physik. Z.* **8**, 145–147 (1907); H. Bateman, "The solution of the integral equation connecting the velocity of propagation of an earthquake-wave in the interior of the earth with the times which the disturbance takes to travel to the different stations on the earth's surface," *Phil. Mag.* [6] **19**, 576–587 (1910); E. Wiechert and L. Geiger, "Bestimmung des Weges der Erdbebenwellen im Erdinnern," *Physik. Z.* **11**, 294–311 (1910).

measured from the surface, of the ray emerging at B, and $p = v_B/v_\Delta$. Putting $x = \Delta$, this equation may be written [7]

$$R \ln \left[\frac{R}{(R - z)}\right] = \frac{1}{\pi} \int_{\Delta=0}^{\Delta=B} \cosh^{-1} \frac{v_B}{v_\Delta} \, d\Delta. \tag{41}$$

Meisser [8] pointed out that when the left-hand member of Eq. (41) is replaced by z_B, its limit as R becomes infinite—in other words, for a plane surface—the equation may be written

$$z_B = \frac{1}{\pi} \int_{\Delta=0}^{\Delta=B} \cosh^{-1} \frac{v_B}{v_\Delta} \, d\Delta. \tag{42}$$

Triple-Valued Travel-Time Curves

A convenient method for examining the effects of various velocity conditions is to compute the paths and travel times for rays incident in the earth at regularly decreasing angles. For the conditions of Fig. 39, rays emerge in the order of their incidence, with increasing distance resulting from decreasing angle of incidence.

The interposition of a discontinuity, as pictured in Fig. 40, may lead to the crossing of certain rays. The resulting travel-

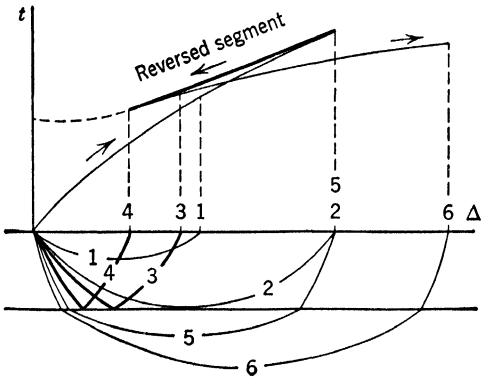

FIG. 40. Triple-valued travel-time graph.

[7] See B. O. Peirce, *A short table of integrals* (Ginn, Boston, ed. 3, 1929), No. 680.
[8] O. Meisser, reference 3, p. 29.

time graph consists of three segments, as shown in the figure. The rays are numbered in order of decreasing angles of incidence, or increasing steepness of incidence. The travel-time line from the origin through 1 to 2 represents direct rays in the upper medium, of which 2 is the one that just grazes the discontinuity. At 2, the curve reverses, and rays 3 and 4, though incident more steeply, emerge at shorter distances. They represent energy incident on the discontinuity at an angle requiring total reflection. At 4, the curve again reverses and becomes the continuous representation of increasingly steeper rays refracted into the second medium.

Slichter [9] has called the segment 2–4 a *reversed segment* and the travel-time graph in its entirety a *triple-valued travel-time curve*. Over the distances between 2 and 4, there are in general three rays with different travel times for a given distance. The reversed segment is concave upwards and meets the other segments tangentially.

Slichter demonstrated that Eq. (42) can be used in this case, the contribution of the reversed segment to the integral being negative. There are as yet no cases on record in which sufficient data were available from field observations for the application of this solution.

Reflected Waves

If there are two layers, in which the velocities v_1 and v_2 are constant, separated by a discontinuity parallel to and at depth h below the surface, the travel time of energy reflected at the discontinuity and recorded at distance Δ is

$$t = \frac{\sqrt{4h^2 + \Delta^2}}{v_1}.$$

If a travel-time graph is plotted, as in Fig. 41, the resulting curve for reflected waves is a branch of the hyperbola with

[9] L. B. Slichter, "The theory of the interpretation of seismic travel-time curves in horizontal structures," *Physics* **3**, 273–295 (1932).

center at (0, 0), asymptote v_1, axis of t the transverse axis, vertex at $(0, 2h/v_1)$, foci at $(0, \pm 2h\sqrt{1 + 1/v_1^2})$ and equation

$$v_1^2 t^2 - \Delta^2 = 4h^2,$$

from which the depth is

$$h = \tfrac{1}{2}\sqrt{v_1^2 t^2 - \Delta^2}. \tag{43}$$

The point P of Fig. 41 represents the travel time of the ray to Δ_c, after reflection at the critical angle i_{12}. It is thus the

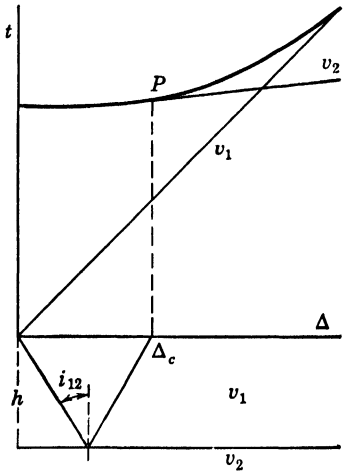

FIG. 41. Travel-time graph for reflected waves.

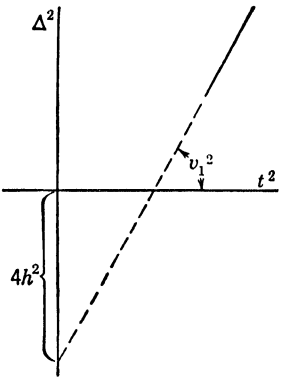

FIG. 42. Graph of the equation for reflected travel times.

beginning of the line v_2, and the point of tangency between the v_2-line and the curve for reflections.

If in the equation for the hyperbola representing reflected travel times, Δ^2 is plotted as ordinate and t^2 as abscissa, a straight line is obtained if h and v are constant (Fig. 42). Each observation determines a value of the depth and of the speed, provided the line is approximately straight. The slope of the line is v_1^2. The negative Δ^2 intercept is $4h^2$, from which the depth h may be found.

Earthquake Waves

The waves from most earthquakes appear to have originated within a relatively restricted zone, almost a point source in terms of global dimensions. This source region is called the *focus*.

The foci of about 75 percent of the world's earthquakes are within the outermost 50 km of the crust. Those which are deeper than that are called *deep foci*. The greatest depth observed to date is 700 km.

Distances are expressed in *degrees*, by the size of the angle subtended at the earth's center by the surface great-circle arc between two points, or in *kilometers* or *miles* for the length of that arc. A recording station a quarter of the way around the globe from an earthquake focus is at a distance of 90° = 10,000 km = 6210 mi.

The symbol P is given to waves of longitudinal type, and S to transverse. Longitudinal waves from a deep focus to the nearest points on the surface are designated p, and transverse waves s. If the path of a wave from focus to recording station is broken by reflection or refraction, with or without change of type, a letter is assigned to each branch of the path. Thus, if an S-wave leaves the focus, is reflected at the surface once and then recorded, its symbol is SS. If it changes type upon reflection, it becomes SP. If it leaves a deep focus and is reflected from the surface nearly vertically above the focus, then reaches a recording station without further reflection or change in type, it is called sS.

0–10°, Normal Focal Depth

Several lines of evidence, both geophysical and geological, have led to the conclusion that the outermost portion of the earth's crust is divided into layers of different chemical composition and elastic properties. The details of this layering control the character of records from distances up to about 10° and, in

turn, can be studied by means of the travel times of elastic waves. Such investigations constitute the transition from commercial and field seismology to so-called pure or earthquake seismology. Small earthquakes and large dynamite blasts have supplied most of the data.

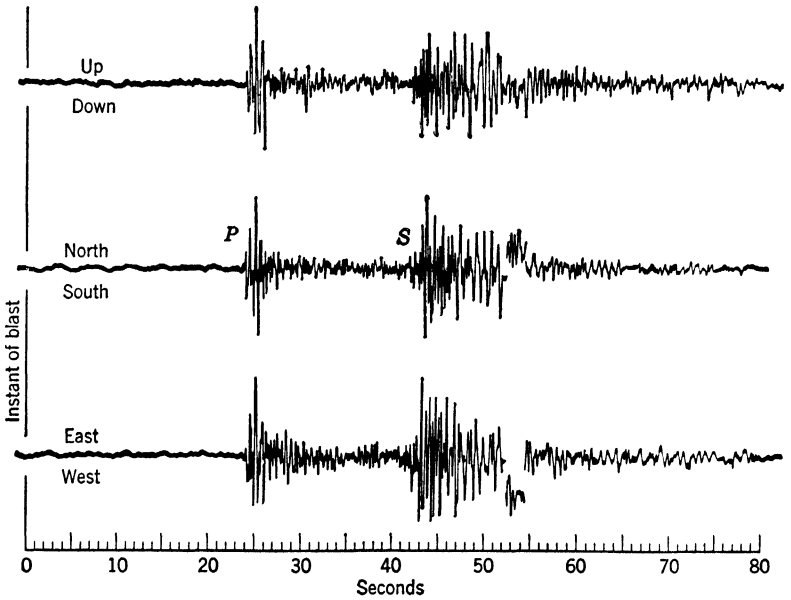

FIG. 43. Waves recorded at Harvard seismograph station from blast of 25,000 lb of dynamite at a distance of 152.5 km on May 25, 1935.

Figure 43 shows three components of the motion recorded at the Harvard Seismograph Station after the firing of a dynamite blast at a distance of 152.5 km (94.7 mi). There are two distinct groups, the longitudinal and the transverse, with surface waves poorly developed following the latter. Registration of waves from dynamite blasts at known places with time of occurrence determined by radio led to the development of the travel-time relations for New England shown in Fig. 44. The *P*- and *S*-waves

that have traveled only in the first layer are given the special symbols P_1 and S_1. Those that penetrate the top of the second layer for part of their travel become P_2 and S_2, and similarly

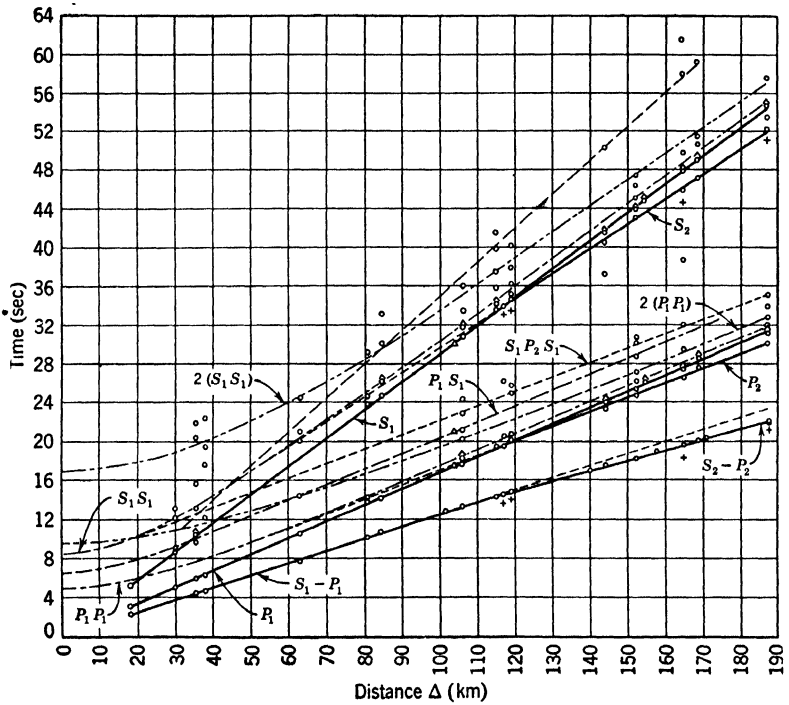

FIG. 44. Harvard travel times for New England, from timed dynamite blasts.

for other layers. Those that reach the material immediately below the base of the crust are sometimes designated as P_n and S_n, the subscript n standing for normal.

These investigations were extended at Harvard by studies of local earthquakes, and the results are listed in Table 7.[10]

[10] L. D. Leet, "Trial travel times for Northeastern America," *Bull. Seis. Soc. Am.* **31**, 325–334 (1941).

TABLE 7. Travel times for P- and S-waves over short distances Δ (km) from a surface focus in New England, and the structures that they represent.

Wave Time (sec)		Wave Time (sec)	
P_1	$0 + \Delta/6.13$	S_1	$0 + \Delta/3.45$
P_2	$2.2 + \Delta/6.77$	S_2	$4.1 + \Delta/3.93$
P_3	$4 + \Delta/7.17$	S_3	$7 + \Delta/4.27$
P_n	$7 + \Delta/8.43$	S_n	$10 + \Delta/4.62$

Thickness (km)		Layer or Zone	Poisson Ratio, μ	Velocity (km/sec)	
From P	From S			P	S
16	15	Layer 1 (Granitic)	0.27	6.13	3.45
13	10	Layer 2	.25	6.77	3.93
7	10	Layer 3	.23	7.17	4.27
—	—				
36	35	Zone of P_n, S_n	.28	8.43	4.62

10°–110°, Normal Focal Depth

In the distance range between 10° and 110°, the pattern of earthquake waves has long been regarded as standard. This is in part because the principal waves were first recognized on seismograms in this range.

In the reading of earthquake records, the word *phase* has taken on a special and restricted meaning. It is employed to designate an event on a seismogram marking the arrival of an impulse or a group of waves, because that arrival usually finds expression as a change in the phase of the motion of the recording light spot or writing point. In this sense, a phase on a seismogram may be defined as a change of period or amplitude, or both. If this change is abrupt, the phase is said to be an *impulse*, and the symbol describing it is preceded by the letter *i*, as *iS*. If it is gradual, it is *emergent* and is designated by the letter *e*, as *eP*.

There is some evidence that a single phase does not cause more than two or three complete oscillations of the ground as it reaches a recording location. Accordingly, if a group of waves exceeds that duration, there is reason to believe that it represents more than one phase.

Records within this distance range are characterized normally by the clear development of *P*, *S*, and surface phases grouped under the generalized symbol *L*, for Long, or Large waves. The *P*-waves commonly have periods from about 1 to 5 sec, *S*-waves from 5 to 15 sec, and *L*-waves from 15 to 60 sec or more. Longer periods tend to be associated with larger earthquakes. Figure 24 is a record from this range and, as previously noted, shows a *P*-wave, with the abnormal period of 15 sec, underlying the usual 1-sec waves.

110°–180°, Normal Focal Depth (Core Earthquakes)

At a depth of about 2900 km (1800 mi) below the earth's surface there is a marked change in composition or physical state, or both, of the materials. It is manifested by a sharp decrease in elastic-wave velocities. Seismic rays which penetrate to approximately that depth emerge between 100° and 110° from their source, so the most prominent effect of this discontinuity appears first in records at about those distances.

Beyond about 100°, the amplitudes of *P*-waves decrease rapidly, and the travel-time line straightens out in a manner suggesting that the waves have reached the surface after being diffracted around the boundary of the core. A new phase, *P'*, which has penetrated the low-velocity core, appears some 3 min or more after *P*. It, too, is very weak in this range and apparently is transmitted in part by diffraction along the core boundary to reach recording stations between about 110° and 145°. At around 145°, defined as the *focal point for P'*, it suddenly becomes prominent and splits into two branches, P_1' and P_2'. The region between 110° and 145° is known as the *shadow zone for P*.

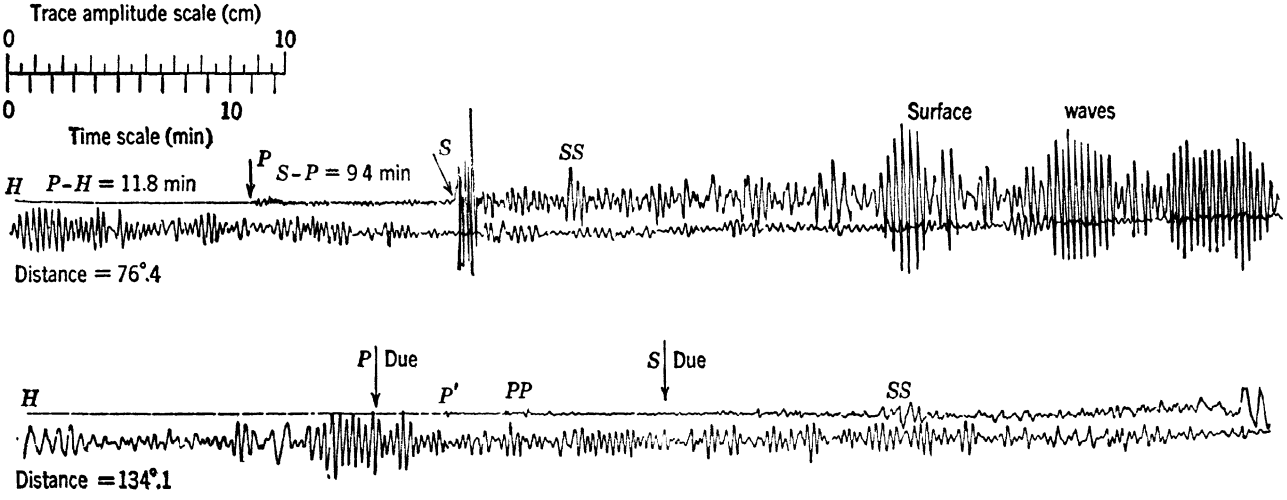

FIG. 45. Core record (lower trace) contrasted with one from middle distance. The nonappearance of *S*-waves is the most striking feature.

Below the boundary of the core, *P*-wave velocities increase again, with at least one discontinuous jump, indicating an inner core.

The *S* phase does not follow a parallel history. Its disappearance beyond about 110° is attributed to the absence of rigidity in the core and is one of the most striking and significant features of the propagation of earth waves through the deep interior.

Terminology for core waves assigns the symbol *K* (from the German *Kern*) to *P*-waves traversing the core, with the exception of waves of longitudinal type that penetrate the core and complete the journey without change of type. These are called *P'*, which is an abbreviation for *PKP*.

The reflected phases, *PP* and *SS*, become prominent, and several transformed core waves are added. The pairing of *P'* and *PP* at the beginning, followed some 20 or 25 min later by the large-amplitude, long-period *SS*, with *L* emerging nearly an hour after the start of the record, are characteristic features by which a normal core record beyond the shadow zone may be recognized at a glance.

Surface waves tend toward a simpler sinusoidal character with more uniform amplitudes than at shorter distances. The motion produced by surface waves lasts longer than at shorter distances because of waves arriving by many paths over which the average velocity is different. *World waves*, *W*, which come in over the major arc from the focus, are sometimes clear.

The contrast between a middle-distance record and a core record is shown in Fig. 45.

Deep Foci

One striking characteristic of records from deep foci at all distances is the decrease in intensity of surface waves as focal depth increases, until they are completely absent for the deepest foci.

Another is the entrance of phases of both *P* and *S* types reflected at the surface near the focus, then transmitted directly to the recording station: *pP*, *sS*, *pS*, and *sP*.

Summary of Earthquake Waves

The positions of the front of the first longitudinal wave from an earthquake are shown after successive intervals of 1 min in

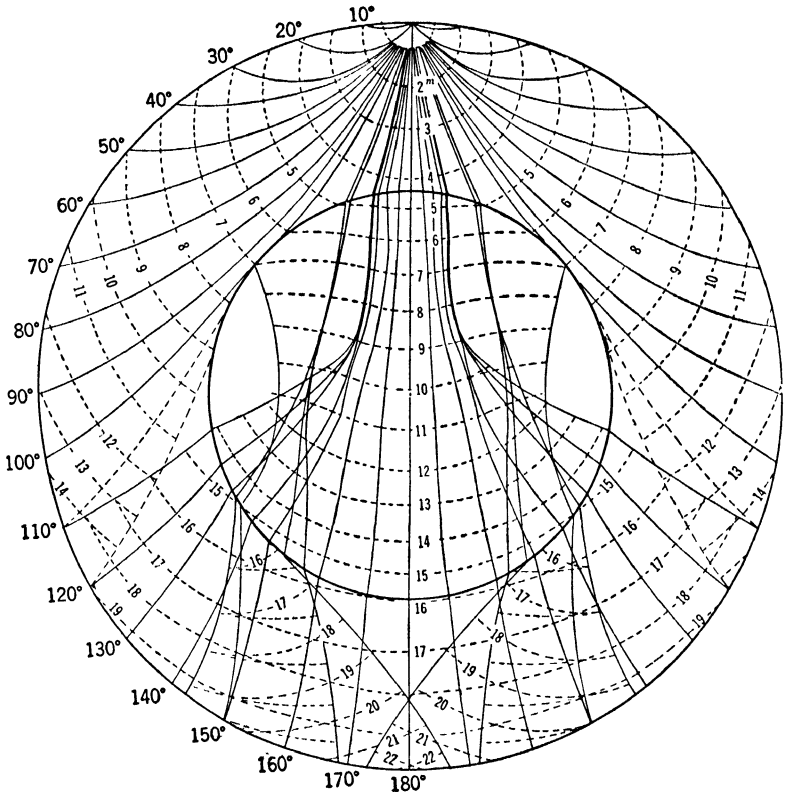

FIG. 46. Front of longitudinal wave from an earthquake, at intervals of 1 min, with rays to surface points 10° apart. (After Gutenberg.)

Fig. 46, together with the paths followed in reaching surface points every 10° from the source.[11]

Paths of a number of prominent phases which have been

[11] B. Gutenberger and C. F. Richter, "On seismic waves. IV," *Gerlands Beitr. Geophysik* **54**, 123 (1939).

identified are assembled in Fig. 47. The travel times for some of these phases from a focus of normal depth are shown in Fig. 48.

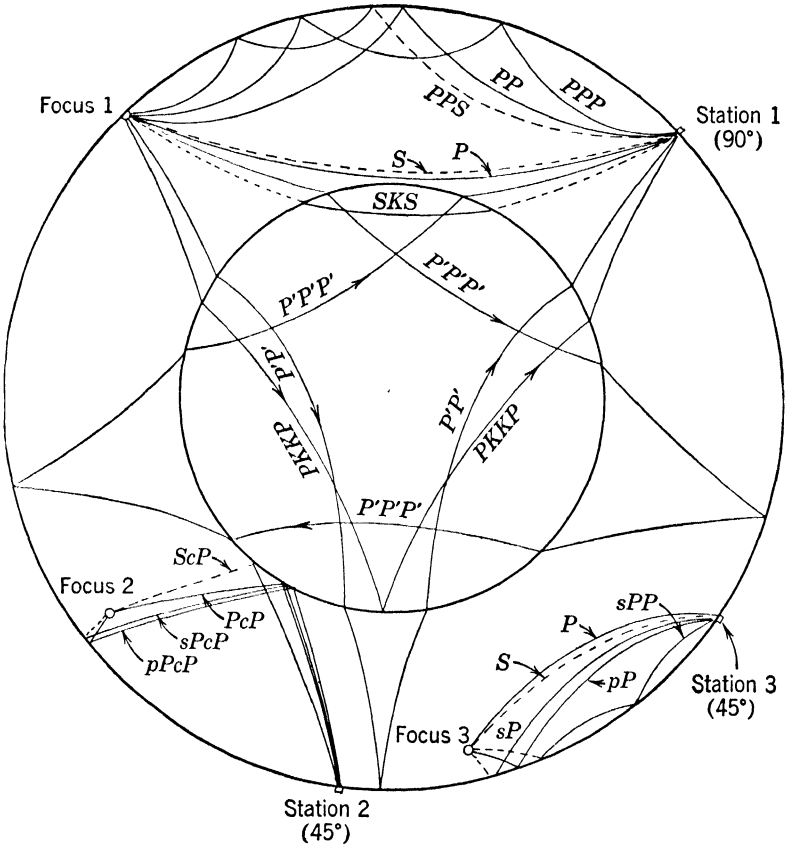

FIG. 47. Paths of certain important earthquake phases.

One of the objectives of the instrumental study of earthquake waves is the unraveling of the travel history along all paths from focus to station. At the present time, a large percentage of the recorded motion, especially at longer distances, remains unexplained.

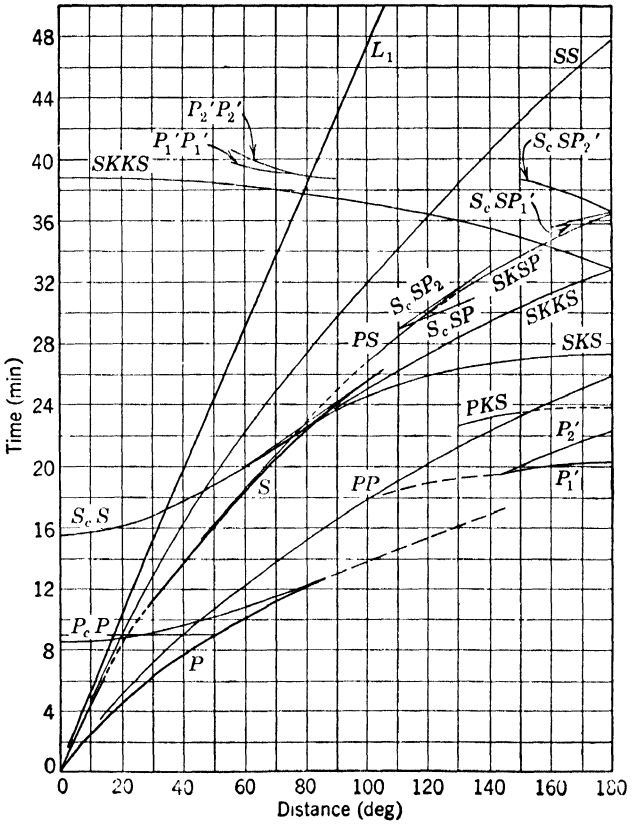

FIG. 48. Travel times for earthquake waves from a normal focus.

Seismic Prospecting

Principles of seismology have been applied to the study of shallow sedimentary structures through the utilization of earth waves generated artificially and recorded on portable seismographs. Such applications are described as *seismic prospecting*, or *seismic surveying*, and have found their chief development in commercial searches for oil.

Seismic-prospecting techniques divide naturally into two types, *refraction methods* and *reflection methods*. Refraction

methods deal primarily with waves that have followed brachistochronic paths and involve a distance from energy source to recording instrument of the order of four times the depth to be investigated, or more. Reflection methods interpret waves

TABLE 8. Velocities of longitudinal waves at the surface, or at shallow depths.

Material	Velocity (ft/sec)
Sand	650– 6,500
Loess	1,000– 2,000
Artificial fill	1,000– 2,000
Alluvium	1,600– 6,500
Loam	2,600– 5,900
Clay	3,300– 9,200
Marl	5,900–12,500
Salt	15,000
Sandstone	4,600–14,100
Limestone	5,600–21,000
Limestone, Arbuckle Mts., Okla.	
Perpendicular to bedding	13,400
Parallel to bedding	17,400
Slate and shale	7,500–15,400
Granite	13,000–18,700
Nepheline syenite	18,000
Quartzite	20,000
Norite	20,500

reflected from velocity discontinuities below the surface, the horizontal spread between energy source and recording instrument seldom exceeding and frequently being only a fraction of the depth to the reflecting horizon.

Seismic methods of mapping delineate planes of velocity discontinuity. An idea of the range of longitudinal-wave velocities is given by the values in Table 8, and the increase of velocity with depth is indicated in Table 9.

TABLE 9. Linear increase of velocity with depth, U. S. Gulf Coast.

(ft)	V_0 (ft/sec)	a (ft/sec ft)	V_0/a (ft)
0– 5,000	5,000	1.25	4,000
5,000–36,000	5,630	0.55	10,250
0–10,000	5,500	1.29	4,260
Penetration of ray reaching 9000 ft			1,900 ft
Velocity at that depth			7,950 ft/sec

Refraction techniques on a small scale are usually applied to the general problem of mapping solid rock overlain by unconsolidated sediments. This problem is of commercial interest in prospecting for alluvial gold, certain types of bauxite accumulation, dam sites in glaciated areas, or bedrock to support building foundations, and in the classification of excavation for highway construction or other engineering projects.

An example of the scale of operations for many such problems is furnished by Fig. 49. These profiles were run where the geological and velocity column were:

Material	Thickness (ft)	Velocity (ft/sec)
sand	55	2,180
clay	165	6,600
syenite		18,130

Some of the records are shown in Fig. 21. The depth to syenite was computed from the profiles as 220 ft at the mirage point nearest shot point *W*. A drill hole at that point encountered the syenite at 218 ft. In general, an accuracy of 5 percent can be obtained in routine work designed for speed and economy of operation.

The earliest applications of seismic methods to prospecting for oil on an extensive commercial scale were aimed at finding salt domes as potential loci for the accumulation of oil and gas. These salt domes are plugs of high-velocity salt driven into surrounding sediments of lower velocity. They are normally between 1 and 2 mi in diameter and their caps have been penetrated at

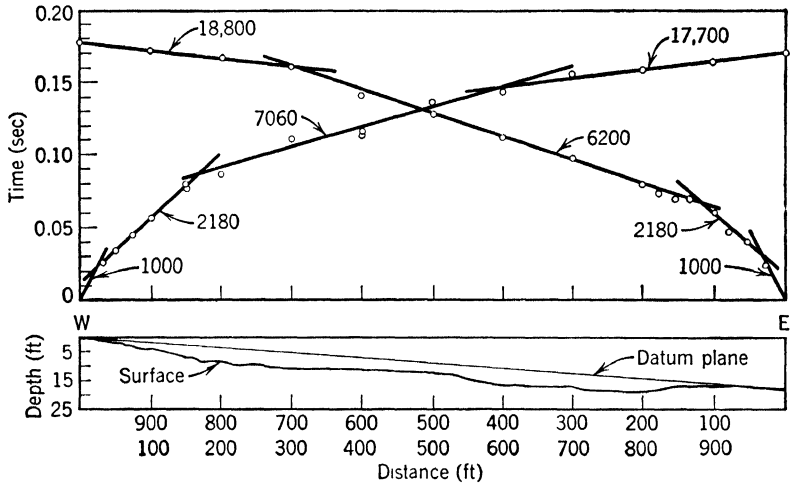

FIG. 49. Reversed profiles for mapping depth to syenite in Arkansas.

depths from 500 ft to nearly 8000 ft. There are many domes in Gulf Coast sediments which are suspected of having salt domes below them, though the drill has not penetrated to salt.

Figure 50 shows the effect of such a salt plug on the wave fronts and travel times of Fig. 31. Waves that have traveled through the salt arrive at surface points ahead of the schedule set by Fig. 31, to form a *salt line* which is below the v_2-line by a time called the *salt lead*. After profiles had fixed the normal travel time to various distances in a region, observing stations were located on the ends of radii branching from the shot, in a pattern called *fan shooting*. Early arrival at one or more radial stations led to more detailed investigation of the region that produced the lead.

Oil associated with a salt dome was first discovered on the Spindletop dome, near Beaumont, Texas, when a fabulous gusher blew in on Thursday, January 10, 1901, from a depth of 1040 ft and spread nearly a million barrels of oil over the plain in the nine days it ran wild.[12] In 1925, production was found on the flank of the dome. Six sands were ultimately developed at depths

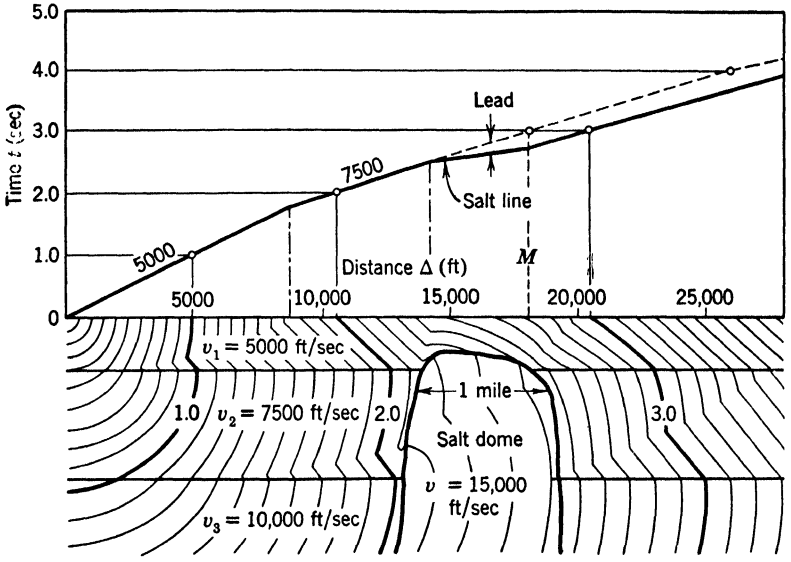

FIG. 50. Wave fronts and travel time through a salt dome. (After Thornburgh.)

from 700 to 5900 ft, over an area of 450 acres. Blue-sky stock promotions gave the place the name of Swindletop in the early days, but in spite of ruinous production practices at the outset, Spindletop yielded enough oil to give a start to such major companies as The Texas Company and The Gulf Refining Company. Through 1933, it had produced 122,000,000 barrels of oil.

Seismic methods were applied to the search for salt domes late in 1923. By that time, 46 domes were known through such

[12] S. W. Tait, Jr., *The wildcatters* (Princeton University Press, Princeton, 1946), pp. 116–126.

evidence as a surface mound, gas seeps, surface geology, and other data. The first discovery credited to the seismograph was the Orchard Dome, Fort Bend County, Texas, found in 1924. In the ensuing 12 years, seismic methods discovered 69 more domes. It was the period of most spectacular success for the method.

Beginning about 1932, the reflection method came into widespread use. Several instrumental and operational problems had to be solved to bring the method to its most productive form. One of the instrumental features was electronic control of sensitivity to suppress the extreme surface turbulence resulting from close proximity to the shot. Another was the use of galvanometers giving 6, then 12, then 24, and more traces on each record. An operational feature that became common was the feeding into each galvanometer channel of the output from several detectors in series, spaced to allow surface waves to partially or entirely cancel one another. Reflected waves hit such an array nearly simultaneously and are therefore strengthened on the record.

The most important single problem in reflection shooting is to determine the average velocity from the surface to the reflecting horizon. Theoretically, this can be done by proper arrangements of detectors and computation by some such means as Fig. 42. In practice, however, extensive use is made of calibration velocities obtained at drill holes.

In spite of the radical differences in details of field procedure and interpretation, the reflection method, of course, is still basically a special case of the refraction method, and principles of the propagation of earth waves are best demonstrated by the latter.

In recent years, refraction methods have been employed in general structural mapping where, for special local reasons, reflected energy cannot be used. A modification of the profile method is substituted for the fans used in salt-dome prospecting. Fully detailed reversed profiles are run for calibration, then the instruments are distributed around a standard reference range,

or distance, and observations are made only in that vicinity for each shot, while the arrival time of waves from a selected horizon is plotted.

When a horizon is being mapped at a depth of several thousand feet, there are often so many intervening velocity discontinuities as to make a full-dress depth computation something of a problem, if not an impossibility. To complicate it further, in many areas, such as Oklahoma and West Texas, low-velocity beds are interspersed with those giving higher velocities. There, a technique is borrowed from reflection procedure and an average velocity from the surface to the horizon being mapped is obtained by calibration. Then the simplest of the depth formulas, Eq. (33), is used for computation.

The laws of geometric optics fail to predict correctly the earth waves that will be recorded from a given structure, if layers are not of sufficient thickness to carry recordable energy to distant points. The exact ratio which is critical has not been determined, but it is probable from theoretical considerations that if a layer is much less than one wavelength in thickness it does not conduct appreciable energy. It is known from evidence like that of Fig. 52 that some critical thickness does exist.

A pair of reversed profiles covering 40,000 ft in northern Oklahoma illustrate the effect of this phenomenon, as well as some other features not previously discussed.[13] The distribution of velocities, and depths to certain geological horizons encountered in a well on the profile line, are shown in Fig. 51. The travel-time graph is given in Fig. 52, and records keyed on this graph are reproduced in Fig. 53.

The period of the waves in first arrivals and later phases shows a systematic increase with distance, and is represented reasonably well over the first 40,000 ft by the expression

$$T_\Delta \text{ (sec)} = 0.015 \text{ sec} + 85 \times 10^{-5} \left(\frac{\text{sec}}{\text{kft}}\right) \times \Delta \text{ (kft)}$$

[13] These records became available through the courtesy of L. A. Scholl, Jr., of The Texas Company. The following analysis was made by the writer.

(1 kft = 1000 ft). This formula yields a period close to 0.05 sec at 40,000 ft. The rate of increase falls off at greater distances, but

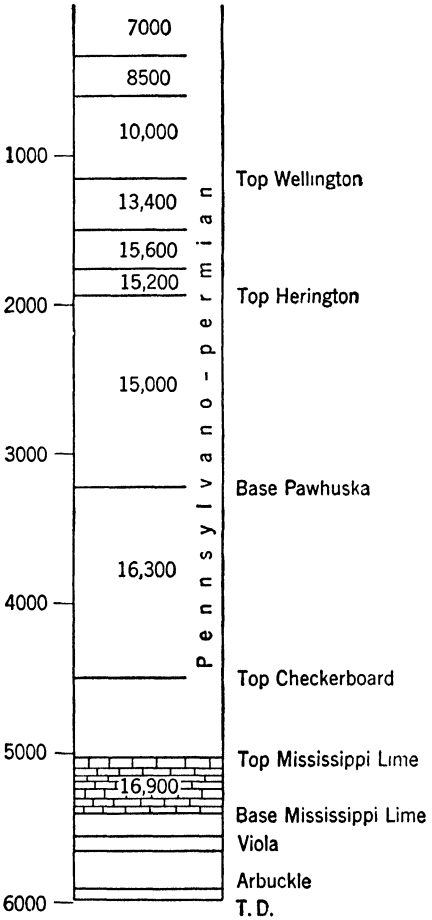

FIG. 51. Geologic and velocity column in the vicinity of the profiles of Fig. 52; depths in feet and velocities in feet per second.

there are no data available at the present time for determining it.

The progressive increase in period with distance also represents a corresponding increase in wavelength. That relation is involved in an explanation of why a layer will show up well on

records at some distances and then fail to transmit recognizable waves at greater distances. This leads in some cases to parallel lines on the travel-time graph, offset in time and representing different layers with the same velocity.

In the region of Fig. 52, a surface zone of velocity between 6500 and 7000 ft/sec carried considerable energy on both profiles for some distance beyond the point where it arrived first. In Record A (Fig. 53) which was shot with insufficient dynamite, the first-layer waves are the only ones that can be picked with consistency. Record B shows a repeat of this shot with more dynamite, which brought out the refracted waves leading the first-layer waves. The duration of this phase is probably due to phenomena discussed in connection with Fig. 55.

The thickness of layer 1, computed from Eq. (33), was 300 ft. Record C shows the same waves out to 15,000 ft. Beyond that distance the records were cut off before these waves would be due, so data are lacking. A wavelength comparable to this thickness, however, would be reached between 20,000 and 30,000 ft, and these first-layer waves should not be a prominent part of any record at greater distances.

Record F shows a new phase breaking away from these first-layer waves. This new phase did not persist, however, and has not been identified.

The formation known as Mississippi Lime was the horizon being mapped in this area. At a well on the profile line near the mirage point for Profile N, it was 5000 ft deep and 400 ft thick. Waves from this horizon appeared abruptly at 13,750 ft on Profile S, as illustrated on Record G, and became well marked beyond 15,000 ft, as illustrated on Records H and J. On Profile N, they disappear with equal suddenness at 29,000 ft, as shown on Record D. At that distance, with a period of about 0.034 sec, their computed wavelength would be 550 ft. The corresponding point on Profile S was 32,500 ft. The disappearance of these waves from the Mississippi Lime was probably due to their wavelength becoming enough greater than the thickness of

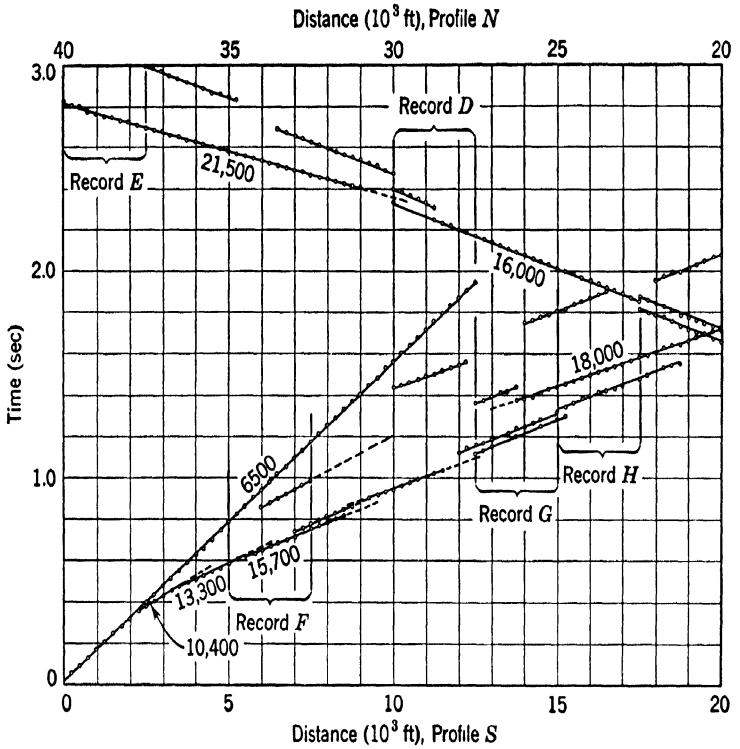

FIG. 52. Reversed profiles in Alfalfa County, Oklahoma, from records given in Fig. 53.

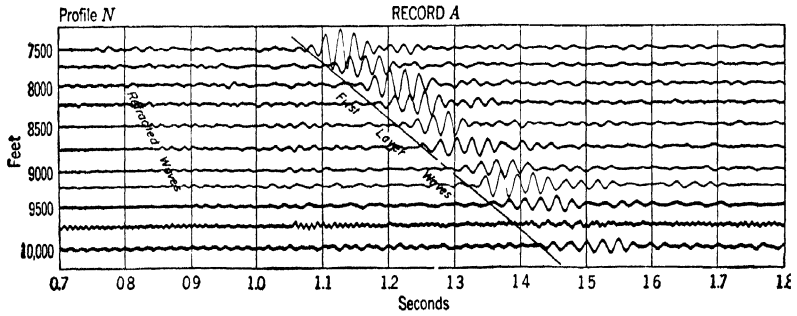

FIG. 53. Seismograph records for Fig. 52.

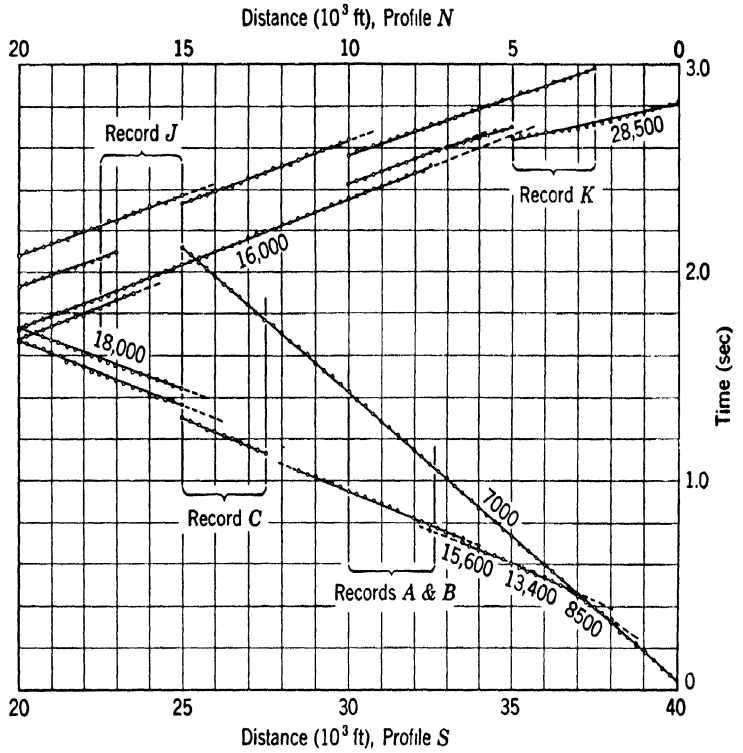

FIG. 52. (*continued*)

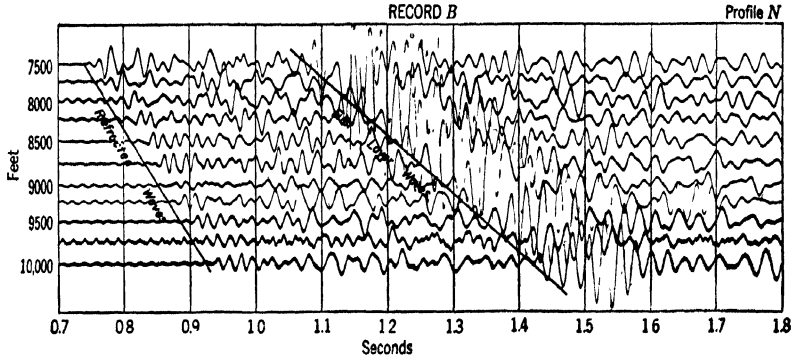

FIG. 53. (*continued*)

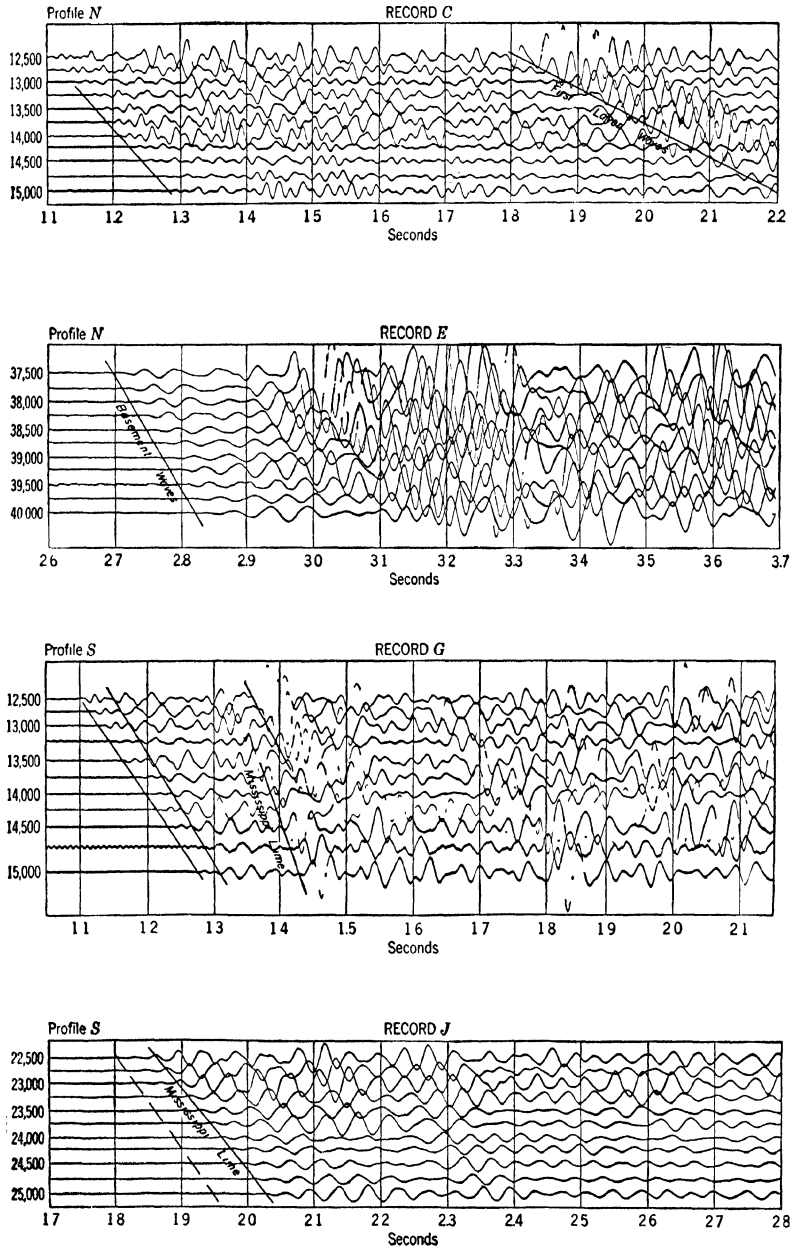

FIG. 53 (*continued*). Seismograph records for Fig. 52.

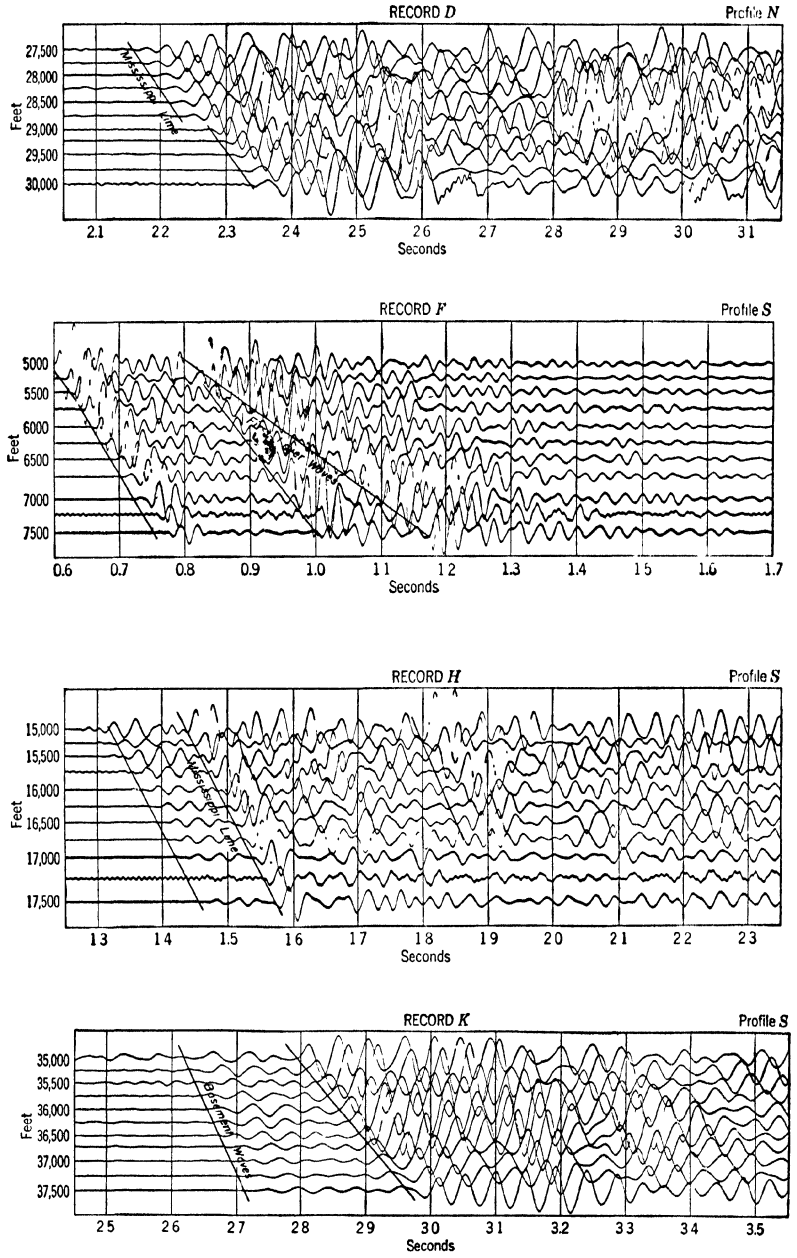

FIG. 53. (*continued*)

the lime to prevent the horizon from carrying appreciable energy.

On Profile S, the Mississippi Lime waves can be followed continuously from 13,750 ft to 32,500 ft. Over the first part of that range, they show a velocity of 18,000 ft/sec, but at 21,000 ft their travel-time line changes slope and beyond that shows a velocity of 16,000 ft/sec. On Profile N, the same effect appears in the opposite direction, with a velocity of 18,000 ft/sec where S shows 16,000 and 16,000 where S shows 18,000. This indicates a structure in the Mississippi Lime, with its crest somewhere close to midway between the shot points of Fig. 52, a slope of the order of 300 ft/mi on either side of the crest, and a true velocity in the Mississippi Lime of 16,900 ft/sec. The use of 12,500 ft/sec for v_1, as an average overburden velocity, in Eq. (33) gives a good check on the depth at the well.

Rocks of the basement underlying the sedimentary formations being prospected for oil, presumably much older and either igneous or metamorphic, were picked up by both profiles. They are shown on Records E and K. There are no data for the identification of the large energy which follows them. With an average overburden velocity of 13,000 ft/sec, the depth between 5000 and 10,000 ft from point N was computed as about 7500 ft, and a similar distance from S as about 10,800 ft. The true velocity in the basement was computed to be 24,400 ft/sec (about 7.4 km/sec), a very high value.

The data represented by Fig. 52 supplied time and distance information for 320 stations distributed over 40,000 ft, at several of which there were repetitions of shots to clarify uncertainties. They were obtained by a commercial crew in two days. In startling contrast to this were the results of a widely quoted application of seismic methods financed by the Geological Society of America for the purpose of mapping basement rocks under the Atlantic Coastal Plain.[14] The key "profile" of that project

[14] M. Ewing, A. P. Crary, and H. M. Rutherford, "Geophysical investigations in the emerged and submerged Atlantic Coastal Plain, Part I, Methods and results," *Bull. Geol. Soc. Am.* **48**, 753–802 (1937).

consisted of two points, one at 35,500 ft and one at 44,030 ft, both more than 150 mi from the nearest velocity calibration. On the basis of those two isolated observations, it was reported that "the thickness of unconsolidated and semiconsolidated material (velocity of longitudinal waves about 8000 ft/sec) near the edge of the Continental Shelf was found to be about 12,000 ft." No part of the extensive information on seismic prospecting now available justifies basing computations of any kind on a two-point "profile." [15]

Reversed profiles to 40,000 ft in a region of young sediments in the U. S. Gulf Coast dominated by three velocity zones, with $v_1 < v_2 < v_3$, developed an interesting set of phases which appear to be multiple surface reflections. The vertical-component records are shown in Fig. 54, with the travel-time graph for one direction in Fig. 55. The graph for the opposite direction was practically identical, indicating horizontal layering. These data were first reported in 1934.[16]

The curve $P_1P_2P_3$ (Fig. 55) corresponds to the first recorded motion and reveals the presence of the three layers. The fact that the lines P_1, P_2, and P_3 are straight indicates that the velocity in each layer is constant. The interpretation of later phases requires the assumption of a surface layer covering layer 1 but too thin to be of importance at the distances of Fig. 55.

A precise interpretation of the subsurface structure can be made from the graph of P_1, P_2, and P_3. The details have been given elsewhere.[16] For present purposes, it is sufficient to say that the approximate thickness of the first layer is 1650 ft, and the velocities are $v_1 = 5900$ ft/sec, $v_2 = 8500$ ft/sec, and $v_3 = 10{,}500$ ft/sec.

The identification of later phases on a seismogram is subject to many uncertainties which cannot be overcome without a large number of records. In the present instance, the numerous

[15] L. D. Leet, "Status of geological and geophysical investigations on the Atlantic and Gulf Coastal Plain," *Bull. Geol. Soc. Am.* **51**, 873–886 (1940).

[16] L. D. Leet, "Some phases on explosion records in a 3-layered region," *Gerlands Beitr. Geophysik* **42**, 246–251 (1934).

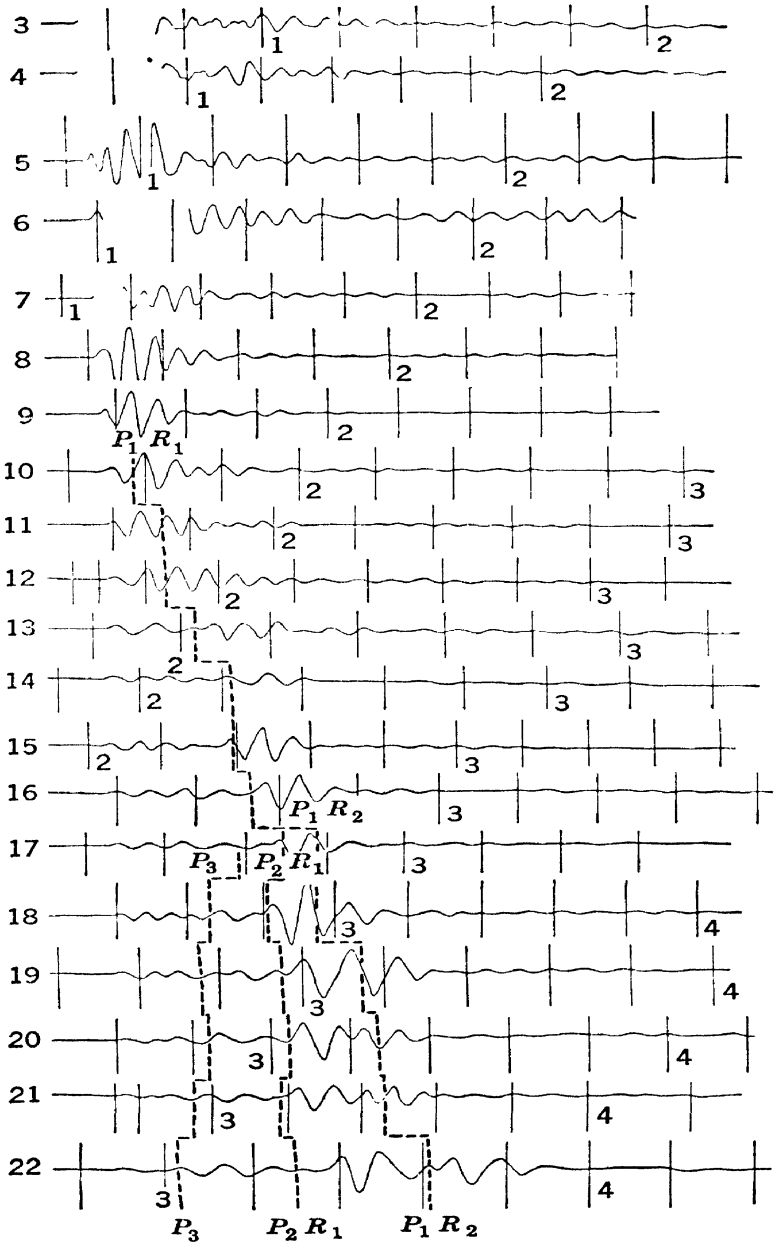

FIG. 54. Records for Fig. 55.

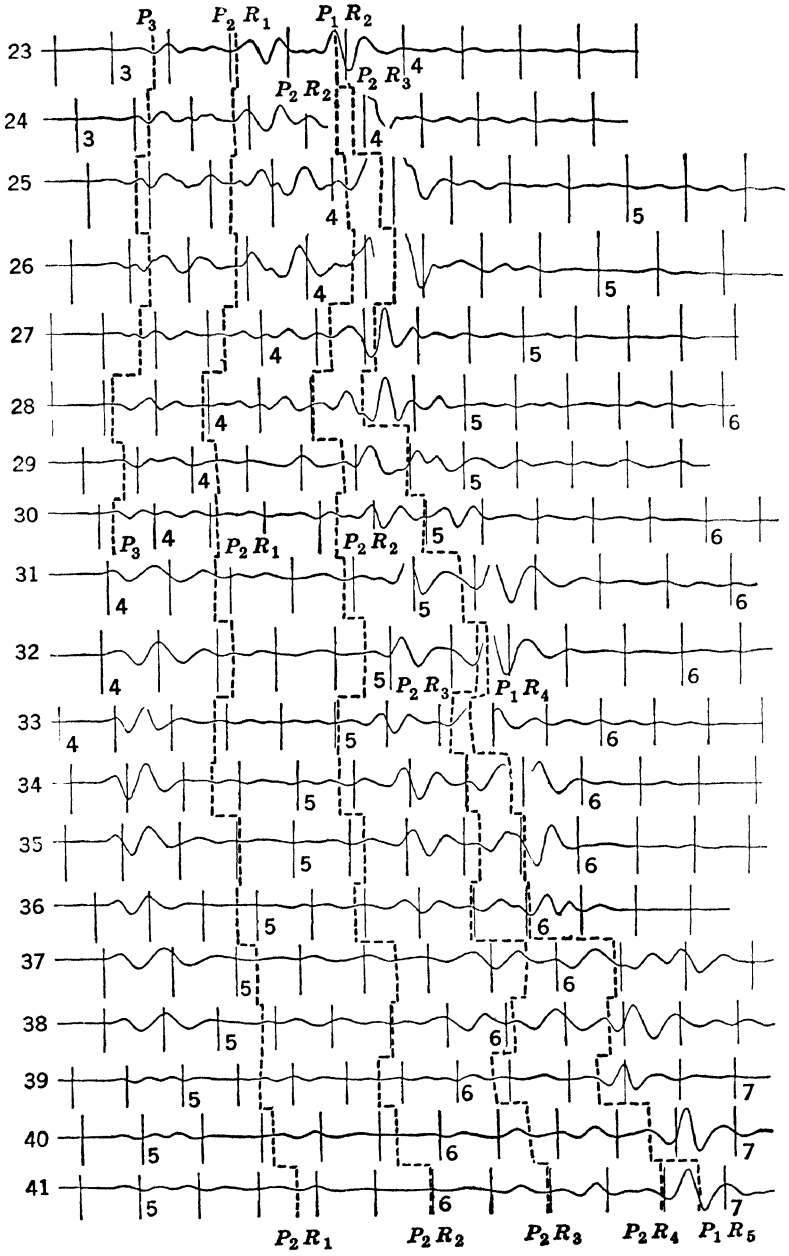

FIG. 54. *(continued)*

closely spaced observations made it possible to trace the various phases from one record to the next solely on the basis of record character. This removed the necessity for relying upon preconceived ideas for guidance in doubtful cases.

One of the facts established by the graph in Fig. 55 is that the phase P_3 appears and can be recognized through the range from

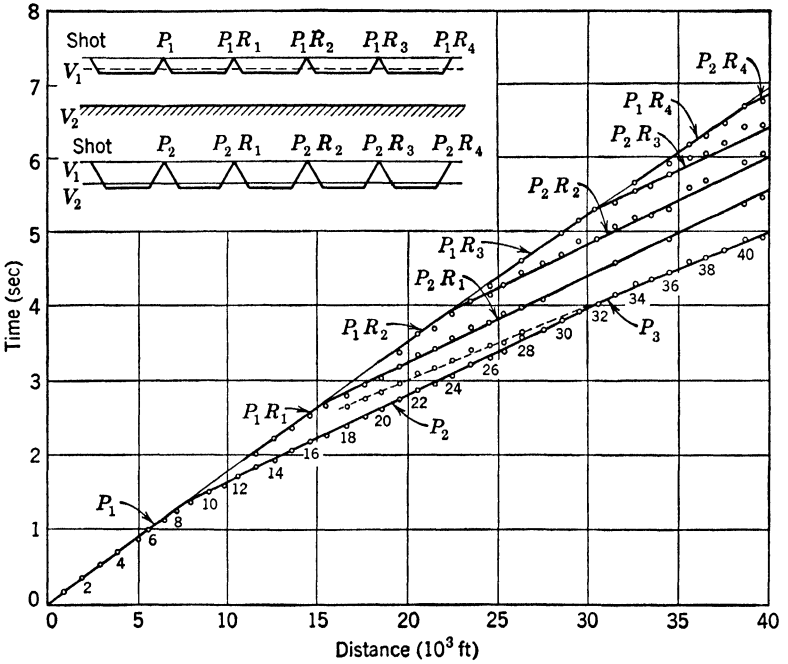

FIG. 55. Travel-time graph in region of three layers, showing multiple surface reflections.

16,000 ft to 31,000 ft within which P_2 is the first arrival. The merging of P_3 and P_2 leads to an increase in the amplitude of the first break, as shown on Records 30 to 36, Fig. 54. The same amount of dynamite was used for each of those shots.

The remaining phases represent rays that have been reflected at the surface one, two, three, and four times, respectively. The

paths are shown diagrammatically in Fig. 55. The travel-time lines for these phases have not been drawn to fit the plotted points. They were all determined from the P_1 and P_2 lines. This may be done by noting from the diagram in Fig. 55 that a P_2R_1 (P_2 reflected once) path is composed of two P_2 paths, or that P_1R_1 is composed of two P_1 paths. Thus, if we double both the time and the distance for a point on P_1 or P_2, we obtain the time and distance for a point on P_1R_1 or P_2R_1. Similarly, multiplication of the time and distance of a first arrival by, say, four gives the time and distance for a point on the R_3 line. All of the lines for reflected phases shown in Fig. 55 were obtained in this manner. The circles represent an attempt to pick the arrival times on the records, and the accuracy with which these plotted points fit the calculated lines is a measure of the correctness of their identification.

Further evidence is found in Fig. 54, where the dashed lines mark the times on each record at which the calculated phases are expected. It should be remembered that these points represent predictions based entirely on the lines for P_1 and P_2 and that they are not choices of phase based on personal opinion. This method facilitates a correlation of phase character from record to record and frequently shows clearly the presence of two phases in what otherwise might be mistaken for a single elongated wave train. It should be noted that not only is every recognizable phase predicted, but for every prediction there is a corresponding phase. The progressive elongation of a wave train with increasing distance is invariably followed by its splitting into two trains. True single pulses appear to consist of no more than two complete oscillations.

CHAPTER IV

Microseisms

Seismographs in routine operation for the registration of earthquakes have always recorded earth waves from other sources as well. Among these are waves, with periods ranging from 1 sec or slightly less to 10 sec, that occasionally grow to large amplitudes for hours or days at a time, and then decrease to small irregular motion. Every seismograph station in the world records them. Early in the history of the science the name *microseisms* (small shakings) was applied to them.

One striking characteristic as a microseismic storm develops is that the waves come in definite groups of two to ten or more complete oscillations, frequently starting gradually, building to a maximum, and then dying down. The pattern at one station is distinctive, yet frequently bears no determinable relationship to the pattern at a nearby station, even though the separation be only a few miles. *This feature establishes the fact that such microseisms are not radiating from a point source, or even a restricted source area, as do the waves from an earthquake, which produce a uniformly spreading pattern that can be followed from station to station for thousands of miles.*

Rayleigh and Q-waves have been identified among microseismic waves. When Rayleigh waves are recorded on a three-component seismograph, the sense of rotation of a particle as they pass determines their direction of travel, in accordance with Eq. (23).

Another method employed for determining the direction of travel of microseisms is illustrated in Fig. 56.[1] With a seismo-

[1] G. L. Schuyler, *Computations of directions of microseisms at tripartite stations* (Office of Naval Research, Washington, 1949).

graph at each vertex of a triangle, the time at which a wave passes each point is observed directly. In Fig. 56, the order of arrival at stations A, B, and C is indicated for the various sectors.

An array of this kind is called a *tripartite network* or *tripartite station*. In 1884, John Milne, a British physicist who became one of the founders of modern seismology while teaching in Japan, set up seismographs at the corners of a triangle on the campus of the Tokyo Engineering College. He supplied them with a circuit for simultaneous time marks at all three stations, and endeavored to determine the direction of travel of earthquake waves crossing the network. The first experiments were not satisfactory because the stations were too close to one another, but Japanese seismologists later got better results by enlarging the triangle until distances between stations ranged from 7500 to 35,750 ft. By selecting a wave that could be recognized at all stations of the network, and measuring the time of passage of the same phase of that wave at each station, these investigators determined the direction of approach for waves from a number of earthquakes.[2] This method was first applied to the study of microseisms in 1927 by F. Kishinouye and N. Nasu of the University of Tokyo.[3] They used three portable seismographs spaced from 1400 to 3600 ft apart. They were able to recognize certain groups of microseisms at all the stations, but decided that the phase relations indicated that the waves were "a kind of free oscillation" of a block of the earth separated by

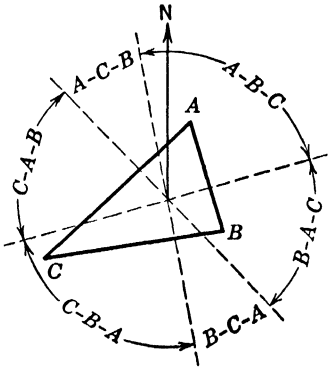

FIG. 56. Tripartite station, showing the order in which waves from different sectors pass stations A, B, C. (After Schuyler.)

[2] A. Imamura, "Seismic triangulation in Tokyo," *Publications of the Earthquake Investigation Committee in Foreign Languages, No. 7* (1902), pp. 5–24.

[3] F. Kishinouye, "Microseisms of four-seconds period," *Bull. Earthquake Research Inst., Tokyo Imperial University* **13**, 146–154 (1935).

fissures from its surroundings, that is, that the oscillations were of the type known as stationary waves. These observations were admittedly inconclusive, for the seismographs used recorded only the north-south component of the waves. When Kishinouye later analyzed other components, however, he did not change his conclusion that the microseisms were stationary waves.[4]

The research was pursued further in 1936 at Göttingen, where H. D. Krug [5] set out two portable stations which, with a central station, defined a triangle with sides approximately 4500 ft long. He was able to trace some of the microseismic wave groups across his network and to determine the direction in which they were traveling. After determining a few bearings, Krug concluded that even with the close spacing of his stations the recorded patterns differed so much at times that they must have been the results of interfering waves from different directions. He calculated that the velocity of the microseisms across his network was 3600 ft/sec but he pointed out that it could not be determined whether this "unexpectedly low value" referred to the transmission of ernegy or to the advance of some phase of a combined wave.

During the last half of 1938, J. Emilio Ramirez, S.J., of St. Louis University, collected records from a tripartite network.[6] The corners of the triangle were at St. Louis University, at Washington University approximately 4 mi nearly due west, and at Maryville College about the same distance nearly due south. The first of these instruments recorded the horizontal motion of the waves in the north-south direction, the second recorded east-west, and the third north-south.

During the period of Ramirez's observations, the most important atmospheric storm in the United States was the New

[4] F. Kishinouye, "On microseisms of four-second period—Second paper," *Bull. Earthquake Research Inst., Tokyo Imperial University* **13,** 608–615 (1935).

[5] H. D. Krug, "Ausbreitung der natürlichen Bodenunruhe (Mikroseismik) nach Aufzeichnungen mit transportablen Horizontal-Seismographen," *Z. Geophysik* **13,** 328–348 (1937).

[6] J. E. Ramirez, S.J., "An experimental investigation of the nature and origin of microseisms at St. Louis, Missouri," *Bull. Seis. Soc. Am.* **30,** 35–84, 139–178 (1940).

England hurricane of September 21, 1938.[7] At 7:00 A.M. EST on September 19, the center of this storm was about 650 mi east-southeast of Miami, Florida. Twenty-four hours later it was 300 mi east of Vero Beach, Florida. On the morning of the 21st it was about 75 mi east of Cape Hatteras, and moving northward at a rate of nearly 60 mi/hr. It passed over the south shore of Long Island at about 2:45 P.M. and swung up the Connecticut River Valley, with maximum winds in the dangerous semicircle reaching nearly 200 mi/hr in Boston. By the following morning, it had become an ordinary low-pressure region north of Ottawa, Canada.

Ramirez reported microseisms coming from the center of this vortex beginning on the morning of the 20th. They radiated from the storm's center as it moved up the coast until it ended on the 22nd. The microseisms reached their greatest amplitude as the storm's eye passed Delaware Bay.

During the war, this observation was followed up with a view to locating hurricanes by the use of microseisms. The first completely equipped tripartite station of the Navy's Hurricane Microseismic Research Project was installed at the Naval Operating Base, Guantanamo Bay, Cuba, in September 1944. It was followed by six others in the Gulf-Caribbean area. Marion H. Gilmore, who was in charge of this program, reported [8] spectacular successes in tracing hurricanes during 1944 and 1945. In July 1948, it was announced that the Navy had expanded this program by the creation of a Pacific Microseismic Project, with stations at Guam, Okinawa, and Subic Bay, near Manila. Gilmore and his associate, William Hubert, reported [9] that "it is now possible to locate accurately the position of a typhoon by the SEISMO method when it is more than 1000 mi from the tripartite microseismic station."

[7] L. D. Leet, *Causes of catastrophe* (McGraw-Hill, New York, 1948), pp. 202–210.

[8] M. H. Gilmore, "Microseisms and ocean storms," *Bull. Seis. Soc. Am.* **36,** 89–119 (1946); "Microseisms classified according to type of storms," *Trans. Am. Geophys. Union* **27,** 466–473 (1946).

[9] M. H. Gilmore and W. E. Hubert, "Microseisms and Pacific typhoons," *Bull. Seis. Soc. Am.* **38,** 195–228 (1948).

The use of microseisms for the study of meterologic conditions has been on a strictly empirical basis up to the present time, and there are a great many lessons yet to be learned. Microseisms come from other sources as well as hurricanes, and the mechanism by which they are generated is not known.

Ramirez concluded from his observations at St. Louis that "the source of microseisms is to be found, not over land, but rather out over the surface of the ocean. The amplitudes of microseisms depend only on the intensity and widespread character of barometric lows traveling over the ocean . . . Special emphasis is laid on the fact that all the determined directions of incoming microseisms at St. Louis point to a deep barometric low over the ocean." According to Macelwane,[10] "it is now reasonably certain from the work of Ramirez and Gilmore that group microseisms . . . originate in the ocean bottom under the center of each hurricane, typhoon, or extratropical cyclone."

On the other hand, studies in New England, even with the relatively crude directional determinations using Rayleigh waves recorded on three components at a single station,[11] showed strong microseisms coming from south, southeast, and east of the Harvard station after an extratropical cyclone center with which they seemed to be involved had moved northeast of the station. They were probably coming from all directions between south and east, but were reported in 45° intervals only because such directions were most clearly defined by the Rayleigh-wave method and there was no need to attempt further refinement of the method at that time. On another occasion, a sharp microseismic storm at the Harvard station accompanied the passage out to sea of a cold front; no cyclonic storm center within the area was reported by the U. S. Weather Bureau. Gilmore stated that "microseisms are generated by meteorological disturbances

[10] J. B. Macelwane, S.J., "The problem of microseisms and ocean storms," *Bull. Seis. Soc. Am.* **36,** 81–82 (1946).

[11] L. D. Leet, "Microseisms in New England—Case history of a storm," *Geophysics* **12,** 639–650 (1947); "Microseisms in New England—Case history II," *Bull. Seis. Soc. Am.* **38,** 173–178 (1948).

such as hurricanes, typhoons, extratropical lows, monsoons, and trade winds." [12] He had previously reported [13] microseisms in the Caribbean area from the passage of a cold front, without data on directions of approach; but on the important point of whether or not microseisms associated with storms radiate exclusively from the center of a storm system, he said that "microseisms . . . are transmitted directly from the central storm area to the various seismograph stations," and he has not reported nearly simultaneous bearings ranging through 90° such as were found at Harvard.

One point of universal agreement is that whatever the mechanism of the origin of microseisms, it appears to operate efficiently only over large bodies of water.

Sources of Error in Tripartite Measurements

There has been a tendency to overemphasize the accuracy of a tripartite station's determination of the bearing of a microseismic wave. Such a determination is based on the assumption that the time of passage of the crest of a specific advancing wave is uniquely observed at each instrument of the network. This is not the case, in general, where waves approach from more than one direction. There is compelling evidence that they do this in many, if not all, storms.

Ramirez, in discussing variations in bearings,[14] said, "The variation may also be due to other microseismic waves, of smaller amplitudes, coming from various directions and overridden by the larger waves. This interference of waves is evident in certain double or superposed storms of different directions and more or less equal amplitudes. Finally, the variation may be due to a rather extensive area as source of origin. The focus or origin of microseisms does not seem to be a point, as in the first motion in earthquakes, but rather a region several hundred kilometers in diameter."

[12] Reference 9, p. 225.
[13] M. H. Gilmore, "Microseisms and ocean storms," reference 8, p. 117.
[14] Reference 6, p. 60.

This reference to "other microseismic waves, of smaller amplitudes," does not, however, state the problem fully. There will be no interference pattern, or evidence in the record of more than one set of waves, if they differ only in amplitude. If two groups of waves of equal period overlap, they combine to form simple sine waves of the same period but with maxima displaced in phase from those of the component waves. This is a situation that the tripartite network with single-component seismographs at each point is powerless to resolve, and one that leads to indeterminate errors in bearings.

For example, if two waves

$$c_1 = A_1 \sin (p_1 t + \kappa_1 x)$$

and

$$c_2 = A_2 \sin (p_2 t + \kappa_2 x)$$

with $p_1 = p_2$, reach a network from different angles and out of phase, say with

$$(p_2 t + \kappa_2 x) - (p_1 t + \kappa_1 x) = 90°,$$

regardless of the ratio A_1/A_2, they combine to form a simple sine wave $c = c_1 + c_2$, with its maximum 45° after that of c_1 and 45° before that of c_2. As these waves sweep on across the tripartite network, their phase relations change and the recorded maximum at each of the other corners of the network leads or lags the true maxima of the components by some angle other than the 45° computed above. Accordingly, the observed time of maximum at each station of the network does not correspond to any individual wave, and the computed bearing is in error.

Interference patterns appear only when p_1 and p_2 are different. Two that are suggestive of many seen in the records of microseisms, are shown in Fig. 57.[15] Here, again, the recorded maxima come at times that differ from those of the true maxima of the component waves, and the phase relations change as the waves sweep across a tripartite network at different angles.

[15] F. B. Galitzin, "Zur Frage der Analyse zusammengesetzter harmonischer Schwingungen," *Bull. acad. imp. sci.* (*St.-Pétersbourg*), pp. 449–474 (1913).

Another aspect of the problem is illustrated by the first microseismic storm studied in detail by Ramirez with records from the tripartite network at St. Louis (1940). It was the largest investigated. It ran from October 23 to 28, 1938. On October 24, Ramirez reported waves from N 8° W and on October 25 a few from N 45° W as well. There was a slight decrease in recorded

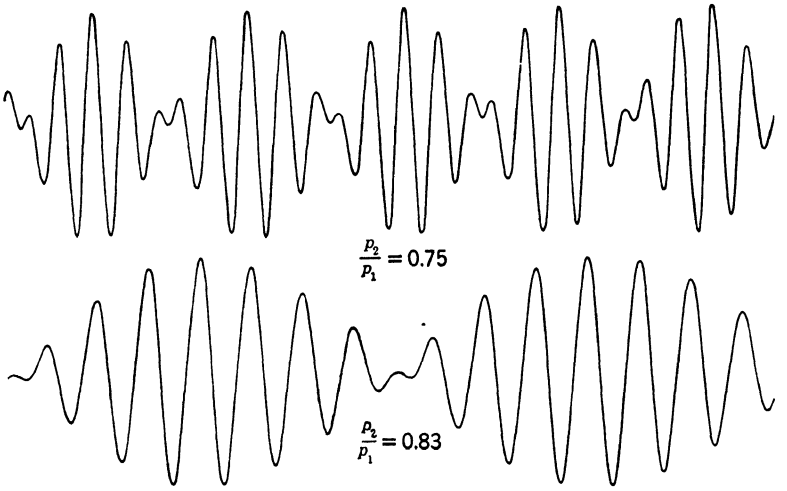

FIG. 57. Interference patterns. (After Galitzin.)

amplitudes late on the 25th, then a strong resurgence leading to maximum trace amplitudes of 14 mm on the 26th, computed as waves arriving from N 33° E. He published a section from the E–W record at St. Louis University between 2:56 and 2:59 P.M., October 26, 1938, and one covering the same time interval from the E–W record at Washington University, 4 mi nearly due west.[16] He stated that these records "give a very fair idea of the microseismic storm of October 26, 1938," and that they "bring out the fact that on this date all the regular waves were arriving at the St. Louis University station earlier than at Washington University. The microseisms were coming from the north-

[16] Reference 6, p. 59.

east . . ." These record sections are shown in Fig. 58. The St. Louis record was printed reading from right to left in the Ramirez report; it has here been changed to read from left to right for direct comparison with the Washington record. Time marks were placed on the original records every 6 sec, but do not all show on the printed copies. They were numbered from 1 through 36 by Ramirez but only 1, 10, 20, and 30 are marked in Fig. 58. An extra minute mark shows at 20.

Ramirez measured the time between the nearest crest or trough and each of 23 time marks for each station. The differ-

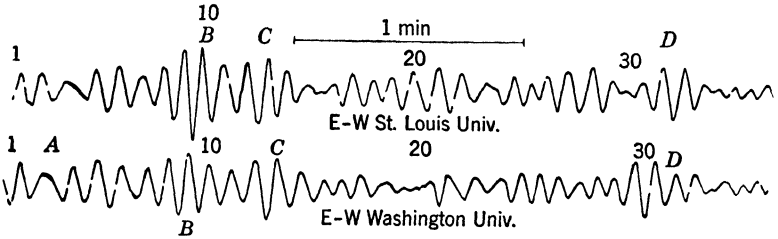

FIG. 58. Microseisms analyzed by Ramirez.

ence between this interval at St. Louis and at Washington ranged from 0.3 sec to 2.0 sec but was always positive. This was interpreted as meaning that *in every case the wave reached St. Louis first.* These time differences represented phase differences ranging from about 20° to 130° between the two stations.

An average of 94 readings of this kind between 2:45 P.M. and 3:15 P.M. local time, which included the time covered by Fig. 58, gave a time difference of 1.15 sec, corresponding to waves approaching the stations from N 33° E.

Examination of Fig. 58, however, opens some questions about the validity of this averaging procedure. The break in sinusoidal character at *A* occurred at the Washington station before it did at St. Louis and the pattern at *B* looks like a group that reached Washington University first. Meanwhile, between *C* and *D* there is a complete breakdown of the point-for-point com-

parability of the two records. This is most striking in the vicinity of time mark 20. On the basis of record character, even in this short 3-min sample, it is clear that these microseisms are not simple trains of waves sweeping past St. Louis and Washington Universities from one or even close to one point of the compass and having a common origin of no greater extent than "a region several hundred kilometers in diameter." Under those conditions, averages of differences in passage time at the two stations, conditioned only by the requirement that they be taken from regular sinusoidal waves, would seem to have limited significance.

In determinations of the velocity of microseisms, a further problem is presented by the employment of horizontal-component seismographs for registration at the corners of a tripartite network, as practiced by Ramirez and Gilmore. Such instruments are unable to distinguish between *R*- and *Q*-waves and there can be no assurance that velocity determinations are being made on the same wave type in all cases. If only one instrument were available for each station, a vertical one would have the merit of not responding to *Q*-waves.

Values for the velocity of microseisms reported at various places are given in Table 10.

TABLE 10. Velocities of microseisms.

Location	Velocity	
	(km/sec)	(ft/sec)
Göttingen	1.1	3,610
St. Louis	2.66	8,730
Guam	3.16	10,370
Richmond	3.25	10,660
Puerto Rico	4.00	13,120

It is reasonable to expect that a solution of this problem will ultimately be found in a combination of the Rayleigh and the

tripartite methods of determining the direction in which microseisms are traveling. With three components recording at each corner of a tripartite network, it may be that the character of the record and wave types can be analyzed in such a way as to spot the occasional isolated microseism that passes without interference from other directions. When this has been done, the direction of its travel can be fixed precisely by the relative times of its passage at the three corners of the network.

INDEX